

**Assessment of Urban Microclimate and Its Impact on Outdoor Thermal
Comfort and Building Energy Performance**

Senwen Yang

A Thesis

In the Department

of

Building Civil and Environmental Engineering

Presented in Partial Fulfillment of the

Requirements For the Degree of

Doctor of Philosophy (Building Engineering)

Concordia University

Montreal, Quebec, Canada

March 2024

© Senwen Yang, 2024

CONCORDIA UNIVERSITY
SCHOOL OF GRADUATE STUDIES

This is to certify that the thesis prepared

By: Senwen Yang

Entitled: Assessment of Urban Microclimate and Its Impact on Outdoor Thermal Comfort
and Building Energy Performance

and submitted in partial fulfillment of the requirements for the degree of

Doctor Of Philosophy (Building Engineering)

complies with the regulations of the University and meets the accepted standards with respect to
originality and quality.

Signed by the final examining committee:

_____ Chair
Dr. Onur Kuzgunkaya

_____ External Examiner
Dr. Afshin Afshari

_____ External to Program
Dr. Hoi Dick Ng

_____ Examiner
Dr. Andreas Athienitis

_____ Examiner
Dr. Ursula Eicker

_____ Thesis Supervisor
Dr. Liangzhu Wang

_____ Thesis Co-Supervisor
Dr. Ted Stathopoulos

Approved by _____
Dr. Chunjiang An, Graduate Program Director

March 14, 2024 _____
Dr. Mourad Debbabi, Dean of Faculty

ABSTRACT

Assessment of Urban Microclimate and Its Impact on Outdoor Thermal Comfort and Building Energy Performance

Senwen Yang, Ph.D

Concordia University, 2024

As urbanization and population growth have increased over the past decade, more construction has been built in urban areas to form large metropolitan areas. Researchers are paying more attention to the link between human activities and the immediate surroundings – urban microclimate –to improve the quality of life and minimize adverse impacts on the environment and climate. This thesis focuses on the urban microclimate and its impact on outdoor thermal comfort and building energy performance. This study will start a comprehensive literature review presenting the latest progress in urban microclimate research on urban wind and thermal environment, covering methods and practical issues.

For the short-term analysis, this research studies how urban configuration affects the urban microclimate and outdoor thermal comfort. In the present work, temperature distribution at three different urban areas will be simulated during a summer heatwave in 2013 in Montreal, Canada. The impact of different building configurations on the flow pattern will be investigated. What's more, thermal comfort and the impact of heatwaves on the human body will be considered by humidex (humidity index). The results show that this model is capable of estimating local microclimate and outdoor thermal comfort.

An artificial neural network (ANN) model is also presented in this study to predict urban microclimates based on long-term measurements from local weather stations near urban buildings and their significance in analyzing building energy consumption. The ANN model could connect local and remote meteorological parameters for a whole year. The 20-year historical weather data at the airport was then used to generate a local TMY, and then building heating and cooling loads were analyzed. This method was evaluated for five weather stations to assess the impact of the local microclimate on the energy consumption of buildings.

This study underscores the crucial role of urban microclimate in building energy consumption through both short-term and long-term evaluations. Accurate prediction of local weather conditions around buildings is essential within urban microclimates. The research introduces a pioneering approach using an artificial neural network model for predicting microclimate parameters based on extensive onsite measurements, emphasizing its significance in building energy analysis.

ACKNOWLEDGMENT

I would like to express my sincere gratitude to the following individuals, without whom the completion of this thesis would not have been possible:

First and foremost, I extend my deepest appreciation to my parents, Mr. Baowei Yang and Mrs. Ling Shen. Their unwavering support, encouragement, and belief in my abilities have been my guiding light throughout this academic journey. Their sacrifices and love have been the foundation upon which I built this thesis, and for that, I am forever grateful.

I am indebted to my supervisors, Prof. Liangzhu (Leon) Wang and Prof. Ted Stathopoulos, for their invaluable guidance, mentorship, and insightful feedback. Their expertise and dedication to my academic development have played a pivotal role in shaping the quality of this research.

I would also like to thank my colleagues and friends, Dr. Dahai Qi, Dr. Cheng-Chun Lin, Dr. Mohammad Mortezaadeh, Dr. Ali Katal, Dr. Chang Shu, Dr. Danlin Hou, Dr. Lili Ji, Dr. Xin Zhang, Dr. Hatem Alrawashdeh, Cheng Zhang, Chen Ling, Bingyan Jia, Dongxue Zhan, Maher Albettar, Jiwei Zou, and Shujie Yan, who provided a stimulating intellectual environment. The exchange of ideas, discussions, and collaborative efforts have enriched my understanding and enhanced the overall quality of this work.

Finally, I would like to express my deepest gratitude to Ms. Qi Xia, whose unwavering love, support, understanding, and encouragement sustained me throughout this academic journey.

Thank you all for your encouragement, support, and inspiration. This achievement is as much yours as it is mine.

CONTENTS

List of Figures.....	viii
List of Tables	xi
Chapter 1. Introduction	1
1.1 Background.....	1
1.2 Statement of Problem	4
1.3 Layout of the Thesis	5
Chapter 2. Literature Review.....	7
2.1 Introduction.....	7
2.2 Review Method	10
2.3 Experimental Approach.....	13
2.3.1 Field measurement.....	13
2.3.2 Wind tunnel measurement.....	15
2.4 Numerical Approach	22
2.4.1 CFD simulation	22
2.4.2 Data-driven models.....	27
2.5 Urban Microclimate: Current Practical Issues	30
2.5.1 Urban wind environment	31
2.5.2 Urban thermal environment	33
2.5.3 Building energy consumption	42
2.5.4 Urban pollutant dispersion	44
2.6 Summary.....	45
Chapter 3. Wind Environment Simulations and Validations	50
3.1 Introduction.....	50
3.2 Methodology	51
3.3 Wind Simulation for Building Configurations.....	53
3.4 Pedestrian-level Wind Environment Simulation.....	57
3.5 Summary.....	60
Chapter 4. Short-term Evaluation of Urban Microclimate and Thermal Comfort Analysis...61	
4.1 Introduction.....	61
4.2 Methodology	63
4.2.1 CFD simulation	63

4.2.2 Building Energy Modelling.....	65
4.2.3 Boundary conditions integration	66
4.2.4 Outdoor thermal comfort	70
4.3 Results and Discussion	70
4.4 Outdoor Thermal Comfort Analysis.....	77
4.5 Conclusion	85
Chapter 5. Long-term Predictions of Urban Microclimate Impact on Building Energy Consumption	88
5.1 Introduction.....	88
5.2 Methodology	92
5.3 Results and Discussion	102
5.4 Conclusion	121
Chapter 6. Conclusions	123
6.1 Contributions.....	123
6.2 Limitations	124
6.3 Future Work	125
REFERENCES	127

List of Figures

Figure 1.1 Climatological scales classified by horizontal extension by Orlanski in 1975 [3] and climatic condition type by region scale.....	2
Figure 2.1 Keyword cloud map of this review with the size indicating the frequency of occurrence, for example, the “Urban Microclimate” (23%), “Urban heat island” (17%), and “CFD” (14%) of the total 563 publications selected.	11
Figure 2.2 (a) Number of studies by turbulence models (b) Number of studies by simulation tools	23
Figure 2.3 (a) Simulation error of wind speed (left axis) and temperature (right axis) by different tools (b) the investigation size for applied urban region cases, ENVI-met (orange), FLUENT (blue).	27
Figure 2.4 Averaged coefficients of determination (R^2) reported in the publications by predicted outputs and by simulation models.....	29
Figure 2.5 Studies related to urban microclimate classified by different issues	31
Figure 2.6 (a) Number of studies by topics (b) Techniques adopted for urban wind studies	31
Figure 2.7 (a) Publication numbers on the landscape and building design parameters (b) Number of studies classified by investigation methods.....	33
Figure 3.1 Multiple buildings with different configurations	54
Figure 3.2 Velocity contours at the height of 2 m, normalized by the reference velocity (1) Reference, (2) CityFFD.....	55
Figure 3.3 Temporal velocity contours for airflow around multiple buildings at 2 m height.....	55
Figure 3.4 Wind distribution along a vertical line at P1, P2, and P3	56
Figure 3.5 Buildings’ configuration in a real urban area (Niigata, Japan).....	57
Figure 3.6 Comparison of simulation results by wind speed contours in an urban area, (1) Tominaga et al.[24][159] (2) CityFFD.....	58
Figure 3.7 Wind flow in Niigata from west direction (1) normalize wind speed at 2 m, (2) Error correlation.....	59
Figure 3.8 Wind flow in Niigata from north direction (1) normalize wind speed at 2 m, (2) Error correlation.....	59

Figure 4.1. vulnerability index and heat-related death map in Montreal (Heatwave: 30 June to 5 July 2018). Source: https://ici.radio-canada.ca/nouvelle/1113457/bilan-deces-chaueur-montreal-sante-publique	63
Figure 4.2. Schematic of the CityBEM model.[161]	65
Figure 4.3. Dynamic urban building and microclimate simulation (CityFFD/CityBEM) workflow	67
Figure 4.4. Temperature and velocity at the inlet of the simulation domain	68
Figure 4.5. Satellite image and geometry of three investigation regions marked with the measurement location.....	69
Figure 4.6. (a) Schematic of the computational domain and boundary condition (b) Satellite imagery of Montreal.....	71
Figure 4.7. Wind velocity (A1, B1, C1)Air temperature (A2, B2, C2) and comparisons between measurements at the airport (blue line) and at the local station (red dash-dotted line), and the simulation at the local station (black dotted line) for Downtown (LCZ1), community (LCZ3) and suburban (LCZ6) case studies.	73
Figure 4.8. Averaged pedestrian level temperature during 48-hour heatwave in LCZ6 area	74
Figure 4.9. Averaged pedestrian level temperature during 48-hour heatwave in LCZ3 area	75
Figure 4.10. Averaged pedestrian level temperature during 48-hour heatwave in LCZ1 area	76
Figure 4.11. Comparison of averaged temperature at pedestrian level in three regions during the heatwave	77
Figure 4.12. Humidex in 48 hours summer heatwave in case LCZ6.....	78
Figure 4.13. Humidex in 48 hours summer heatwave in case LCZ3	79
Figure 4.14. Humidex in 48 hours summer heatwave in case LCZ1	80
Figure 4.15. Comparison of averaged humidex.....	81
Figure 4.16. Distribution of humidex among different urban locations	82
Figure 4.17 Thermal discomfort exposed duration comparison for 3 regions	84
Figure 4.18. Maps of the 48-hour averaged velocity, temperature, and humidex for the LCZ6 (a), LCZ3 (b), and LCZ1 (c) case studies.....	85
Figure 5.1 Overall schematic for using ANN to estimate building energy.....	92
Figure 5.2 Structure of proposed ANN model.....	95

Figure 5.3 (a)location and installation of roof-mounted weather stations (b) weather station sensors and configuration and installation in LOC1.	97
Figure 5.4 DOE Building archetype of primary school.	101
Figure 5.5 (a)Air temperature comparison between prediction and measurement from June 18th to 23rd (b) Air temperature prediction accuracy in the testing dataset. (c) air temperature error distribution at LOC1.	104
Figure 5.6 (a) Wind speed comparison between measured, predicted, and calculated from power law distribution, (b) wind prediction error distribution for LOC1.	106
Figure 5.7 Wind speed comparison and wind prediction error distribution for all other locations	108
Figure 5.8 (a) Temporal wind direction performance in July (b) Wind rose for testing dataset comparing the measured and predicted wind direction (c) Wind direction prediction error distribution for LOC1.....	109
Figure 5.9 Wind direction comparison and wind direction prediction error distribution for all other locations.....	110
Figure 5.10 TMY air temperature (a) and wind speed (b at LOC1 from July 18 th to 23 rd	113
Figure 5.11 Local 20 years weather prediction air temperature variation and related TMY and related annual cooling load and heating load evaluation for 5 Locations(LOC 1-5).....	115
Figure 5.12 Overall cooling energy and heating energy changes in comparison to the traditional method using airport weather for TMY.	116
Figure 5.13 Meteorological parameters impact ranking on building energy modeling for LOC1	120

List of Tables

Table 2-1 Previous review articles related to the urban microclimate.....	8
Table 2-2 Field measurement studies for the urban thermal environment.....	14
Table 2-3 Wind tunnel experimental studies on the urban thermal environment.....	20
Table 2-4 CFD simulation and validation studies for the outdoor urban thermal environment in actual regions.....	25
Table 2-5 Average SUHII (°C) in 419 cities around the world [121] by daytime and nighttime..	36
Table 3-1. Dimensions of in 3 building configurations in Figure 3.1.....	54
Table 4-1 RMSE of validation results for three regions	72
Table 5-1 Machine learning model performance of temperature predictions	103
Table 5-2 ANN model performance at multiple locations.	105
Table 5-3 Wind speed performance and error in all 5 locations.....	106
Table 5-4 Wind component and directions for 5 locations.	111
Table 5-5 Building energy sensitivity analysis.....	118

Chapter 1. Introduction

1.1 Background

Urbanization and rapid industrialization have made the urban environment more vulnerable to degradation over the past decade. According to the United Nations (UN) and the World Bank, the global population will increase rapidly by the end of the 21st century, and the population will continue to grow rapidly in the following decades [1]. Fast urbanization involves replacing natural surroundings with man-made environments that have different physical properties. Under changing climates, the constantly changing physical properties of man-made urban features directly impact the immediate living environment of city dwellers to create an urban microclimate in which most human activities take place.

A microclimate refers to the climate conditions within a relatively small and localized area, which may differ from the surrounding larger climate. Various factors contribute to the development of microclimates, including topography, vegetation, water bodies, and human activities. These factors can create variations in temperature, humidity, wind patterns, and other climatic elements within a specific region. According to Figure 1.1, microclimates are defined as climate conditions at a "microscale" on the earth's underlying surface [2] as opposed to macroscales and mesoscales. Based on Orlanski [3], climate studies were classified by the region of investigation. In urban microclimate, climatic phenomena are considered at a variety of scales, from the neighborhood and small community scales of several kilometers [4] to street canyons of a few meters [5].

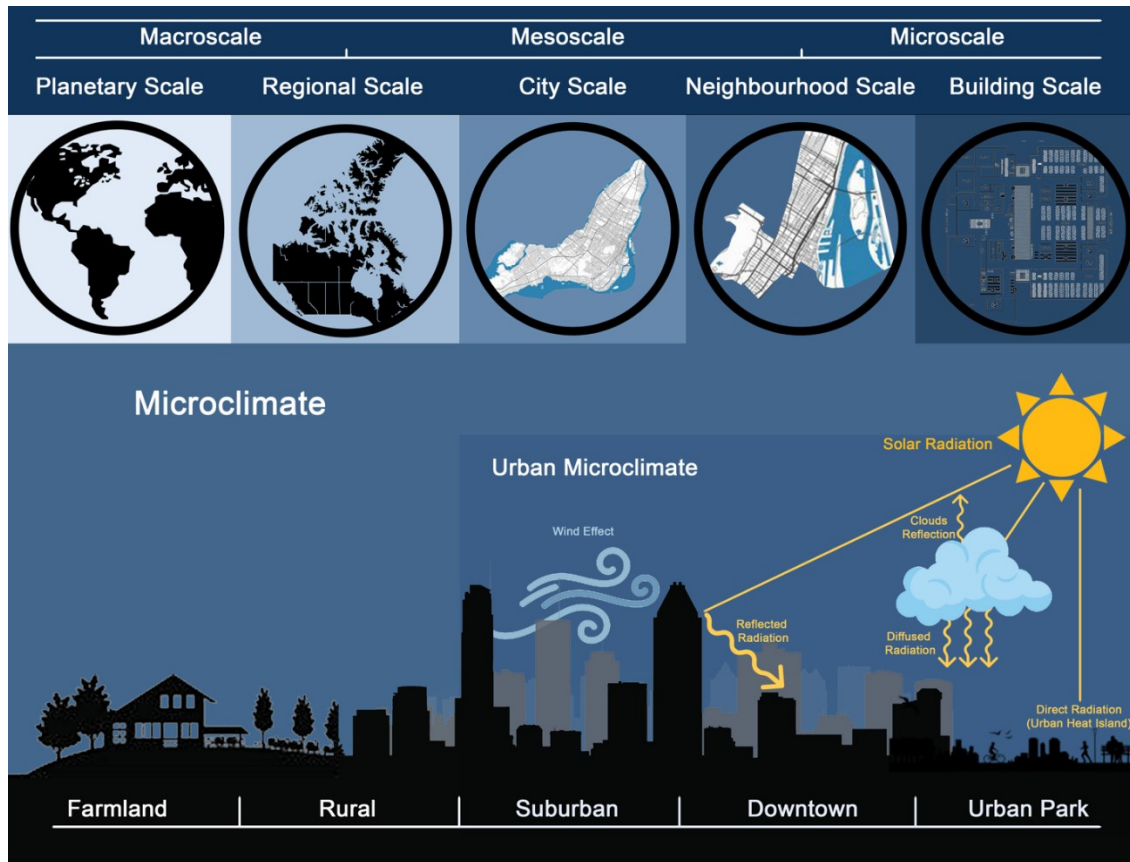


Figure 1.1 Climatological scales classified by horizontal extension by Orlanski in 1975 [3] and climatic condition type by region scale.

In the review study by Toparlar et al.[6], urban microclimate only referred to the scenarios considering the impact of temperatures, while isothermal scenarios, in which airflow is regarded to be dominated by the wind, so the thermal buoyancy effects are usually neglected, were excluded, representing a narrow definition of urban microclimate. Some other studies applied a broader definition: any climatic phenomenon of urban physics is considered a part of the urban microclimate [4], such as wind aerodynamics [7], wind thermal comfort, energy demand, pollutant dispersion, and wind-driven rain [8]. As such, this review encompasses a broader perspective on the subject.

Among the most discussed topics in urban microclimates are urban heat islands (UHI). According to Howard [9], urban areas can retain and generate more heat than rural regions, leading to higher ground surface and air temperatures near the ground. The UHI is the result of inadequate urban development control [10]. Besides UHI, urban surface morphing also modifies the urban wind environment and urban pollution dispersion due to the thermal buoyancy from heated surfaces. The underlying urban surfaces can also affect building energy consumption. For example, urban thermal aerodynamics affects pollution dispersion in street canyons, especially in stratified conditions [11], and indoor air quality, especially for naturally ventilated buildings [12].

Urban Microclimate is profoundly influenced by various parameters, each playing a critical role in shaping the microenvironment within urban areas. Temperature variations, particularly the formation of Urban Heat Islands (UHI), result from factors such as building materials, urban disturbances, and anthropogenic heat generation[13]. Heatwaves, intensified by sustained heat stress, pose health risks, with developing countries experiencing casualties due to unplanned urbanization [14–17]. Precipitation patterns in urban areas are affected by surface roughness, convergence, and air pollution, leading to altered precipitation rates and increased lightning incidents. Humidity, closely linked to air temperature, experiences changes in urban areas, contributing to thermal stress during high temperatures and moist urban air during winter [18]. Wind patterns are hindered by densely constructed areas, influencing speed and direction and impacting temperature differentials between urban and countryside areas [19]. Surface characteristics, such as albedo, influence urban microclimate (UMC), with high-albedo surfaces mitigating the heat island effect [20]. Urbanization's demand for transportation and infrastructure contributes to increased fuel consumption and air pollution, further affecting microclimate

attributes. Anthropogenic activities alter natural microclimate factors, creating distinct UMC patterns, compounded by background pollutant concentration and transboundary movement.

There are two scientific approaches to how urban microclimate affects the building environment: the experimental approach, which entails full-scale field measurements and wind tunnel tests, and the numerical approach, which has been enacted lately through CFD and data-driven models. A number of studies have been conducted using CFD to simulate thermal comfort at the pedestrian level [21] and buoyancy-driven flows in street canyons [22,23]. Compared with the conventional CFD simulation, more novel methods based on data-driven models, including artificial intelligence ones, have been developed that integrate multiple parameters of urban microclimate, which cannot be easily accomplished with conventional CFD simulation. Thus, these approaches are also discussed in this literature review section.

1.2 Statement of Problem

Predicting urban microclimates is challenging due to the intricate interplay of various factors. The complex morphology of urban landscapes, characterized by diverse building layouts and densities, creates dynamic wind patterns, sunlight exposure, and temperature variations. The composition of surface materials, such as pavements and buildings, further complicates predictions as different materials absorb and release heat at varying rates.

The simulation for urban microclimate requires detailed boundary conditions. However, most of the factors are not well defined in the simulations. The existing simulation tools are not fulfilled to cover all the physical boundary conditions. Meanwhile, the existing simulation studies on urban microclimate can only evaluate the urban microclimate in the short term due to the high computational cost for large applied regions.

This thesis will focus on how to simulate the urban microclimate to cover the building information, including the detailed building shapes and building surface temperature. Meanwhile, to assess the impact of urban microclimate on building performance, long-term monitoring, and machine learning models are applied to evaluate the impacts on buildings.

1.3 Layout of the Thesis

To delineate the research gaps addressed in this study concerning urban microclimate and its implications, the thesis is structured into six chapters as follows:

Chapter 2 presents a systematic review of current advancements in urban microclimate research. Beginning with the definition of urban microclimate, it navigates through methodologies, approaches, factors influencing urban microclimate, and related research topics, with a specific focus on their impacts on building environments.

Chapter 3 describes the application of Computational Fluid Dynamics (CFD) simulations to assess wind environments in urban regions. Examining three distinct cases—generic street canyons, building blocks, and applied urban regions, this chapter explores simulation performance using detailed validation data. The outcomes of these simulations have contributed to multiple publications.

Chapter 4 presents the urban microclimate simulation, incorporating considerations for the urban heat island effect across three diverse locations. This chapter concentrates on the spatial and temporal variations in urban microclimate during summer heatwaves, emphasizing their impacts on outdoor thermal comfort.

Chapter 5 is dedicated to constructing a machine-learning model based on on-site monitoring results. This model aims to establish connections between public meteorological weather stations

and local urban microclimate. Given the impracticality of long-term simulations for urban regions due to high computational costs, the proposed machine learning approach serves as an alternative method for analyzing the influence of urban microclimate on building energy performance.

Chapter 6 serves as the conclusion for the overall research, encompassing contributions, limitations, and future directions. This chapter discusses factors overlooked in the present study and outlines potential avenues for improvement in future research.

Chapter 2. Literature Review

2.1 Introduction

This section focuses on the literature review concerning the topics' necessity and contribution, which can be explained by comparing it to previous reviews¹. Table 2-1, Previous reviews focused either on approaches or practical issues. The CFD simulation studies on urban microclimate were reviewed by Toparlar et al. [6], where they found that more validation studies need to be conducted. Laboratory studies are not linked to field implementations, according to Bherwani et al. [24]. The thermal environment was studied by Priya et al. [25] with the conclusion that trees, water bodies, and green walls and roofs lower ambient temperatures and improve thermal comfort. Ampatzidis et al. [26] confirmed the cooling effects of water bodies during the daytime but noted that they could also play a negative role at night because of thermal storage. For the impacts of building configurations, Ai et al. [27] found that street canyons lead to hotspots of traffic-related noise and pollutants, so more high-resolution field measurements are needed to support wind tunnel tests or CFD. In another review [28], it was demonstrated that water bodies provide significant cooling effects in tropical cities, but the study was restricted to coastal regions with significant water evaporation. Among the mitigation strategies for urban overheating discussed by Li et al. [29], water and vegetation, along with reflective building surfaces, however, may affect pedestrian thermal comfort. Liu et al. [30] conducted a review of the field measurement in urban microclimate, and a four-step framework for the overall measurement process was generalized and discussed in detail. The review investigated the factors or approaches for urban microclimate in the past decade

¹ 1 This chapter has been published as a peer-reviewed journal article: Senwen Yang, Liangzhu (Leon) Wang, Ted Stathopoulos, Ahmed Moustafa Marey. (2023) "Urban microclimate and its impact on built environment – A review." Building and Environment. Volume 238, 15 June 2023, 110334.

and provided insights on how and what to investigate regarding urban microclimate. When comparing the previous reviews, it could be necessary to conduct a new review study on a broader sense of urban microclimate and its close impacts on the built environment. Meanwhile, the emerging methods of interest should also be reported for a timely update of our knowledge base on urban microclimate, including data-driven models and artificial intelligence applications.

In this review, we examine the related research over the past decade, focusing on 1) the development of existing approaches to urban microclimate since 2010, 2) the impact of the various parameters of urban microclimate and their interactions, and 3) an update on urban climate literature. In this review, four topics are addressed: 1) urban wind environment, focusing on neutral wind conditions, where the airflow is dominated by the incoming wind so the thermal aspect may be neglected; 2) urban thermal conditions, including UHI; 3) urban building energy consumption; 4) urban pollution dispersions.

Table 2-1 Previous review articles related to the urban microclimate.

Review papers	Concentration	Year	Key Findings
Ai et al. [27]	Natural ventilation	2014	Street canyons are hotspots for both traffic-related pollutants and noise. Large-scale, long-term, high-resolution, standardized onsite measurements in typical urban street canyons should be conducted to accumulate microclimatic data.
Toparlar et al. [6]	CFD simulation	2015	To improve reliability, CFD results should be subjected to detailed validation in the future.

			Most studies used the RANS model, even though LES has the potential to be more accurate. More turbulence models should be covered.
Shafaghat et al. [28]	Costal zones	2016	Coastal zones have not received much attention compared with the other zones in tropical areas. Water bodies can provide a significant cooling effect by lowering the ambient temperature that was supported.
Bherwani et al. [24]	Methodology	2019	Demonstrate the missing link between microclimate research and implementation of policy.
Lai et al. [29]	Mitigating strategies	2019	The urban environment can be cooled by vegetation and water bodies. The cooler surface, which has a high reflection of solar radiation, may worsen the thermal comfort of pedestrians.
Priya et al. [25]	Vegetation	2020	Trees and water bodies can reduce air temperature and provide better thermal comfort. The green roof and green wall can also cool the ambient temperature
Ampatzidis et al. [26]	Water bodies	2020	Blue spaces may not provide cooling all day long and may provide warming at night.

			Night-time should be included when water bodies are investigated.
Liu et al. [30]	Measurement	2022	A four-step workflow was generalized and discussed, including formulating a field measurement plan, preparing for field measurements, sustaining measurement quality, and curating data.

2.2 Review Method

The review considered 563 studies, with the majority coming from well-known databases or publishers like ScienceDirect and Springer and a few more from peer-reviewed conference proceedings, covering topics such as urban outdoor environments and their interactions with indoors. The publication selection focused on the interactions between urban microclimate and buildings. Some studies only investigated microclimate at the metrological scale, such as weather observations, without considering the phenomena inside the street or neighborhood scales, so they were not counted (e.g., Hu et al. [31]). Meanwhile, some others focusing only on indoor climatic conditions without considering the spatial and temporal microclimatic impacts (e.g., Mu et al. [32]) were also excluded from this review. Figure 2.1 shows how frequently keywords were used in all reviewed publications except those relating to indoor environments or building energy consumption. Microclimate or urban microclimate is the most cited term, followed by “urban heat islands” and “thermal comfort,” and “CFD” the most frequently used research approach keyword. “ENVI-met” [33] is frequently listed as a software tool in the keywords.



Figure 2.1 Keyword cloud map of this review with the size indicating the frequency of occurrence, for example, the “Urban Microclimate” (23%), “Urban heat island” (17%), and “CFD” (14%) of the total 563 publications selected.

Keywords in a descending frequency of occurrence for the three main categories and their subcategories are presented as follows:

- The methods or tools applied to urban microclimate:
 1. Numerical simulation (i.e., CFD, ENVI-met, SOLENE, validation, simulation model)
 2. Experiment (i.e., remote sensing, experimental, onsite measurement)

3. Wind tunnel (i.e., Sub-scale, wind tunnel experiment)

- Practical issues related to urban microclimate:
 1. Urban heat island
 2. Climate (i.e., urban climate, microclimate, climate change)
 3. Outdoor thermal comfort (i.e., thermal stress, mitigation strategies, UTCI)
 4. Energy demand (i.e., building energy consumption, space cooling, space heating)
 5. Urban ventilation (i.e., pedestrian wind comfort)
 6. Urban physics
 7. Pollutant dispersion
- Landscape and building design parameters:
 1. Urban geometry (street canyon, building blocks)
 2. Vegetations (i.e., urban greenery, urban park)
 3. Water bodies (i.e., coastal cities)
 4. Building characteristics (i.e., albedo, green roof)

For the investigation methods, the most commonly applied approaches are numerical simulations (e.g., CFD), followed by experimental studies, such as onsite measurements and wind tunnel experiments. The urban heat island is investigated the most, except for the urban microclimate, among all the research topics from this review. For the landscape and building aspects, street canyons are most interesting to researchers.

2.3 Experimental Approach

2.3.1 Field measurement

It is essential to conduct field measurements or field measurements to determine the realistic state of urban microclimate. Field monitoring appears to be a relatively new approach, with only a few studies being conducted every year, although they have increased with only a slight decrease in the past two years. The number of publications on field measurements is extremely limited when compared with numerical simulations. As shown in Table 2-2, the parameters investigated include air temperature, relative humidity, wind speed, building surface temperature, and solar radiation. The majority of the studies measured air temperatures, relative humidity, wind speed, and direction, which are relatively easier to measure than solar radiation with less expensive instruments. For the measurements of the parameters of interest, several measurement devices/techniques were used: thermocouples for air temperature and façade temperature [34]; LiDAR [35,36] and sonic anemometers [34,37,38] for wind speed/direction. In addition to recording temperature, humidity, wind speed, and solar radiation, a weather station can also be installed for long-term field monitoring [39]. The temperature distribution on building and ground surfaces was measured using portable infrared thermography [40]. For city-scale temperature distribution measurements, thermal images were taken by helicopters or satellites [41]. Field measurement studies are summarized in Table 2-2. In most of the studies, neighborhood scales were studied instead of city scales. The majority dealt with UHI, which explains why temperate/hot climates were most commonly studied.

Table 2-2 Field measurement studies for the urban thermal environment.

Author	Location	Scale	Parameter	Detail
Nikolopoulou et al. [39]	Athens	Neighborhood	AT, ST, RH, WS	Outdoor spaces, microclimate
Emmanuel [42]	Colombo	City	AT, RH, WS	UHI, urban geometry, coastal city structure
Neophytou, et al. [43]	Nicosia	Neighborhood	WS, AT, ST	UHI, heatwave
Maxime, et al[44]	La Rochelle	Building scale	AT, ST	UHI, passive cooling, cool paints
Sharhrestani, et al. [45]	London	Neighborhood	AT, ST, SR, WS	Microclimate, wind pattern
Gabriele, et al. [37]	Rome	Neighborhood	AT, WS, RH, SR	UHI, UCTI, ENVI-met
Liu et al. [38]	Changsha	City scale	AT, RH, WS, GT	outdoor thermal comfort, microclimate parameter
Wong [46]	Hong Kong	Neighborhood	AT, RH, WS	Urban microclimate, urban habitat
Tong et al. [47]	Tianjin	City scale	AT, RH, WS	UHI, greenery, outdoor thermal comfort
Zaki et al. [48]	Kuala Lumpur	Neighborhood	AT, ST, RH	urban morphology, green cover ratio

Hong et al.	San Francisco	City scale	AT, SR, RH,	Urban	microclimate,
[49]			WS		building energy use

AT: air temperature; ST: surface temperature; RH: relative humidity; WS: wind speed; SR: solar radiation; GT: global temperature

In summary, air temperature and wind speed were the most investigated for experimental urban microclimate studies. Humidity was also widely concerned in outdoor thermal comfort research. Solar radiation measurement was often neglected, whereas it is a major thermal parameter of urban microclimate. Other weather phenomena, such as fog or snow, are barely investigated by researchers. Due to the increasing impact of climate change, extreme weather, in addition to heatwaves and UHIs, will be studied more in the future. A building's operation is not considered in field measurements for most studies, and their contribution is neglected, despite the fact that building properties and land properties play a significant role in urban heat islands.

2.3.2 Wind tunnel measurement

In atmospheric boundary layer wind tunnel studies, researchers often use dimensionless numbers to characterize and analyze the behavior of the atmospheric boundary layer. Some of the key dimensionless numbers in this context include:

1) Reynolds Number (Re): the Reynolds number is a fundamental dimensionless number used in fluid dynamics. In the context of atmospheric boundary layer studies, the Reynolds number is often defined based on the characteristic length (e.g., height of vegetation or buildings) and the wind speed. It helps determine whether the flow is laminar or turbulent.

$$Re = \frac{\rho \cdot U \cdot H}{\mu} \quad \text{Equation 2-1}$$

where:

- ρ is the air density,

- U is the characteristic wind speed,
- H is the characteristic length, and
- μ is the dynamic viscosity of air.

2) Grashof number (Gr): The Grashof number (Gr) is a dimensionless number used in fluid dynamics to characterize the natural convection flow of a fluid. It is particularly relevant in situations where buoyancy forces dominate over viscous forces.

The formula for the Grashof number is given by:

$$Gr = \frac{g \cdot \beta \cdot \Delta T \cdot L^3}{\nu^2} \quad \text{Equation 2-2}$$

where:

- g is the acceleration due to gravity,
- β is the coefficient of volume expansion of the fluid,
- ΔT is the temperature difference between the solid surface and the surrounding fluid,
- L is a characteristic length (typically the height of the object or the distance between parallel plates), and
- ν is the kinematic viscosity of the fluid.

The Grashof number is used to predict the onset of natural convection and to assess the relative strength of buoyancy forces compared to viscous forces. The flow is considered to be in the laminar natural convection regime when Gr is less than a critical value (typically around 10^8). For Gr values above this critical value, the flow may transition to turbulent natural convection.

The Grashof number is commonly encountered in problems involving heat transfer, such as in the design of cooling systems, and it helps in predicting the heat transfer characteristics of fluids undergoing natural convection.

3) Prandtl Number (Pr): The Prandtl number is the ratio of momentum diffusivity to thermal diffusivity. It is particularly relevant in atmospheric boundary layer studies where heat transfer is a significant factor. The formula is given by:

$$\text{Pr} = \frac{\nu}{\alpha} \quad \text{Equation 2-3}$$

where:

- ν is the kinematic viscosity of air, and
- α is the thermal diffusivity of air.

The Prandtl number is important in understanding the thermal structure of the atmospheric boundary layer.

4) Richardson Number (Ri): The Richardson number is used to assess the stability of the atmospheric boundary layer. It is the ratio of buoyancy to the effects of wind shear and is defined as:

$$\text{Ri} = \frac{g \cdot \beta \cdot \Delta T \cdot H}{U^2} \quad \text{Equation 2-4}$$

where:

- g is the acceleration due to gravity,
- β is the coefficient of volume expansion,
- ΔT is the temperature difference between the ground and a reference height,

- H is the height of the atmospheric boundary layer, and
- U is the characteristic wind speed.

The Richardson number helps classify atmospheric stability conditions of urban thermal airflow.

5) In thermal fluid dynamics, the Froude number (Fr) is a dimensionless parameter that characterizes the relative importance of inertial forces to buoyancy forces. It is particularly relevant in situations where both fluid motion and thermal effects are significant, such as in natural convection or mixed convection flows.

The general definition of the Froude number in thermal fluid dynamics is similar to its definition in regular fluid dynamics, with the addition of thermal terms. The Froude number in thermal fluid dynamics is expressed as:

$$Fr = \frac{V}{\sqrt{g \cdot L \cdot \beta \cdot \Delta T}} \quad \text{Equation 2-5}$$

where:

- V is the velocity of the fluid,
- g is the acceleration due to gravity,
- L is a characteristic length,
- β is the volumetric thermal expansion coefficient of the fluid, and
- ΔT is the temperature difference between the fluid and its surroundings.

The Froude number in thermal fluid dynamics is used to predict and analyze the behavior of buoyancy-driven flows. It helps to determine whether the flow is dominated by inertial effects or

buoyancy effects. Similar to the non-thermal Froude number, when Fr is less than 1, buoyancy forces dominate, and the flow is considered to be in the buoyancy-dominated regime. Conversely, when Fr is greater than 1, inertial forces dominate, and the flow is in the momentum-dominated regime.

However, most existing wind tunnel studies did not consider thermal buoyancy flow, even though these factors are crucial nowadays, for example, in the study of UHI. Consequently, field measurements have been focused primarily on understanding the real state of the urban environment, particularly UHI issues, while laboratory studies have lagged behind. For wind tunnel tests of urban microclimates, more attention should be paid to the thermal aspect. A limited number of wind tunnel studies have examined the thermal conditions and radiation of urban street canyons. Currently, the only method for analyzing thermal conditions and radiation is to add heat to the building surface.

To investigate thermal conditions by wind tunnel experiment, the similarity should be considered. In most studies in Table 2-3, the Reynolds number and Richardson number are used to determine the similarity, and then wind speed and air temperature are calculated accordingly. Meanwhile, most studies on pedestrian wind comfort neglected thermal buoyancy, so for urban microclimate studies, further research is needed for thermal conditions. As an example, during the summer, thermal buoyancy affects wind speed in the urban center quite a bit, which is something worth investigating further.

Table 2-3 lists the studies that consider the non-isothermal process in the wind tunnel. In most studies, building shape and building height are investigated using a single building or building blocks for generic building types. Due to the complexity of similarity criteria for thermal scaling as well as the difficulty in controlling the temperature of multiple building façades, limited studies

have used the wind tunnel in the applied urban region. Furthermore, the most accepted similarity method for turbulence and thermal conditions is based on the Reynolds number for turbulence and the Richardson number for thermal conditions. The fulfillment of both similarities requires a wind tunnel with a scaling ratio preferably greater than 1:10.

To summarize, wind tunnels have been used to study urban wind flow in an urban region or street canyon for over a century, and most wind tunnel studies focus on urban wind flow, while more attention is needed to address thermal conditions. Moreover, for other studies on thermal stratification and thermal stability, non-isothermal conditions are used with heat sources [50,51]. A variety of measurement equipment was used in the wind tunnel to measure wind velocity, including hot-wire anemometry, hot-film anemometry, Laser-Doppler anemometry, and particle image velocimeter [52], thermocouples [50] or infrared thermal images [53] for temperature measurements, and tracer gas like SF₆ and water vapor tracer [54] for pollutant dispersion measurement.

Table 2-3 Wind tunnel experimental studies on the urban thermal environment.

	Author	Similarity	Parameter	Details
1	Uehara et al. [50]	Re, Ri	WS, AT, TI	Building blocks; Buildings and streets; Air pollution; Atmospheric stability
2	Larsen et al. [55]	/	WS, AT	Single building; Single-sided natural ventilation; Air-change rate; Wind tunnel

3	Zhang et al. [56]	Re, Ri	WS, AT, TI	Single block; Atmospheric boundary layer; Convective boundary layer; Thermal stability
4	Yassin [57]	Re, Ri	WS, AT, TI, PC	Building blocks; Atmospheric diffusion; Dispersion emissions; Thermal stability
5	Allegrini et al. [52]	Re, Fr	WS, AT, TI	Street canyon; Buoyancy; Wind tunnel; PIV; Froude number
6	Zhang et al. [58]	/	WS, AT	Single building; Building energy efficiency Evaporative cooling; Climatic wind tunnel
7	Cui et al. [12]	Gr, Ri, Re	WS, AT	Building blocks; Buoyancy effect; Mixed flow; Pollutant dispersion
8	Allegrini et al. [53]	Re, Fr	WS, AT, TI	Building blocks; Particle image velocimetry; Infrared thermography; Buoyancy; Street canyon
9	Huang et al. [59]	Re, Gr, Ri	WS, AT, TI, PC	Building blocks; Thermal buoyancy effect; Pollutant dispersion; Richardson number

10	Lin et al. [60]	Re, Ri	WS, AT	Building blocks; Flow field; Temperature; Street canyon
----	-----------------	--------	--------	--

Re: Reynold number; Ri: Richardson number; Gr: Grashof number; Fr: Froude number; WS: wind speed; AT: air temperature TI: turbulence intensity, PC: pollutant concentration

Wind tunnels, however, still do not consider other important factors of urban microclimate, including solar radiation, shading, vegetation, and thermal storage of buildings. Although some studies have been conducted on the effects of thermal buoyancy, many wind tunnel studies have only examined air temperature and wind velocity and generic building blocks or single-street canyons. Urban regions with realistic geometries were seldom studied in wind tunnels. This is primarily due to the difficulty of preserving both dynamic and thermal similarities. There is a need for more in-depth research on the limitations of the similarity and/or dimensionless-independence studies and the possibility of maintaining a weak form of different similarities. These new approaches will enable the investigation of the urban microclimate in more realistic conditions by wind tunnel measurements.

2.4 Numerical Approach

2.4.1 CFD simulation

A CFD simulation is often used to study urban microclimates due to its accessibility and flexibility. The Navier-Stokes equations are derived from Newton's second law and are used to determine the airflow governing equations in urban microclimate studies. Fig. 4(a) and 4(b) include the publications for CFD studies with both thermal and isothermal scenarios, considering the neighborhood scale and larger area. CFD studies on a single building block are not included. With different processing methods for turbulence modeling, the Large Eddy Simulation (LES) computational demand is less than that of Direct Numerical Simulation (DNS) but still higher than

Reynolds-Averaged Navier-Stokes (RANS) [61,62]. Due to the high computational costs of LES, CFD simulations were mostly based on RANS, with more than six times more publications than those using LES, as shown in Figure 2.2 (a). As computing power has advanced in recent years, more LES studies have been conducted because LES is widely considered to be more accurate than RANS for urban microclimate simulations [63–65]. In terms of simulation tools (Figure 2.2 (b)), CFD simulations of urban microclimate were dominated by the commercial tool ANSYS FLUENT [66], followed by ENVI-met [67], and OpenFOAM [68]. These three tools accounted for more than 90% of all simulations.

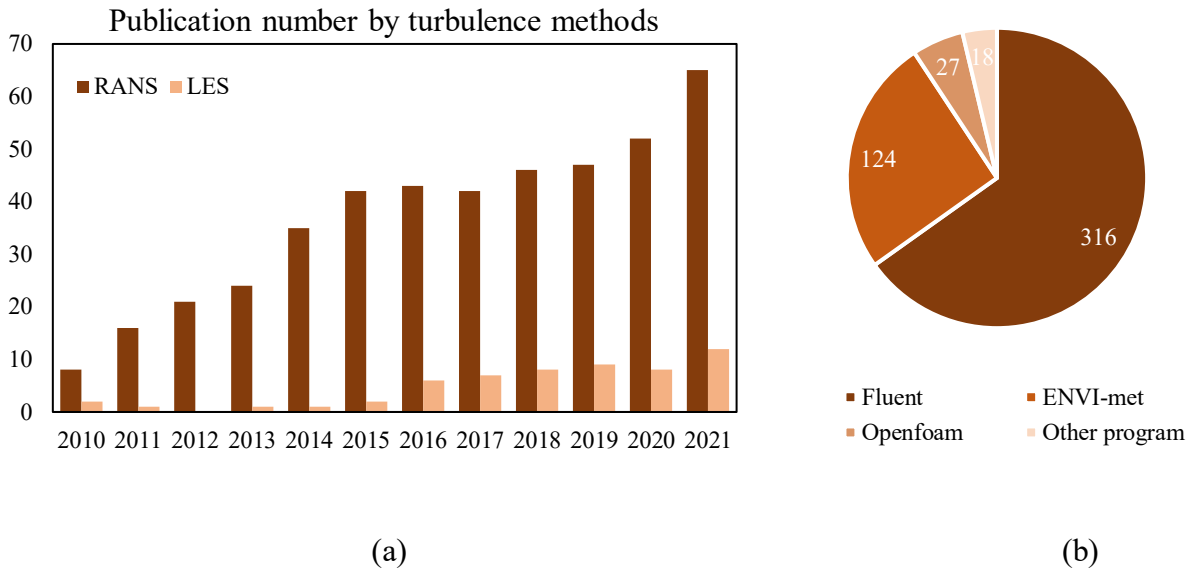


Figure 2.2 (a) Number of studies by turbulence models (b) Number of studies by simulation tools.

A few studies have applied Urban Weather Generator (UWG) to consider the urban microclimate [69–71], and researchers have utilized it to analyze its impact on building energy consumption [69]. A few researchers also implemented the PALM-4U model to evaluate the urban microclimate and urban heat island covering multiple parameters by microscale simulation [70–72]. Researchers also implement the CFD approach with building energy consumption (BES) to investigate the

impact on building energy performance [13,73]. Several studies have adopted the coupling simulation method by combining CFD and Building energy simulation (BES) [74–76] for implementing detailed building information into CFD simulation. Coupled simulations have enabled cross-scale investigations both on timescales and length scales. Simulating outdoor-oriented problems requires using larger scales like WRF [77] or SOLENE [78] or providing detailed boundary conditions that include solar radiation, building surface temperature, or wind in urban environment simulation, or obtaining information about building façade from building energy simulations (such as EnergyPlus [79] or TRNSYS [80]). For indoor-oriented issues, the coupling methods implement outdoor ambient weather conditions from CFD for building energy simulation, as well as air temperature, wind pressure, or heat transfer coefficients for calculating energy consumption [75]. The coupling methods allow local spatial data as detailed boundary conditions for pressure-driven or buoyancy-driven natural ventilation. There are, however, limited validation studies for most coupling methods. More validation and calibration studies are required. For coupling methods that include the radiation effect, most studies ignore longwave radiation between building surfaces.

A summary of the 3D studies of actual urban regions with thermal effects is shown in Table 2-4. Table 2-4 lists the publications on urban simulations with validations of winds and temperature. The majority of the studies (seven out of ten) cover an area of less than 1 km² with a grid resolution from 0.15 m (Brozovsky et al. [81]) to 30 m (Fintikakis et al. [82]). The predictions of temperatures seem more accurate than those of wind speeds: the surface temperature predictions with an error of 0.1 °C ~ 2.5 °C and air temperature error of 0.1 °C ~ 1.35 °C (2.5% ~ 9.3%) compared with the wind speed error of 17.3% ~ 38.8%.

Table 2-4 CFD simulation and validation studies for the outdoor urban thermal environment in actual regions.

Author	Location	Size	Model	Validation error	Tool	Mesh size
Fintikakis et al. [82]	Tirana	2.4 km ²	Steady RANS	Maximum error: Surface temperature:0.4 °C Air temperature: 0.3 °C	PHOENICS	3 m
Shahidan et al. [83]	Persiaran Perdana	1.7 km ²	Steady RANS	Average error: Air temperature 0.1 to 0.8 °C Surface temperature 0.1 to 2.5 °C	Envi-met	20 m
Antoniou et al. [40]	Nicosia	0.247 km ²	Unsteady RANS	RMSE: Wind speed: 0.57 m/s air temperature: 1.35 °C	FLUENT	0.3 m
Toparlar et al. [84]	Rotterdam	1.13 km ²	Unsteady RANS	Average deviation: Surface temperature 7.9%	FLUENT	0.5 m
Yang et al. [85]	Guangzhou	0.05 km ²	Unsteady RANS	MAE: Air temperature: 0.84 to 1.01 °C Surface temperature: 1.98 °C	Envi-met	0.5 m
Ma et al [86]	Shenzhen	0.38 km ²	RANS	MAE: Wind speed: 0.3 m/s Air temperature:0.5	In-house code	N/A
Brozovsky et al. [81]	Trondheim	0.48 km ²	Steady RANS	NRMSE: Wind speed: 17.3% to 38.8% Air temperature: 2.5% to 6 %	FLUENT	0.15 m
Brozovsky et al. [87]	Trondheim	0.16 km ²	Steady RANS	NRMSE: Wind speed:27% Air temperature: 9.3% Relative humidity:7.7%	ENVI-met	3 m
Berardi and Wang. [88]	Toronto	0.42 km ²	Unsteady RANS	MAE: Air temperature: 1.3 degree	Envi-met	0.5 m
Tominaga et al. [89]	Hadano city	0.25 km ²	Steady RANS	Not quantified	FLUENT	0.6 m
Mohammad et al. [90]	Montreal	4 km ²	LES	RMSE: temperature: 0.6 °C RMSE: wind velocity 0.265 m/s	CityFFD	2 m

Figure 2.3(a) reports the simulation errors of the papers reviewed, including the cases of outdoor air temperatures and both actual urban regions and generic building blocks. The bar shows the

average values of the dots, which is the specific value from each study. Simulation studies using ANSYS FLUENT are generally more accurate than simulation studies using other tools, such as ENVI-met, for applied urban regions. In comparison to wind speeds and surface temperatures, including building façade temperatures and ground temperatures, air temperature predictions seem more accurate. It appears that surface temperatures are the most difficult to predict, probably because of the simulation limitations: it is common to neglect solar radiation, shading, and longwave radiation from hot surfaces when predicting surface temperatures. In the summer, these factors can have a significant impact on outdoor thermal stress as well as building energy consumption, especially during the daytime. Figure 2.3(b) shows the annual number of studies with the bubble size for the numerical simulation domain size of an investigation. Due to limited geometry information from the reviewed publications, the comparison is only presented with ENVI-met and FLUENT. Both ENVI-met and FLUENT can be used on an urban scale or building scale. However, FLUENT is required to provide more detail and a larger number of grids than ENVI-met. Both ENVI-met and FLUENT can handle large urban areas of up to 4 km² in size.

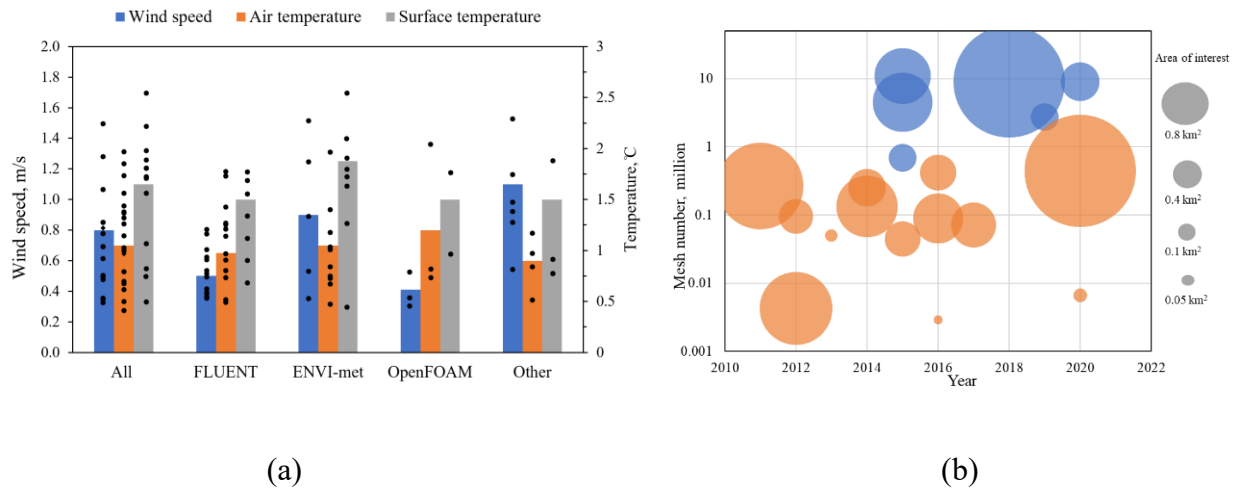


Figure 2.3 (a) Simulation error of wind speed (left axis) and temperature (right axis) by different tools (b) the investigation size for applied urban region cases, ENVI-met (orange), FLUENT (blue).

In summary, CFD simulations are versatile and can be applied to many different applications. Based on the literature, the error for simulations could be around 0.5 m/s for wind speed and ~ 1 °C for temperature. When it is applied to urban region simulation, FLUENT requires at least 1 million meshes, and in large cases, it can reach 10 million meshes, requiring more computing power than ENVI-met.

2.4.2 Data-driven models

The rapid development of machine learning and data science technologies in the 2010s led to new methods for studying urban microclimates using data-driven models. When this review was conducted, limited data-driven studies were found on the interaction between microclimate and the built environment. Data-driven methods and the so-called artificial intelligence approach have been developed for a long time [91]. However, the current computing power could not handle high-dimensional data and complex artificial neural networks. Increasing computational power and data memory is therefore important. As a result of the advancement of data sciences, urban microclimate models and methods will become more efficient. One of the first applications dates back to 2016 [92] to category the climate zones with various landscape features, and the number of applications increased in the following years. For data-driven models applied to urban physics topics, four data sources are available: historical weather station records, field measurements, wind tunnel measurements, and CFD simulations. It is common to use the coefficient of determination (R^2) to evaluate the performance of machine learning models [93–95]. Figure 2.4 shows the parameters investigated previously by data-driven models and the reported training performance

of different models. Most current work focuses on predicting wind speed, temperature, and building energy consumption. Artificial intelligence models were applied based on the parameters of interest, including multiple linear regression (MLR) [93][96], nonlinear regression (NLR) [97][96], random forest (RF) [93][96], and artificial neural networks (ANN) [95,98]. Based on the reviewed articles, the ANN is the most widely used model due to its superior performance for multiple inputs. The coefficient of determination (R^2) in the reviewed articles is around 0.8-0.9, which indicates high prediction accuracy.

For predicting wind speed and power, Mortezaazadeh et al. [99] adopted the machine learning method with CFD simulation results to assess the wind power potential in an urban region. According to a recent study by Alonso [93], multiple machine-learning models were developed to investigate the relationship between air temperature and different factors (vegetation, sky view factors, the density of water bodies, buildings, moisture, radiation, etc.), and the results showed satisfactory results. The performance of this model still needs further confirmation due to the lack of long-term and multi-location testing data. Recently, a recurrent neural network was applied to model the variation in time-series temperature under the urban street canyon. Zhang et al. [94] implement the long short-term memory (LSTM) model to forecast the wind speed, wind direction, relative humidity, and solar radiation. Then, the study applied the predicted weather parameters for building energy estimation. This method shows more reliable energy estimation than when using Typical Meteorological Year (TMY) weather data.

As for the analysis of the urban surface temperature as well as surface heat island, Yao et al. [100] developed a machine-learning method for monitoring land surface temperature through downscaling satellite thermal images. A spatial resolution of 30 m can be obtained by downscaling measurements from 100 meters to 30 meters. The proposed method performs well under specific

conditions, and it is not affected by rain and clouds. As a result of limited validation data and sites, how the approach performs in other regions is unknown.

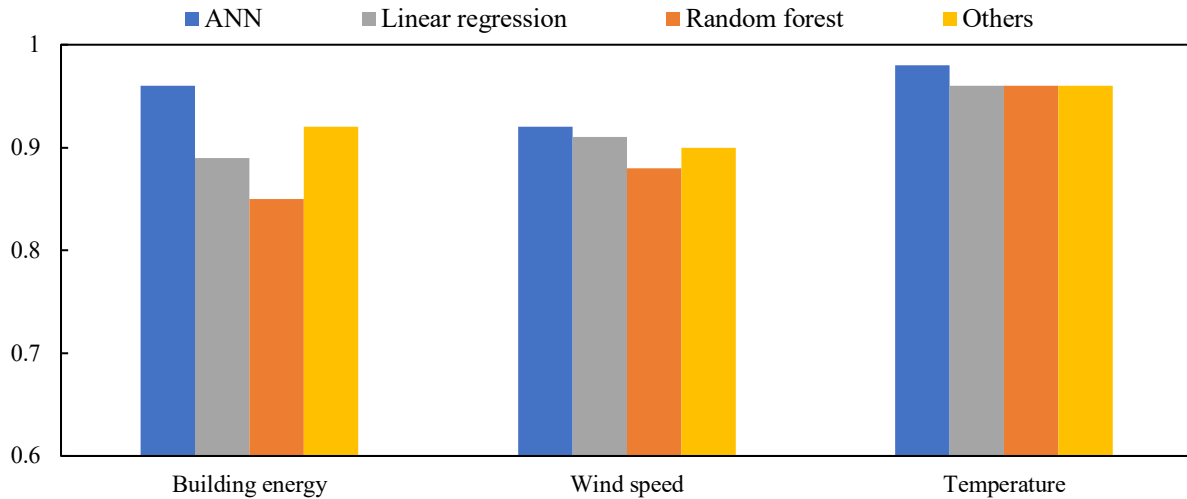


Figure 2.4 Averaged coefficients of determination (R^2) reported in the publications by predicted outputs and by simulation models.

In general, data-driven or machine-learning methods for urban microclimate applications are still in the early stages of development, and there are no general guidelines and criteria for applying them yet. In order to develop data-driven models for urban microclimates, it is still unclear how much data and how many parameters should be included. The existing studies used a variety of models for predictions, but most models used in the studies were tailored to a specific situation, and the robustness of the trained model was not validated. Additionally, other machine learning models are less explored and applied to the microclimate of cities, such as Recurrent Neural Networks (RNNs), such as Long Short-Term Memory (LSTM), and Transformers.

2.5 Urban Microclimate: Current Practical Issues

There are four main categories of topics related to urban microclimate: urban wind environment (neutral wind condition neglecting thermal buoyancy), urban thermal environment, building energy consumption, and pollutant dispersion. According to Figure 2.5, the number of research articles on urban microclimate topics has increased from 2010 to 2020. The majority of research studies consider isothermal conditions as the basis for urban wind comfort, pedestrian wind comfort, and wind-driven rain. A major topic in urban microclimate is the study of urban thermal comfort and urban heat islands. Additionally, there are several studies investigating how the urban microclimate affects the increase in building energy consumption and the dispersal of pollutants. Several factors are discussed and examined in order to determine their relationship with the urban microclimate, including:

- Ambient conditions: air temperature, surface temperature, moisture, wind speed, radiation.
- Urban configurations: building arrangement, building heights, sky view factor, floor-area ratio, building coverage ratio, building heights, etc.
- Vegetation: trees, parks, etc.
- Water bodies: lakes, rivers, seas, etc.
- Other properties: soil properties, building properties.

This section focuses on each of these practical issues and discusses the associated design factors in Section 2.

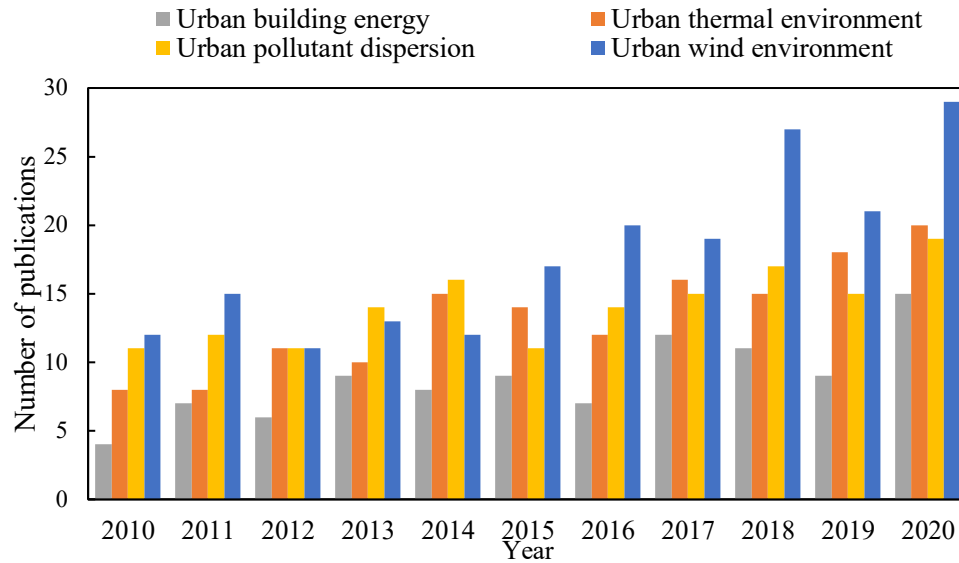


Figure 2.5 Studies related to urban microclimate classified by different issues.

2.5.1 Urban wind environment

This section focuses on the neutral wind environment inside urban regions, where the airflow is dominated by the wind, so the thermal buoyancy effects are usually neglected. Figure 2.6 gives the distribution of investigation topics and approaches. Most studies used CFD simulations.

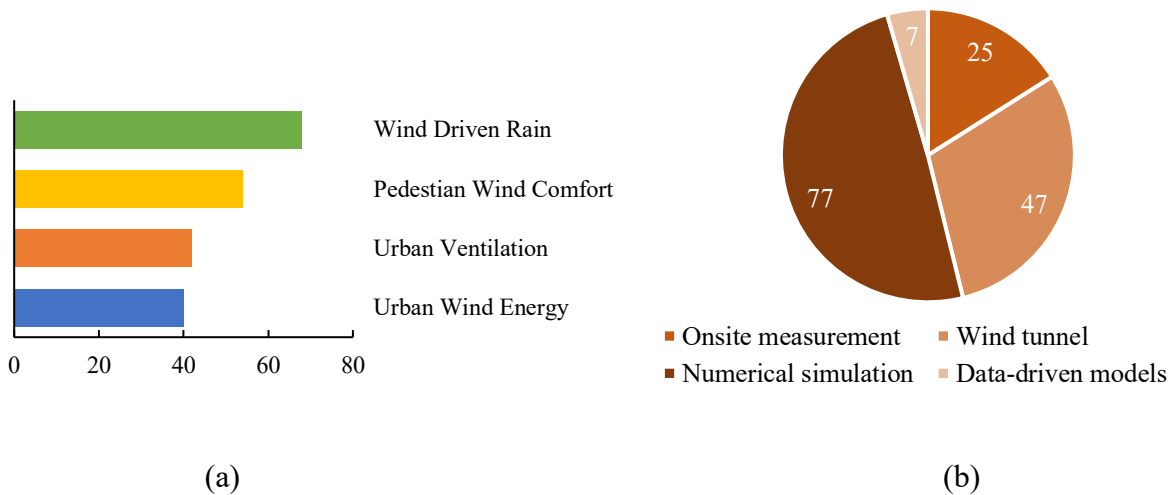


Figure 2.6 (a) Number of studies by topics (b) Techniques adopted for urban wind studies.

Among the factors that influence urban wind, urban configuration and shapes are considered in most studies. Abohela et al. [101] found that a roof-mounted wind turbine with a taller building has a higher potential for generating energy than one mounted on top of a low-rise building. Based on numerical simulation, Abohela et al. [101] optimized wind turbine installation locations on a roof based on the impact of roof shape on performance. Wind flow around a building is also influenced by surrounding buildings, as shown by Liu et al. [102]. It was determined that to obtain sufficiently accurate wind flow and pressure distributions around a building, a region within a $3L$ radius of the building should be simulated with detailed building structures. CFD simulation was used by Iqbal and Chan [103] to investigate pedestrian wind comfort under high-rise buildings of different shapes. Janssen et al. [104] Also, different wind comfort criteria were compared by conducting the CFD simulation to assess pedestrian wind comfort around buildings and the significance of standardizing the procedure for evaluating wind comfort. Wind-driven rain, which is defined as rain load subject to the horizontal velocity component of wind, was also investigated under the impact of urban microclimate [100, 101].

The urban wind environment can also be affected by vegetation or trees. Yuan et al. [107] developed a semi-empirical model for the effect of trees on the urban wind environment. In place of costly fluid mechanics calculations, the semi-empirical model was developed by Yuan et al. [107] to calculate indices of urban density and tree geometry. A practical alternative to CFD simulation and wind tunnel experiments, empirical models provide direct modeling results that can guide the planning process and design process. A study by Giometo et al. [108] examines the effect of trees on wind, turbulence, and momentum exchange in and above urban areas. It was found that the total drag caused by all vegetation elements during the summer season exceeded the drag caused by buildings. Kang et al. [109] simulate pedestrian wind comfort based on tree effects in

an urban area. Based on the results of the study, trees planted 90° to the dominant wind direction decreased wind speeds by more than 50% near the tree.

In summary, the urban wind environment has been focusing on the effects of building configuration, building shape, and building aspect ratio in the recent decade. As trees and parks have been found to have a huge impact on nearby wind comfort in recent years, their impact has become an essential topic. The impact of vegetation terrains like city parks and their distance to the building need to be further assessed.

2.5.2 Urban thermal environment

The publication numbers on urban thermal environment, landscape, and building design parameters are categorized in Figure 2.7(a), and the research methods are shown in Figure 2.7(b). Building configurations and vegetation were mostly investigated, whereas limited research was on water bodies on an urban scale. Most researchers relied on numerical simulations by CFD, and the application of data-driven models was limited but emerged with six studies recently.

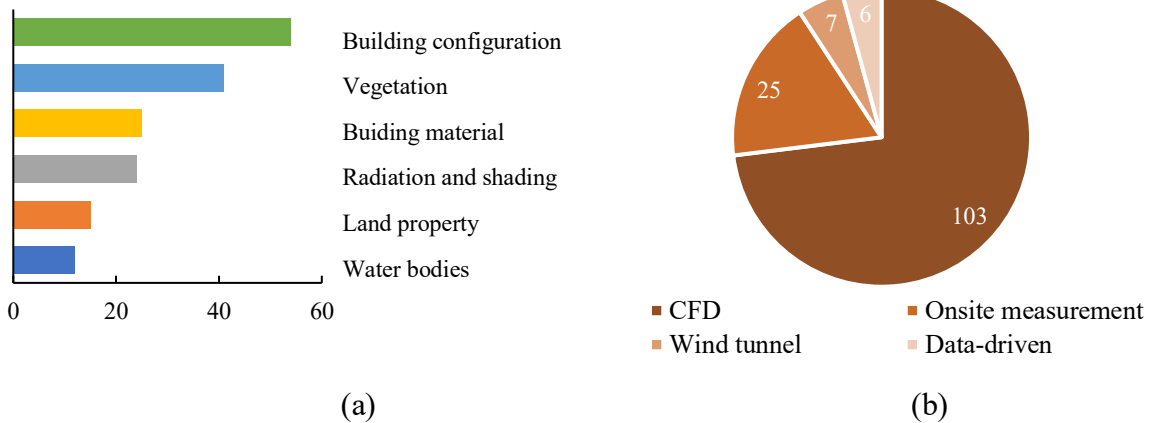


Figure 2.7 (a) Publication numbers on the landscape and building design parameters (b) Number of studies classified by investigation methods.

To evaluate the urban thermal environment, researchers adopted different thermal indices. The physiological equivalent temperature (PET) is based on the Munich Energy-balance Model for Individuals (MEMI) for modeling the thermal comfort conditions of the human body in a physiologically relevant method [110]. The equation is shown as follows with the unit of W:

$$M + W + R + C + ED + Ere + Esw + S = 0 \quad \text{Equation 2-6}$$

The PET is calculated by taking into account metabolic activity (M), physical work output (W), body net radiation (R), convective heat flow (C), latent heat flow for the skin (ED), heat flow to heat and humidify the inspired air (Ere), evaporative heat flow (Esw) and storage heat flow (S) for the body mass.

Meanwhile, UTCI (Universal Thermal Climate Index) [111] is the air temperature (T_a) of the reference weather conditions that cause the same model response as actual thermal comfort conditions [112]. It can be defined as:

$$UTCI(T_a, T_{mr}, V_a, pa) = T_a + OFFSET(T_a, T_{mr}, V_a, pa) \quad \text{Equation 2-7}$$

Where T_a is air temperature ($^{\circ}\text{C}$), T_{mr} is the mean radiant temperature ($^{\circ}\text{C}$), V_a is wind speed (m/s), pa is water vapor pressure (hPa). The UTCI is a climatic thermal comfort index considering the impact of weather conditions without the effect on the human body, which is suitable for representing urban microclimate.

Using a seven-point thermal sensation scale, the PMV is designed to predict the average vote value of a group of occupants during indoor conditions. As a result of its determination to describe human sensations instead of ambient climate conditions, the PMV is a commonly used thermal

index. Another commonly used thermal index is the Standard Equivalent temperature (SET*). It is also expressed in terms of air temperature in the hypothetical environment with a relative humidity of 50%, an air speed of less than 0.1 m/s, and $T_a = T_{mr}$. In addition, the humidity index (Humidex) is an index used in Canada to describe outdoor thermal comfort by combining temperature and humidity. For evaluating the impact of urban microclimates on outdoor thermal comfort, the UTCI is found to be the most commonly used and the most appropriate index.

Urban heat island (UHI) is another phenomenon related to the urban thermal environment characteristic to describe the urban microclimate. It is possible to influence the intensity of urban heat islands by a variety of factors, including building and land properties, including thermal inertia of the built area, radiative properties of urban surfaces, urban morphology and aerodynamic, resistance to impervious and vegetation surfaces [17,113–115] density and size of the city [116,117], and anthropogenic heat generated by industrial activities [118]. UHI can be classified into four types based on the vertical layers used to calculate it - the subsurface/soil UHI, the surface UHI, the canopy layer UHI, and the boundary layer UHI [119,120]. As a result of their prevalence in areas closest to human activity, surface and canopy UHIs have been the most extensively investigated [120].

Two UHI calculation methods were developed by pioneer researchers. In the first method, the UHI is calculated as the temperature difference between urban areas and surrounding rural areas. The urban area is defined as grids dominated by urban land cover types in the city, and the rural area with less constructed regions constructed area surrounding the urban region like a ring, so this method is named the “rural-ring” (RR) method [121,122]. Some researchers [115,123,124] mentioned that the rural area should be at least 2 km away from the urban to eliminate the local effect and be within 10 to 30 km distance to avoid uncertainties from father geospatial areas.

According to the other method, called "urban-increment", the UHI is determined by calculating the temperature difference over urban areas based on two sets of simulations: one where urban land cover is left unchanged and one where cropland replaces urban land cover. The "urban-increment" (UI) method quantifies the impact of urbanization on the local climate by comparing assumed and realistic land cover conditions before and after urbanization [125]. In this section, the impact of different factors on the urban thermal environment and urban heat islands will be discussed.

Underlying surface

In terms of urban thermal climate, the temperature of the underlying surfaces is crucial. In Table 2-5, a satellite thermal imaging analysis of 419 cities in 2010 shows the surface urban heat island intensity (SUHII), which represents the temporal temperature difference between urban and LCZ6 areas. Table 2-5 presents the average temperature difference value (SUHII) for daytime and nighttime. All the reported locations were reported with the surface urban heat island effects during the summer daytime, with an average temperature between 1 and 3 °C, which is higher than in winter. Among all the cities, European and American cities have more surface urban heat island intensity, which means the central city land and surface temperature is higher than that of the rural area. A surface urban heat island occurs every year, and the highest value is during the summer daytime due to solar radiation. According to the global average, the surface temperature of urban areas is one to two degrees higher than the surface temperature of rural areas.

Table 2-5 Average SUHII (°C) in 419 cities around the world [126] by daytime and nighttime.

		Africa	Asia	Europe	North America	South America	Oceania	World
--	--	---------------	-------------	---------------	----------------------	----------------------	----------------	--------------

Annual	Daytime	0.9	1.2	2	2.3	2.4	1.5	1.2
	Nighttime	0.9	1.1	0.8	0.9	1.1	1	1.1
Summer	Daytime	1	1.5	2.1	2.5	3	2.3	1.9
	Nighttime	0.7	1	1	1	1.3	1.3	1
Winter	Daytime	0.8	0.9	1.7	2.2	1.7	0.8	1.1
	Nighttime	1.1	1.2	0.4	0.9	0.9	0.8	1

Meanwhile, another statistical study [127], which focuses on the air temperature difference between the city center and rural area (Urban heat island intensity: UHII), investigates the urban heat island in 101 Asian and Australian cities and regions, demonstrating that the magnitude of the UHI has fluctuated between 0.4 °C and 11 °C. There is a 4° C average intensity across all studies and a 2.3 °C standard deviation. About 23% of studies had UHIs below 2 °C, while 58% had UHIs below 4 °C. In almost 27% of studies, the UHI intensity exceeded 5 °C. A clear relationship has not yet been quantitatively established between surface urban islands (or land surface temperatures) and urban heat islands (air temperatures). The land surface temperature was found to affect the thermal stresses of pedestrians, together with the air temperature.

In another recent study, Yao et al. [100] also developed a new machine-learning method to monitor the land surface temperature by the satellite thermal image, to examine the urban heat island for a city. This study indicates a good direction for investigating the relationship between land surface temperatures and air temperatures based on downscaling measurements from 100 m to 30 m. Due to the lack of validation, the downscaling method needs to be further investigated or improved.

Building configurations

Many researchers have focused on the urban heat island effect, and building configuration has an important role to play in the urban thermal environment. Dimoudi et al. [128] examined the microclimate parameters of an urban center. In dense urban environments, natural and night ventilation is restricted because of the severe reduction of wind speed in urban canyons. Thus, the city's blocks are not adequately ventilated. A lack of natural ventilation contributes to problems like elevated ambient air temperatures, urban heat island effects, and poor air quality in urban areas. Dimoudi et al. [128] also found that in the city of Serres, the air temperature during the afternoon and night was about 5.0–5.5 °C higher than in the LCZ6 area. In the morning, the air temperature in the city is 7.0 °C lower than in LCZ6 areas due to the thermal storage of buildings at night. Their findings on negative UHI in the morning need further confirmation. Peron et al. [129] show that during the summer, the temperature difference between urban areas with high-density buildings and LCZ6 areas is usually greater than 4 °C, and sometimes greater than 7 °C. The UHI documented in a tropical city in Muar was 4 °C during the day and 3.2 °C at night, according to Rajagopalan et al. [130], which studied wind flow characteristics and their impacts on urban heat islands. This study showed that Muar's random building configuration reduced ventilation in urban canyons. As a result of tall buildings and narrow streets enclosing heat and reducing airflow, high temperatures occur. In a typical tropical coastal city, Ndetto and Matzarakis [131] analyzed the effects of urban configuration on thermal conditions. Based on the simulations, the studies found that building configurations and elevations have a significant impact on pedestrian comfort and that open spaces such as parks can help to reduce thermal stress.

Therefore, according to studies on building configurations, dense buildings may reduce incoming airflow and thereby worsen urban ventilation. As a result, buildings absorb more solar radiation

and store more heat, which increases the surface temperature. In the urban street canyon, high-density buildings can cause the air temperature to rise from 3 to 7 °C. Few studies have been conducted on the longwave radiation emitted from building surfaces despite its significant impact on pedestrian thermal sensation.

Vegetations and canopies

It has been suggested that vegetation plays an important role in the urban thermal environment as well. Klok et al. [41] reported that during the heatwave in July 2006, due to the difference of underlayer, the average surface temperature difference between the warmest and coolest districts was 12 °C maximum during the daytime and 9 °C at night. Districts that experienced a significant difference in temperature between night and day also differed in terms of their nighttime surface heat island (SHI) and daytime SHI. The difference in SHI will also contribute to spatial differences for UHI. Priya and Senthil [25] found that vegetation in tropical urban areas reduces the air temperature by up to 12 °C. For a variety of tree species, Souch and Souch [132] found that in the early afternoon, the maximum air temperature under the canopies of individual trees and clumps of trees decreased by 0.7–1.3 °C. A subtropical park's air temperature below the tree canopy at midday was 0.64 to 2.52 °C lower than in the open. As a way to mitigate the urban heat island impact on the street canyon, Aboelata et al. [133] examined the vegetation for different street orientations. In order to reduce air temperature and enhance thermal performance, the streets canyon should have 70% grass and 50% trees. Due to the weak influence of vegetation, the air temperature was reduced by 2–3 degrees by the trees, and the buildings' energy demand was reduced by 2% – 5% as a result. It has been demonstrated by Salata et al. [20] that vegetation can have an important impact on the environment, and the widespread use of those plants can affect

the direction and speed of the wind. In the summertime, Salata et al. suggested that vegetation with less foliage density, such as palm trees, should be chosen for better wind-cooling effects.

According to the studies mentioned above, urban vegetation reduces the ambient temperature of the urban thermal environment. This can still alleviate thermal stress in urban areas due to transpiration and less absorption of solar radiation. Vegetation may perform in a wide range of ways, lowering ambient temperatures from about 1 °C to 7 °C, with the reduction impact being greater in the summer than in the winter. Further research is needed to determine how these mitigation levels can be quantified in each region.

Building properties

An urban area's thermal conditions can also be affected by its building properties. In their study, Li and Norford [134] showed that cool roofs could reduce surface and near-surface temperatures during the daytime (especially at noon), but they do not have a negligible effect at night. However, when UHI intensity is high at night, the deployment of greenery can reduce the near-surface air temperature by more than 1 °C compared with the concrete underlayer. A field measurement and numerical simulation are used by Battista et al. [37] to examine how different constructions affected the July 2014 summer heatwave in Rome. As a result of the newly developed configuration, the air temperature in the area increases by 3.5 °C during the daytime, and the maximum UTCI index increases by 2.7 °C. With five different configurations, Salata et al. [20] conducted simulations and experiments to calibrate their model. They found that high albedo materials can reduce the thermal load on buildings while increasing the thermal stress on pedestrians. Mughai et al. [135] conducted a CFD simulation to determine the impact of urban parks on air temperatures and thermal comfort. An incoming wind speed of 2.3 m/s results in a

cooling intensity of 1 °C within a region of 27 m from the park, which reduces to 0.6 °C at 117 m from the park. The thermal comfort index (UTCI) also indicates a reduction in and around the park.

Due to the thermal storage of buildings and urbanized regions, during heat waves, urban heat islands can be intensified and make outdoor thermal comfort more vulnerable. Through numerical simulation, during a heatwave, Ramamurthy et al. [136] analyzed the UHI in New York City increased by more than 1.5 °C, compared with the UHI under no heatwave. Li and Bou-Zeid [137] reported a similar phenomenon by observation and numerical simulation by analyzing the heatwave in 2008. The intensified UHI during the heatwave in the summertime was also found in other large cities [138–141].

As part of their study, Dimoudi et al. [142] examine the material of roads as a means of mitigating urban heat islands by measuring the reflectivity and emittance of the surfaces. A discussion of mitigation strategies is provided by comparing the different thermal properties of land to the CFD simulations. However, due to a lack of validation results, the mitigation demonstrates a trend of improvement.

It is thus concluded that the thermal environment is affected by a number of factors, and wind, temperature, solar radiation, and longwave radiation can be affected in both spatial and temporal aspects by the landscape and building design. Observation and demonstration are the most common types of studies of urban thermal environments, but few researchers have studied the complex and fundamental physics of urban microclimates and the interactions of the associated parameters. Meanwhile, due to different building configurations, geometry, and properties for every city and community in the applied urban region, the conclusion of a specific location may not be valid elsewhere. Future studies require a generalized model that connects building materials and thermal storage to all ambient conditions when analyzing outdoor thermal conditions.

2.5.3 Building energy consumption

The study on building energy consumption has increased in urban microclimates from 2010 to 2020. To analyze building energy consumption, numerical simulation is used the most. It is common to use CFD and BES to investigate how outdoor urban environments influence indoor building energy consumption. Meanwhile, solar radiation is crucial for evaluating building energy consumption in urban regions. A number of models have been developed to quantify radiation flux on buildings: DART [143], SOLENE [78], and SOLWEIG [144], and the models calculate the mean radiation temperature for analyzing outdoor thermal conditions. Several other tools, such as FLUENT [66] and ENVI-met [33], compute the energy and mass conservation equations taking ambient heat and solar radiation into account.

Through the use of BES (building energy simulation), Allegrini et al. [75] demonstrate the importance of urban microclimates in the street canyon to building energy consumption. Based on the information from street canyon airflow, the model was improved with a radiation model and convective heat transfer correlation. By using this numerical method, Allegrini et al. [75] examined the urban microclimate impact by combining BES with the heat transfer coefficient correlated with previous CFD results, and the authors suggested that directly coupling CFD and BES at each time step would yield better estimates. They [62] proposed a simplified coupled method to CFD and BES to improve the predicted space cooling and space heating demand of buildings by BES and the prediction of the local microclimate in an urban area, in which temperature and convective heat transfer act as an agent between the two. Since CFD simulations are much more expensive than BES simulations, it is important to minimize CFD simulations in coupling procedures. Using a coupling model, Dorer et al. [145] found that solar and longwave radiation effects had the greatest effect, followed by UHI effects and convection heat exchange between the canyon walls and the

free-stream shear layer. In order to model climate in large urban areas, a multi-scale method is proposed, which includes models at the meteorological mesoscale through microscale models of radiative and convective exchange, as well as links between the individual building and ground surface elements in the simulation of building and urban energy usages. The meteorological measurements were conducted in Belgium in July 2013 by Toparlar et al. [146]. On average, air temperatures at urban sites away from and close to the park are 3.3 °C and 2.4 °C higher, respectively, than those in the rural area, resulting in an additional cooling demand of up to 90% monthly.

Moreover, building energy consumption in urban areas can also be affected by vegetation or local greenery. Using the coupling simulation, Malys et al. [147] developed a hydrothermal model to assess the impact of green walls on urban microclimate and building energy consumption. Based on their prototype cases, they found that incident sunlight on the substrate is divided almost equally between evaporation from the surface and storage at the location, followed by the transmission to the wall. When compared with the convective flux between vegetation cover and the outside air, the heat exchanged with plant cover remains rather limited.

Urban microclimate is also important for building energy performance of cross-ventilation potentials. Ding and Lam [97] developed a method coupled with CFD for indoor and outdoor use to evaluate the cross-ventilation potential and implement a machine-learning method for prediction. And it has also been proven that cross-ventilation can be affected by the surrounding environment from multiple researchers [148–150]. However, cross-ventilation with thermal buoyancy and building energy impacts still requires more research.

In general, many studies have found that the urban microclimate is important to building energy consumption and that the urban heat island can increase building cooling demand in the summer.

As part of the evaluation of building energy consumption in urban street canyons, it was also stressed that CFD and BES must be coupled. However, due to the lack of on-site temporal monitoring of building energy consumption, only a few studies focus on the validation of the coupling simulation models, and their accuracy has not yet been confirmed. During heatwaves, excessive urban energy consumption deteriorates the urban thermal environment, according to a limited number of studies. As air conditioning units for dense building areas add extra heat sources in the street canyons, it is important to monitor and research how these systems affect the ambient temperature in the street canyons.

2.5.4 Urban pollutant dispersion

Dispersion of urban pollutants, as well as transportation, which takes into account wind and thermal conditions, are also important topics for urban microclimates. The publications have been increasing since 2010. In most urban pollution dispersion studies, building configurations and urban ventilation from different weather conditions are examined. In most studies, CFD simulation [151–154] is used on pollutant dispersion, compared with field measurements or wind tunnel experiments [155].

In order to understand urban pollutant dispersion, most researchers examined pollutants by CFD simulations or wind tunnel experiments with the thermal buoyancy effect neglected from the urban street canyon. Wind speed and building configuration are the most important factors. Using wind speed, wind direction, and building configurations as parameters, Soulhac et al. [156] developed a parametric law for defining urban pollutant dispersion. The prediction model was compared with a wind tunnel experiment conducted in an idealized urban district. Carpentieri et al. [157] measured vertical concentration flux in the wind tunnel. In their study, turbulent exchange increased at the roof level at intersections, confirming its importance in the exchange between canopy and external

flow. As part of their study, Yuan et al. [158] studied the interaction between air pollution dispersion and urban morphologies using CFD simulations and wind tunnel simulations. According to the research, building configuration has an important role to play, and pollutants pose a significant risk in deep street canyons. Since no field monitoring methods exist for urban pollution dispersal, most validation works rely on wind tunnel measurements. For urban pollutants to be dispersed effectively, more applied urban region monitoring is necessary.

Limited studies examined the thermal effect of pollutant dispersion, which could have an important impact under low wind conditions. Sini et al. [159] found that differential heating of building surfaces can affect the transport and exchange of pollutants, which is also confirmed by Ai et al. [27]. During summertime, thermal buoyancy becomes significant, especially under low-wind conditions. Therefore, more research is needed on the role of thermal buoyancy on urban pollutant dispersion.

2.6 Summary

The literature review found that field measurement is always the most direct method for exploring the urban microclimate from a physical perspective. However, the techniques applied still lack the ability to capture all the essential parameters necessary to evaluate urban microclimate. Quantification of the thermal storage performance of buildings and soil is still a work in progress. When field measurements are not feasible, many researchers seek solutions through wind tunnels. The majority of wind tunnel studies are isothermal scenarios; however, a few have considered the thermal impact of a subscale wind tunnel. For sub-scaling, similarity criteria for wind tunnels based on Re , Ri , and Fr are inconsistent. The similarity criteria between the applied urban region and the sub-scale urban region must be considered. Furthermore, it is necessary to consider the distribution of temperature across various surfaces because the shading effect, as well as thermal

properties, have an impact on building surface temperatures. Additionally, a real microclimate is influenced by a variety of factors, such as radiation, shading, terrain, trees, etc., which must be investigated in a wind tunnel. Over the past few decades, many new models and methods have emerged, and many of these models are capable of providing accurate predictions.

For numerical simulation, CFD is often a versatile method for urban microclimate applications. Compared with wind tunnel and field measurement, CFD can generate detailed 3D flow fields and has been applied the most in the past [160][161]. As a result of the detailed boundary conditions from measurement, accurate results, including wind, thermal, and radiation, were required for the CFD, as was a detailed building model for the large applied urban area. There is still a need for investigation of the boundary conditions for the city's thermal storage system. CFD performance can be limited by the difficulty of acquiring complex boundary conditions and implementing them internally. When it comes to the application of data-driven models or artificial intelligence to urban microclimates, there are no guidelines or comprehensive studies on the procedure or criteria. Meanwhile, model training requires a large range of datasets, either from field measurement, wind tunnel measurement, or CFD simulation, making it challenging to estimate urban microclimates. Nevertheless, existing artificial intelligence models will face a problem when they expand from a traditional geometry to a new geometry. Data science and computer science are expected to develop more artificial intelligence models in the future, leading to an increase in their applications to urban microclimates. The combination of CFD simulations and data-driven models is a potential direction for urban microclimate studies due to the expense of collecting on-site or wind tunnel measurement data.

According to the literature review, many factors play a significant role in urban microclimates, such as building configuration, wind, solar radiation, and vegetation. As a result of the review, it

is clear that there are limitations either due to a lack of investigation or a lack of method development. Most of these factors are studied individually, but there are no studies that include all impactors for parametric analysis. The thermal storage of an entire city is essential to a sustainable urban thermal environment, and it contributes to an urban heat island, according to many studies. It has not yet been explored how to define and quantify urban thermal storage and how it relates to urban configurations. In some studies, urban heat islands were defined as surface urban heat islands based on the differences in surface temperatures between rural areas and urban centers derived from satellite images. Although it is a worthwhile endeavor to determine the thermal storage of underlying surfaces, the impact of surface urban heat islands must also be investigated. It is unknown exactly how much surface urban heat islands will contribute to urban heat islands.

As far as microclimate and building energy consumption are concerned, many studies have shown that urban heat islands increase cooling demand during the summer because of urban heat islands. Limited studies, however, have explored how building energy usage affects the surrounding urban microclimate, especially in summer when everyone in the city cools the indoor heat into the outside environment. Also concluded is that a building's albedo can be used to reduce cooling loads. Meanwhile, the heat retained from the outside will increase the temperature outside. Most studies on urban pollutant dispersal focus on non-isothermal conditions, including wind. The effect of thermal buoyancy on pollutant dispersion, especially in low wind speed conditions, has been highlighted in a few studies and needs more exploration in the future.

Overall, the thermal impact is more complicated than the wind effect, as many factors can influence the temperature of buildings and air in urban areas, including materials, solar radiation, greenery, shading, and so on. Currently, it is unclear how all these parameters interact to determine

the temperature of building surfaces as well as urban air. Because of their complexity, urban heat islands and thermal environments are affected by many variables, including wind, temperature, solar radiation, shortwave radiation, urban configuration, and greenery on the terrain. It is difficult to quantify the influence of each of these many parameters on the urban microclimate because many of them are coupled together. Due to the complexity of building geometry and wind and thermal conditions, conclusions drawn from one city may not apply to other cities. Therefore, future urban microclimate research must be conducted from the multi-physics, multi-scale, and multi-disciplinary perspectives.

From the literature review, this section presents previous research on (a) approaches to urban microclimates, including physics and numerical approaches, and (b) issues related to urban microclimates, such as wind and thermal environments, building energy consumption, and building pollutant dispersal. A summary of urban microclimate studies since 2010 was presented in this review. Existing approaches to the urban microclimate continue to face the following challenges based on existing knowledge:

- On-site monitoring focuses on wind, temperature, and humidity parameters, but building surface temperatures are often neglected. The thermal storage of buildings is not quantified as well. A number of studies fail to measure longwave radiation as a factor in the urban microclimate.
- Fewer studies explore non-isothermal conditions in wind tunnels. Fundamental studies of thermal impact are lacking.
- Urban microclimate has been extensively studied using CFD since 2010, and many detailed case studies and validations have been conducted. Detailed boundary conditions, such as thermal storage of buildings, especially at the urban scale, soil,

façade temperature, longwave radiation, and vegetation details, remain difficult to apply in CFD simulations.

- In recent years, data-driven models have appeared in urban microclimates; however, they are still in the early stages of development. Despite many studies showing encouraging results, many uncertainties remain regarding the required training data, the performance of models, and the robustness of models.

Aside from the challenge of the investigation approach, there are still a number of areas that need to be explored in the urban microclimate:

- It is well known that the urban microclimate is the result of interactions between multiple weather variables and urban characteristics. However, a lack of urban physics fundamentals has hindered our understanding of how these parameters interact.
- Many studies have observed and predicted surface urban heat islands. However, how the surface urban heat island is related to urban heat islands or pedestrian thermal comfort needs further understanding.
- It is shown that combining CFD with BES is a viable way to estimate building energy consumption, but the method is often less reliable due to the lack of validations and calibrations.
- Urban pollutant dispersion dominated by thermal buoyancy is often neglected, despite the fact that it is significant for urban street canyons at low wind speeds, and more non-isothermal studies are needed.

Chapter 3. Wind Environment Simulations and Validations

3.1 Introduction

This section focuses on urban wind simulations. The simulations are conducted in isothermal conditions without considering the building surface temperature, ground temperature, solar radiation, etc. The study in this section will present the simulation method and validation performance for the proposed CFD method. This section focuses on how urban regions interact with wind flow patterns and wind comfort.²

Urbanization plays a pivotal role in a nation's development, with the construction of tall buildings becoming a prominent trend in both developed and developing countries. However, the proliferation of tall structures in urban areas has significant impacts on wind flow patterns and pedestrian comfort at ground level. Municipal authorities now emphasize the importance of assessing wind conditions during the planning of new buildings, employing a combination of meteorological data, aerodynamic insights, and specific criteria for safety and comfort. Tall buildings can alter wind patterns, redirecting high-speed winds to the ground and creating potentially hazardous conditions for pedestrians. This phenomenon adversely affects air movement at ground level, leading to the accumulation of pollutants and increased air pollution.

² This chapter has included the contribution of the author in multiple publications:

1. CityFFD – City fast fluid dynamics for urban microclimate simulations on graphics processing units. Mohammad Mortezaadeh, Liangzhu Leon Wang, Maher Albettar, Senwen Yang (2022). *Urban Climate*. Volume 41, January 2022, 101063
2. CityFFD/CityBEM – Modeling Urban Microclimate, Thermal, and Energy Performances. Mohammad Mortezaadeh, Senwen Yang, Jiwei Zou, Ali Katal, Sylvie Leroyer, Wang Leon (2021). *Proceedings of Building Simulation 2021: 17th Conference of IBPSA*.
3. Estimating Urban Wind Speeds and Wind Power Potentials Based on Machine Learning with City Fast Fluid Dynamics Training Data. Mohammad Mortezaadeh, Jiwei Zou, Mirata Hosseini, Senwen Yang, Liangzhu Wang (2022). *Atmosphere* 2022, 13(2), 214; <https://doi.org/10.3390/atmos13020214>

Consequently, a thorough examination of pedestrian-level wind conditions is deemed essential in the early design stages of large urban projects. Historically, on-site field measurements were employed to study pedestrian-level wind speeds. However, due to practical limitations, wind tunnel measurements on scaled models have become a feasible method for investigating the effects of building design changes in the early stages of urban projects. Various measurement techniques, including hot wire or film anemometry, Irwin probes, laser Doppler anemometry, particle image velocimetry, infrared thermography, and thermistor anemometry, have been utilized to assess pedestrian-level wind speed.

The rise of computational fluid dynamics (CFD) has provided a viable alternative for studying pedestrian-level winds supported by high-performance computational resources. Steady Reynolds-averaged Navier-Stokes (RANS) modeling has been commonly used, offering cost and time efficiency. However, its accuracy in predicting low wind speed regions is lower compared to more expensive techniques like large eddy simulation (LES) and detached eddy simulation (DES). The adoption of CFD introduces challenges related to accuracy and reliability, leading to the establishment of best practice guidelines to enhance the fidelity of CFD simulations in urban planning and building design.

This chapter introduces a comprehensive simulation of pedestrian wind comfort in urban settings using CFD. Validation of the simulation results is carried out by comparing them with the CityFFD simulation compared to the results in the previous literature.

3.2 Methodology

In this section, the wind environment simulations are conducted by CityFFD, which solves the following conservation equations for the mass and momentum:

$$\frac{\partial \vec{U}}{\partial \vec{x}} = 0 \quad \text{Equation 3-1}$$

$$\frac{\partial \vec{U}}{\partial t} + U \frac{\partial \vec{U}}{\partial \vec{x}} = -\frac{\partial P}{\partial x} + (\nu + \nu_t) \frac{\partial^2 \vec{U}}{\partial x^2} + \vec{f} \quad \text{Equation 3-2}$$

where \vec{x} , \vec{U} , t , P , ν , ν_t , and \vec{f} are dimensionless length, velocity, time, pressure, kinematic viscosity, turbulent kinematic viscosity, and source term, respectively. These equations are defined in the Eulerian coordinate. CityFFD solves Eq. 3-2 based on three sub-equations for advection, diffusion, and pressure terms:

$$\frac{\partial \vec{U}}{\partial t} + U \frac{\partial \vec{U}}{\partial \vec{x}} = 0 \quad \text{Equation 3-3}$$

$$\frac{\partial \vec{U}}{\partial t} = (\nu + \nu_t) \frac{\partial^2 \vec{U}}{\partial \vec{x}^2} + \vec{f} \quad \text{Equation 3-4}$$

$$\frac{\partial \vec{U}}{\partial t} = -\frac{\partial P}{\partial \vec{x}} \quad \text{Equation 3-5}$$

Then, solving the Poisson equation (Equation 3-6) updates the pressure domain using the intermediate velocity.

$$\frac{\partial^2 P}{\partial \vec{x}^2} = \frac{1}{\Delta t} \frac{\partial}{\partial \vec{x}} \cdot \vec{U} \quad \text{Equation 3-6}$$

In the end, velocity is updated by using the new pressure domain. The most complex term in Eq. (3-3) is the advection term (Eq. 3-4). This term is nonlinear and can cause numerical constraint and stability problems. Thus, CityFFD converts Eq. (3-3) from its Eulerian coordinate to the Lagrangian perspective and overcomes stability issues, especially for large time steps. The advection equation in the Lagrangian form is as follows:

$$\frac{\partial \vec{U}}{\partial \vec{S}} = 0$$

Equation 3-7

where \vec{S} is the characteristic curve of the flow particles inside the computational domain. Details of this method have been revealed in our previous works.

3.3 Wind Simulation for Building Configurations

Wind flow passing different arrangements of buildings is also very important. It is related to the local wind comfort and also related to the local convection heat transfer coefficient which could contribute to building energy consumption in summer and winter periods. In this case, three different building configurations are investigated to study wind flow inside the community (Figure 3.1). The results generated from CityFFD will be compared to the experimental results and simulation results of conventional CFD from previous literature [162,163]

Figure 3.1 shows the details of the building's geometry and arrangement. The building height is 18 m. The distance between buildings is set as the certain ratio shown in Table 3-1. Their locations (P1, P2, P3) are selected for wind speed analysis. P1 and P2 are located in at open street canyon, while P3 is at the back of the building blocks. The wind speed is 4.5 m/s at the elevation of 10 m and comes from west of the buildings, with a power law vertical profile (the exposure is 0.22). In this case, the size of the minimum grid is 0.5 m, and the total grid number is 11.6 million.

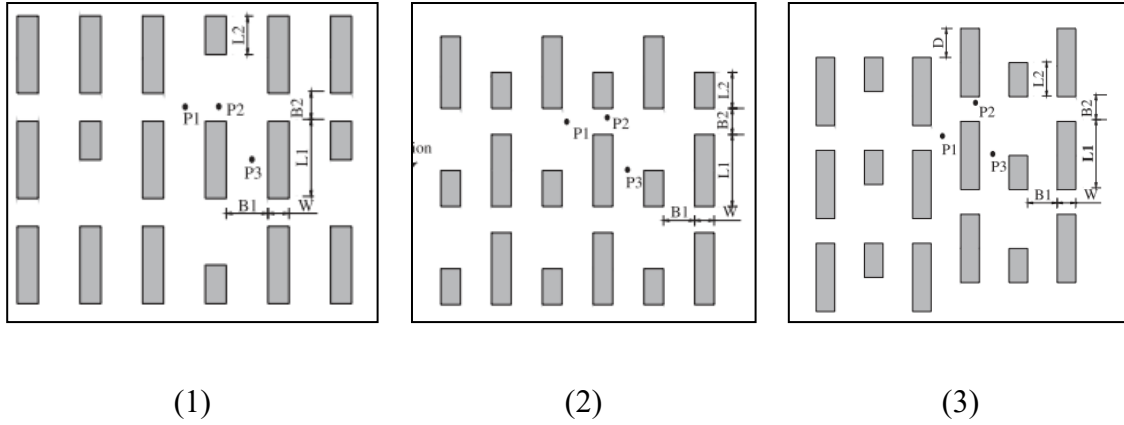


Figure 3.1 Multiple buildings with 3 different configurations [162].

Table 3-1. Dimensions of in 3 building configurations in Figure 3.1.

Scheme	B1/H	B2/H	D/H
1	1.0	0.67	0
2	0.7	0.67	0
3	0.7	0.67	0.78

Figure 3.2 shows the airflow pattern at 2 m near the ground surface when the wind comes from the west in Scheme 1. The velocity pattern generated by CityFFD is generally similar to the previous study. There is higher induced wind between buildings which close, and the dimensionless velocity is above 1. The airflow is also accelerated at the top and bottom boundary of the building cluster.

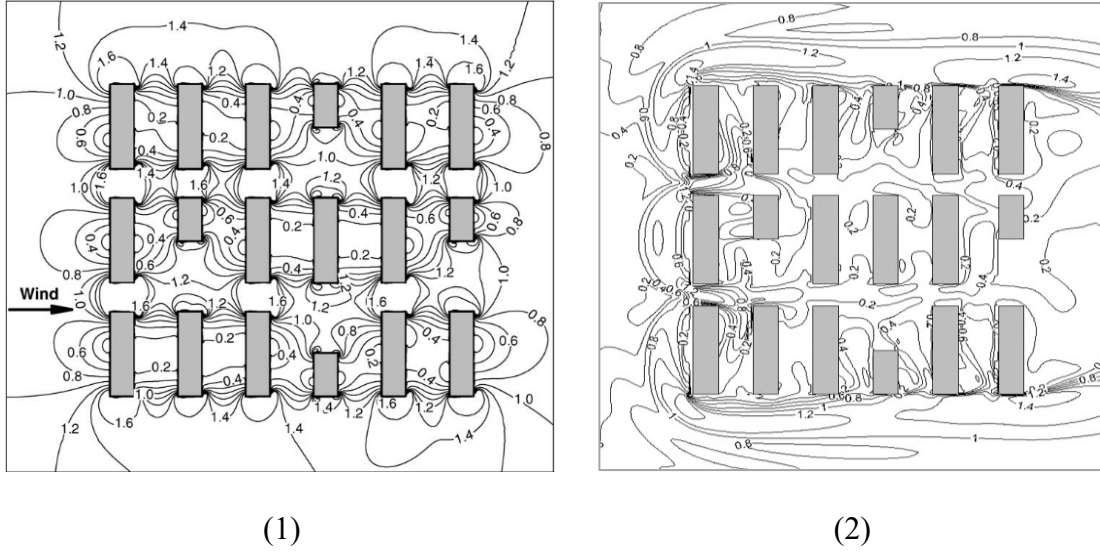


Figure 3.2 Velocity contours at the height of 2 m, normalized by the reference velocity (1) Reference[162], (2) CityFFD.

Since the CityFFD simulates the urban wind with the LES method, the airflow will fluctuate with each time step. Figure 3.3 shows the temporal results at an elevation of 2 m for simulation time from 200 s to 220 s. The figures show that there are numerous small vortices inside the domain, especially at the locations close to the building surface. The velocity magnitude is similar to the result shown in the reference.

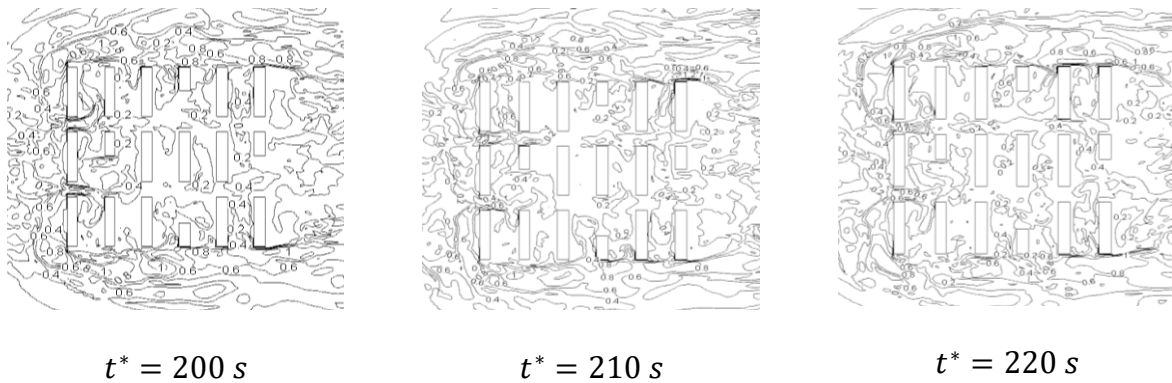


Figure 3.3 Temporal velocity contours for airflow around multiple buildings at 2 m height.

Figure 3.4 shows the results for 3 different configurations, comparing simulation results with the experiment and simulation results in the previous literature [162]. The overall comparison shows good agreement with previous studies, especially if the height above dimensionless height Z/H is higher than 1, and the results in the high elevation are almost the same. However, in the low elevation zone close to the ground, results show some deviation, which is probably due to wall effects. Further improvement can be obtained by using wall functions.

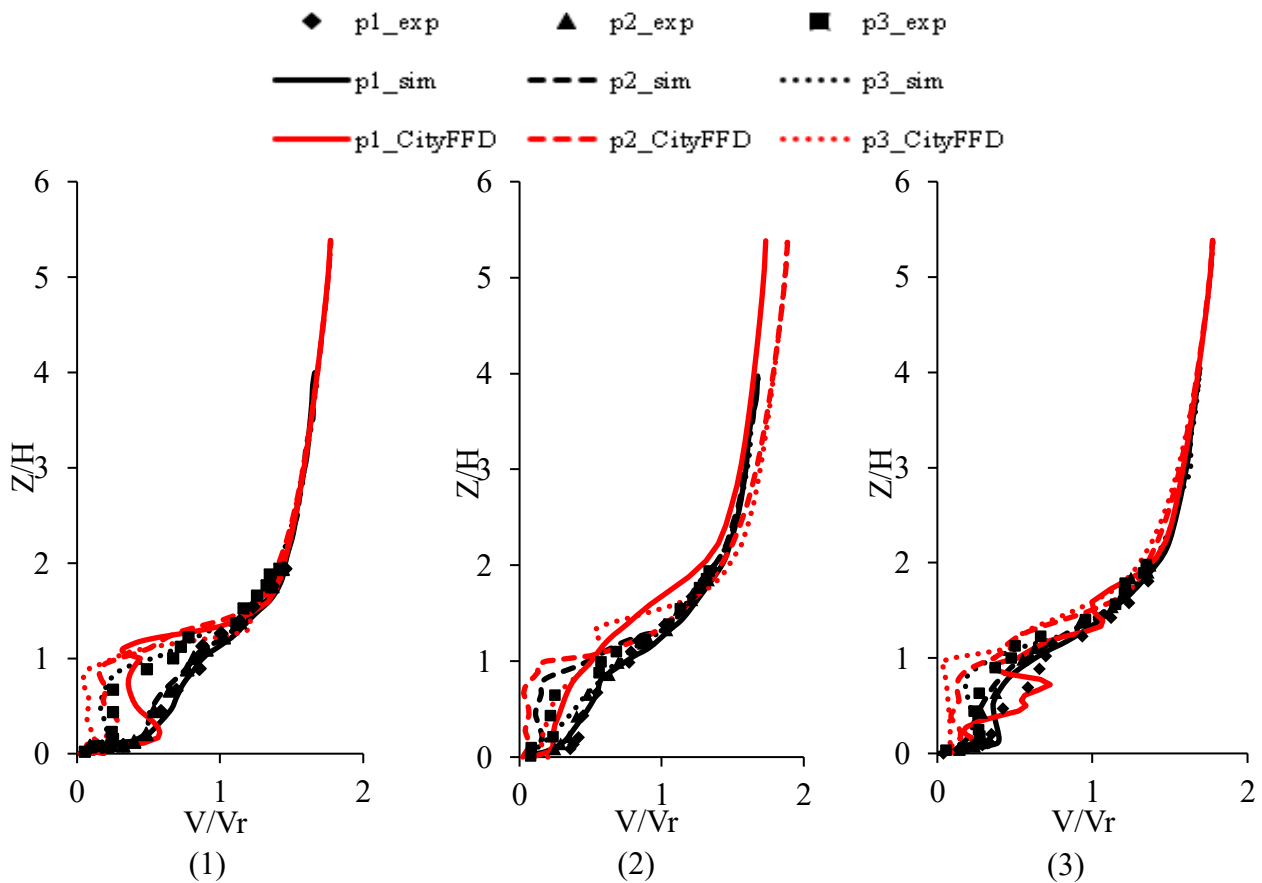


Figure 3.4 Wind distribution along a vertical line at P1, P2, and P3.

In Figure 3.4(1) for Scheme 1, the results for P3 are quite close to the literature, while results for P1 and P2 show some difference, and especially at the height Z/H from 0.2 to 1.2, wind speed is much lower than the experiment results. Note that P1 and P2 are located in a street canyon parallel

to the wind direction which can accelerate the flow and cause difficulty in modeling airflow. For Scheme 2, the results are similar to the experiment and previous CFD results. For Scheme 3, the results, the difference from CityFFD shows a similar trend as Scheme 1. However, due to the difficulty of simulating the turbulent flow near the ground boundary, the results from the proposed method are still acceptable.

3.4 Pedestrian-level Wind Environment Simulation

In this section, a large city region in Niigata, Japan which is studied by previous researchers [164] is selected to validate the performance of the proposed method. The target region is included in the circle with 400 m diameter (Figure 3.5 (1)). The total computational domain is set as a square with a 500 m length, which is the same as the simulation setting by Tominaga et al. (2005). The spatial resolution is 1 m with a uniform grid. The total grids number 75 million. It takes around 20 hours to achieve converged results on a PC with GPU Nvidia Titan V.



Figure 3.5 Buildings' configuration in a real urban area (Niigata, Japan).

Figure 3.6 shows 23 locations in a street that are selected to compare the velocity between CFD and CityFFD. Wind from west and north are considered. The reference wind speed is 7.8 m/s at

250 m height. Figure 3.6 shows the wind contour around three target buildings A, B, and C. Both results from CFD and CityFFD show the induced wind around building A. The wind is accelerated in the street canyon. However, wind has less impact around buildings B and C. The velocity contour of CityFFD in Figure 3.6(b) shows good agreement with the contour in the literature in Figure 3.6(a).

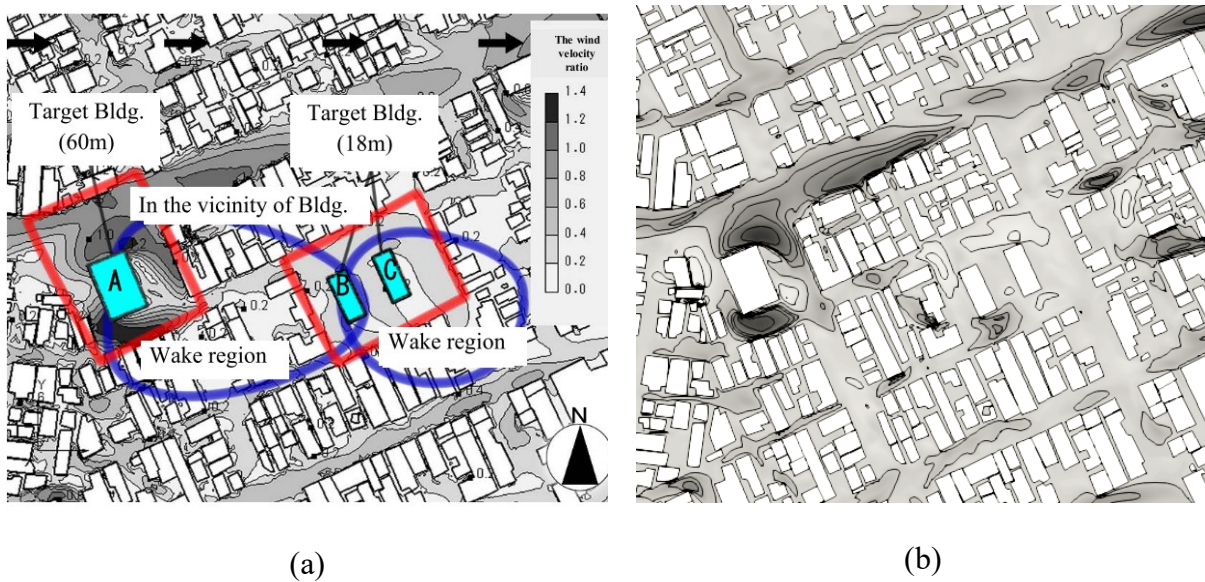


Figure 3.6 Comparison of simulation results by wind speed contours in an urban area, (a) Tominaga et al. [24][165] (b) CityFFD.

Figure 3.7 and Figure 3.8 show the wind speed comparison between CFD and CityFFD in 23 locations on the street canyon. Figure 3.7 (a) shows the normalized wind speed at 2 m (the wind speed is normalized by the wind velocity at the inlet) when the wind comes from the west. Overall, the results show good consistency; the normalized root mean square deviation (NRMSD) is 23.3%, and the error for most results is less than 30%, as shown in Figure 3.7(b). Some locations under weak wind (like locations 11, and 12) show a higher difference than the average. According to previous works, airflow modeling in an urban area with this amount of error is acceptable [4].

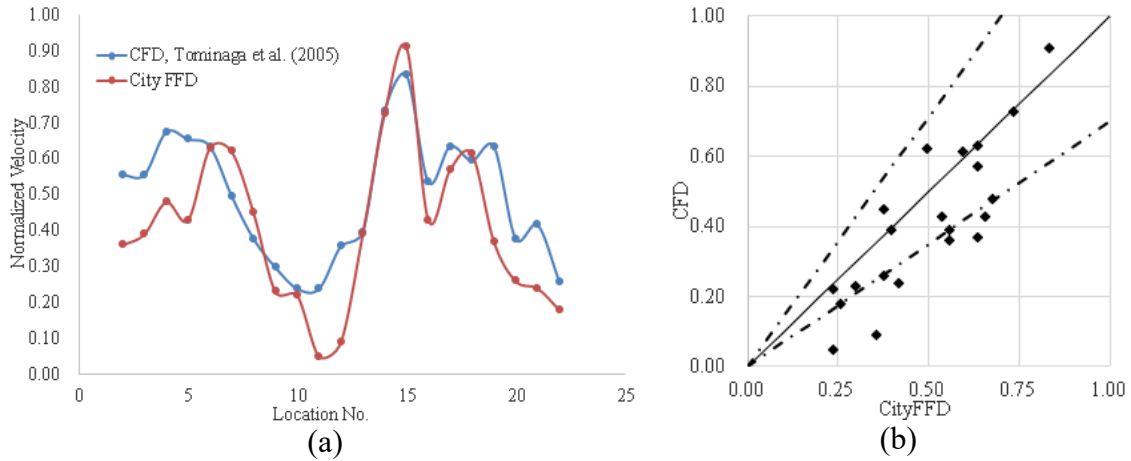


Figure 3.7 Wind flow in Niigata from west direction (a) normalized wind speed at 2 m, (b) Error correlation.

Figure 3.8(a) shows the results with north wind. In general, the results show good consistency. As shown in Figure 3.8(b), most errors are located inside the 30% line. The NRMSD for this north wind condition is 28.1%. It is higher than the west wind condition, but it's still acceptable. Figure 3.8 for wind speed at location 11 shows the results from CityFFD are lower than the CFD results because location 11 is quite close to the building wall, and it is difficult to achieve accurate results. The source of discrepancies can be caused by the flow turbulence or differences in simulation methods.

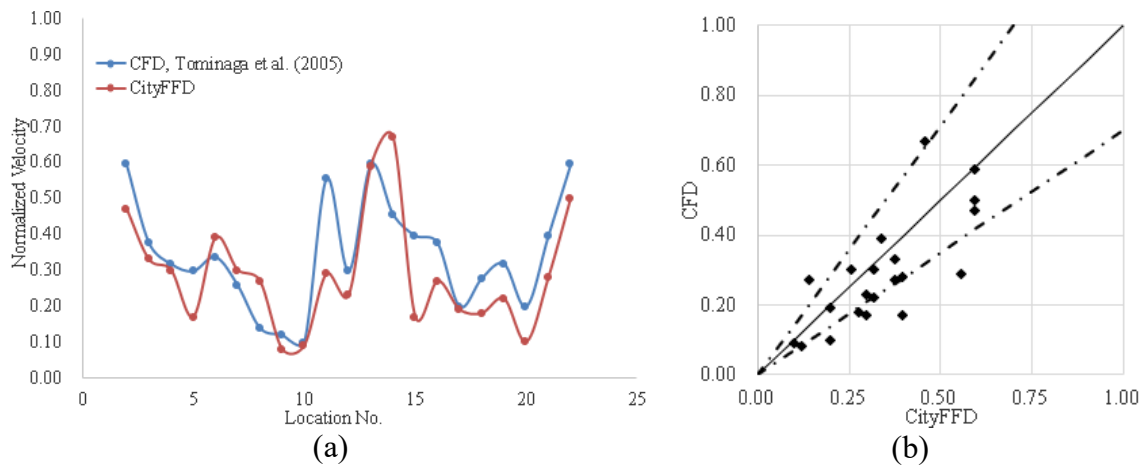


Figure 3.8 Wind flow in Niigata from north direction (a) normalized wind speed at 2 m, (b) Error correlation.

3.5 Summary

This section using the CityFFD considering isothermal conditions, shows that the CityFFD can be used for urban wind environments simulation. The CityFFD can provide good accuracy compared to results in the literature review. From the generic building configurations, the CityFFD can simulate the wind velocity at the pedestrian level as well as the vertical profile. For the applied urban regions, the CityFFD can simulate wind patterns for different locations.

Simulations for the urban wind environment offer a versatile set of applications. There are several potential applications for urban wind simulations by CityFFD in future studies. The technology extends its utility to microclimate analysis, considering factors like temperature, humidity, and air quality to understand how local weather conditions are influenced by the urban layout. Furthermore, urban wind simulations can study natural ventilation within urban spaces, contributing to the optimization of building designs for efficient airflow and pedestrian comfort. The simulations also enable the modeling of pollutant dispersion and assessment of the Urban Heat Island effect, aiding in the development of strategies for improved air quality and temperature regulation. Moreover, it can assess the wind energy potential, supporting sustainable energy planning. Finally, urban wind simulations may contribute to emergency evacuation studies by modeling the dispersion of smoke or contaminants, optimizing evacuation plans, and enhancing public safety considerations.

Chapter 4. Short-term Evaluation of Urban Microclimate and Thermal Comfort Analysis

The evaluation of urban microclimate, including both thermal and wind conditions, is more challenging compared to the isothermal urban environment, as presented in Chapter 3. With the satisfying isothermal simulation and validation in Chapter 3, the study in this Chapter investigates the urban microclimate by combining the wind and heat sources by coupling the Computational Fluid Dynamics and Building Energy Modelling.

4.1 Introduction

The section focuses on the use of computational fluid dynamics (CFD) to analyze urban thermal microclimates and heat stress. CFD is increasingly employed in various urban microclimate studies, including wind flow around buildings, pedestrian thermal comfort, and pollutant dispersion. While CFD provides detailed flow-field data and allows efficient parametric studies, complexities in urban microclimate studies necessitate simplifications, impacting simulation accuracy. Validation typically requires high-quality experimental data, obtainable through on-site measurements, thermal remote sensing, or reduced-scale modeling. On-site measurements offer real-world insights but are costly and limited in spatial coverage. Thermal remote sensing, despite technological improvements, demands caution due to various influencing parameters.³

In the past decades, summer heat waves have become a significant issue in urban microclimates because of their direct impact on human health. The prediction of outdoor thermal comfort in cities

³ This chapter has been partially published in the conference paper: Study of Urban Building Configuration Impacts on Outdoor Thermal Comfort Under Summer Heatwave via CityFFD and CityBEM. Senwen Yang, Mohammad Mortezaadeh, Jiwei Zou, Ali Katal, Sylvie Leroyer, Liangzhu Leon Wang, Ted Stathopoulos. International Conference on Building Energy and Environment, 2022

during heatwaves is important to avoid economic and life losses. Urban morphology, a parameter that will significantly affect urban microclimate, addresses its importance in outdoor thermal comfort study. In the present work, temperature distribution at three different urban areas will be simulated over two subsequent days during a summer heatwave (2013, July 15 to July 16) in Montreal, Canada. Urban microclimate simulation is done by using two new methods: CityFFD (City Fast Fluid Dynamics, an urban-scale fast fluid dynamics model for urban microclimate modeling-based graphics card unit computing) and CityBEM (City Building Energy Model, a new urban building energy model with a library of 1700 building archetypes for facilitating urban model creation). These numerical models are validated by on-site measurement data of the above-mentioned heat wave. The impact of different building configurations on the flow pattern is investigated, whereas thermal comfort and the impact of heat waves on the human body are considered by Humidex (humidity index). The results show that this model is capable of estimating local microclimate. The outdoor thermal comfort based on humidex in three regions during the summer heatwave is analyzed in this study.

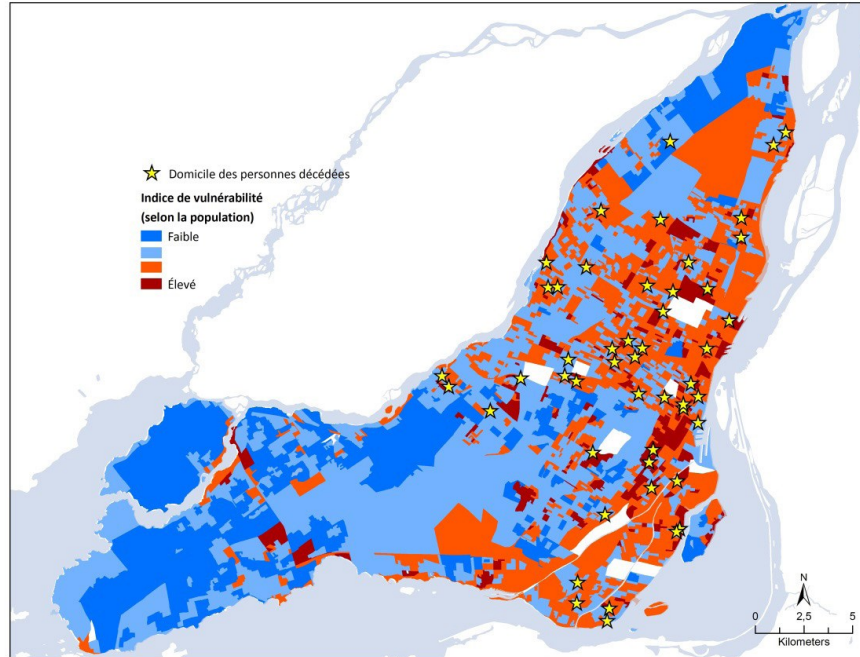


Figure 4.1. Vulnerability index and heat-related death map in Montreal (Heatwave: 30 June to 5 July 2018). Source: <https://ici.radio-canada.ca/nouvelle/1113457/bilan-deces-chaueur-montreal-sante-publique>.

In the present work, urban microclimate simulation is carried out by using two novel and in-house numerical tools, CityFFD (City Fast Fluid Dynamics) and CityBEM (City Building Energy Model). These two models will be introduced in the following section.

4.2 Methodology

4.2.1 CFD simulation

CityFFD is based on the semi-Lagrangian approach and fractional stepping method running on the graphics processing unit (GPU) to simulate urban microclimate features for modeling large-scale urban problems [90,166]. CityFFD solves the following conservation equations:

$$\nabla \cdot \vec{U} = 0 \quad \text{Equation 4-1}$$

$$\frac{\partial \vec{U}}{\partial t} + (\vec{U} \cdot \nabla) \vec{U} = -\nabla p + \left(\frac{1}{Re} + \nu_t \right) \nabla^2 \vec{U} - \frac{Gr}{Re^2} \theta \quad \text{Equation 4-2}$$

$$\frac{\partial \theta}{\partial t} + (\vec{U} \cdot \nabla) \theta = \left(\frac{1}{Re \cdot Pr} + \alpha_t \right) \nabla^2 \theta \quad \text{Equation 4-3}$$

where \vec{U} , θ , and p , Re , Gr , Pr , ν_t , and α_t are the velocity, temperature, pressure, Reynolds number, Grashof number, Prandtl number, turbulent viscosity, and turbulent thermal diffusivity, respectively. The advection terms of Eqs. 4-4 and 4-5 are solved by using the Lagrangian approach:

$$\frac{\partial \vec{U}}{\partial t} + (\vec{U} \cdot \nabla) \vec{U} = \frac{d\vec{U}}{dS_c} \quad \text{Equation 4-4}$$

$$\frac{\partial \theta}{\partial t} + (\vec{U} \cdot \nabla) \theta = \frac{d\theta}{dS_c} \quad \text{Equation 4-5}$$

where S_c is the characteristic curve and shows the fluid particles' path. The fluid-particle positions, S_c^n at the time n and S_c^{n+1} at the time $n + 1$ can be related by the following equation:

$$dS_c = \vec{U} dt \quad \rightarrow \quad S_c^n \approx S_c^{n+1} - \vec{U} \Delta t \quad \text{Equation 4-6}$$

To calculate the values for the unknown variables (e.g., velocity and temperature, \vec{U} and θ) at the position S_c^{n+1} , it is necessary to compute the values of \vec{U} and θ at the position S_c^n in Eq. 4-6. Thus, an interpolation scheme is needed. CityFFD is equipped with a 4th-order interpolation scheme to model airflow on the coarse grids and overcome the high dissipation errors. Details of the proposed method have been comprehensively investigated in our previous work. The LES-SGS turbulence model is applied to capture the turbulence behavior of the flow. Based on this model, turbulent viscosity is calculated by:

$$dv_t = (c_s \Delta)^2 |\bar{S}| \quad \text{Equation 4-7}$$

where c_s , Δ , and \bar{S} are the Smagorinsky constant, the filter width, and the large-scale strain rate, respectively. Smagorinsky constant is mostly in the range of $0.1 < c_s < 0.24$ (Klaus and Hoffman, 2000).

CityFFD has been well validated by several CFD benchmarks and represented acceptable accuracy for modeling an urban microclimate [166].

4.2.2 Building Energy Modelling

CityBEM is a building energy model for urban thermal loads and energy prediction. The model's inputs include building information, such as geometry, construction materials, lighting, etc.; and building uses and operations, such as occupancy schedules, lighting, etc. The schematic of the model is shown in Figure 4.2.

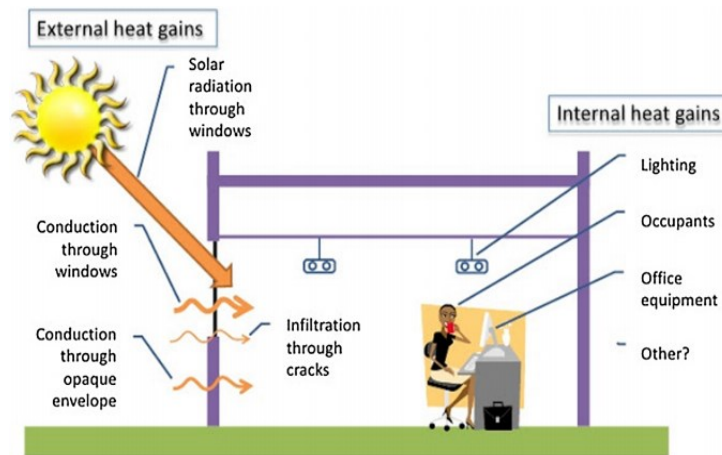


Figure 4.2. Schematic of the CityBEM model [167].

CityBEM considers the building as a single zone with a well-mixed assumption. The total thermal load of each building (Q_t) is a combination of convective heat transfer from indoor surfaces,

fenestration radiation heat, infiltration heat transfer, and internal heat gains. The model was validated in the previous study [76].

$$Q_t = Q_{wall} + Q_{fes} + Q_{inf} + Q_{int} \quad \text{Equation 4-8}$$

Details of each component in Eq. 4-8 can be found in the previous work [76].

Building information, such as building thermal properties, occupancy schedules for internal load calculations, and Window-Wall-Ratio (WWR) for solar heat gains, are provided based on an archetype library. This library was developed and implemented into CityBEM based on the building year of construction and usage [76]. Then, the required parameters are assigned to each group of buildings. 19 reference building types, including single-family houses, Multi-Unit Residential Buildings (MURB), and 17 commercial buildings, are used to estimate WWR. Building envelope properties were estimated based on the classification of buildings' years of construction. To estimate the internal load, the building stock was divided into 10 building types. The operation hours, average loads by occupants, appliances, lighting, and the average usage rate are the parameters defined for each group and used to estimate the transient internal load of buildings. Comprehensive information about the proposed archetype library can be found in the reference [76].

4.2.3 Boundary conditions integration

Proposed urban microclimate and building energy models are automatically integrated using the Ping-Pong coupling strategy [168]. Based on this model, CityFFD and CityBEM run in sequence (i.e., one data exchange at each time step). The integration method is shown in Figure 4.3. The typical timestep of integrated simulation is 1 hour, which is suitable for microclimate simulation. The typical internal timestep of CityFFD and CityBEM is 1 to 10 seconds and 5 minutes, respectively. At each time step, CityFFD simulates the urban microclimate and obtains an average

air temperature and wind speed for each façade or specified sections of a building facade. CityBEM uses these data to calculate the thermal load, indoor air temperature, and building surface temperature. The simulated surface temperature of each building facade is transferred to CityFFD as a surface temperature boundary condition for the next timestep simulation.

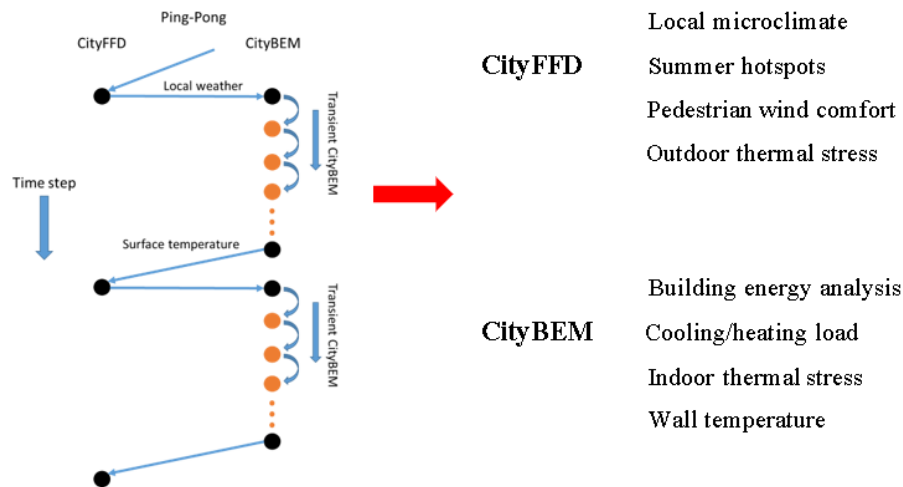


Figure 4.3. Dynamic urban building and microclimate simulation (CityFFD/CityBEM) workflow [76].

In this study, three regions in Montreal, Canada, with different urban configurations, will be simulated: the downtown region (LCZ1), the urban region in the residential community (LCZ3), and the suburban region (LCZ6) in Montreal. For the LCZ1 area investigated in this article, buildings with a maximum of 100 m height are included in the region. The large LCZ3 area contains densely arranged low-rise buildings with an average elevation of around 10 m. The LCZ6 area includes sparse single houses, and the average building elevation in this area is around 5 m. The boundary of the computational domain maintains 10 times the highest buildings' height in the domain to the edge of the investigation region.

In the present work, weather station data collected by Environment Canada in the 2013 heatwave from July 15th to July 16th are used for validation. 48 hours duration was simulated in this study, and the time interval selected is 1 hour[40]. As shown in Figure 4.4, the weather station data flow speed and profile at Dorval airport were selected as simulation input parameters at the domain inlet.

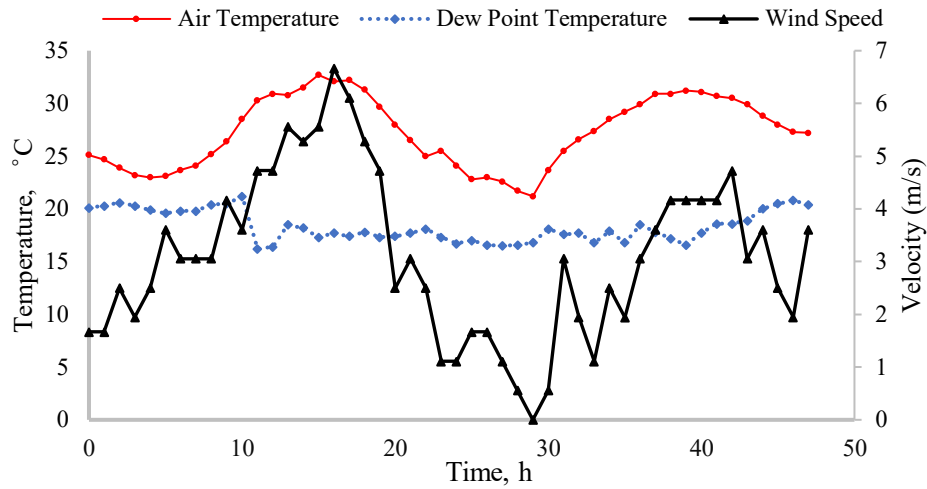
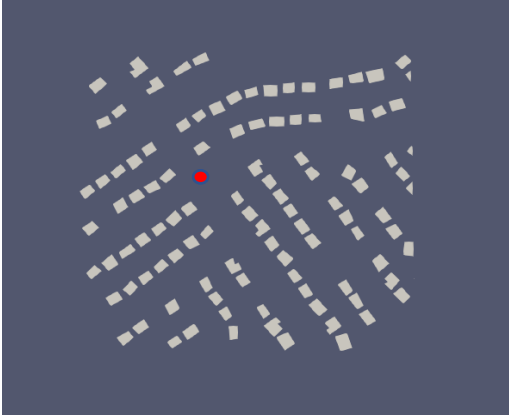
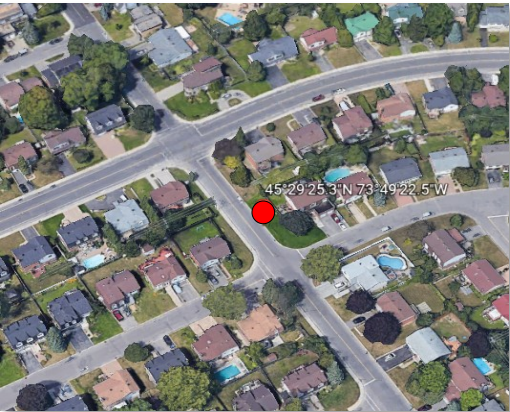


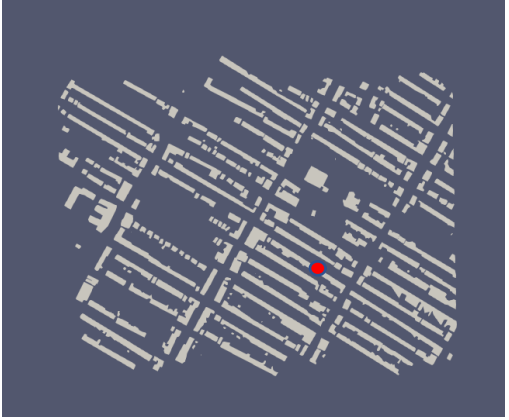
Figure 4.4. Temperature and velocity at the inlet of the simulation domain.

The building cluster with the size of $0.3 \text{ km} \times 0.3 \text{ km}$ is located in the LCZ6 area. The overall domain size is $0.6 \text{ km} \times 0.6 \text{ km}$. The total mesh number is 29 million, and the minimum mesh size near the building is 1 m. 48 simulations are conducted, and the timestep is 1 hour. The computational cost is around 3 hours for each case on the Nvidia DGX server with Tesla V100 GPU (5120 CUDA cores). The building cluster is with a size of $1 \text{ km} \times 1 \text{ km}$, and the overall domain size is $1.6 \text{ km} \times 1.6 \text{ km}$. The total mesh number is 96 million, and the minimum mesh size near the building is 1 m. The computational cost is around 8 hours for each case. The building cluster with the size of $1.5 \text{ km} \times 1.5 \text{ km}$ is located in LCZ1 Montreal. The overall domain size is $4 \text{ km} \times 4 \text{ km}$. The total mesh number is 54 million, the minimum mesh size near the building is 1

m, and the computational cost is around 6 hours for each case. For all three cases, 48 simulations are conducted, and the timestep is 1 hour. Figure 4.5 shows the geometry of the three regions.



LCZ6



LCZ3



LCZ1

Figure 4.5. Satellite image and geometry of three investigation regions marked with the measurement location.

4.2.4 Outdoor thermal comfort

Humidex has been adopted to study the impact of thermal comfort on the human body. The Humidex (H) is an index used by Canadian meteorologists to evaluate how hot the weather feels to a person, considering the combined effects of heat and humidity. It was derived from hourly observations of dry bulb and dew point temperatures taken at 126 climatological stations. The calculation format is proposed by [169,170], and shown below:

$$H = T_{db} + \frac{9}{5} \left(6.11 \times e^{5417.75 \left(\frac{1}{273.16} - \frac{1}{T_{dew}} \right)} - 10 \right) \quad \text{Equation 4-9}$$

where T_{db} is the dry bulb air temperature ($^{\circ}\text{C}$), and T_{dew} is the dew point temperature (K). The value 5417.753 is a constant number based on the molecular weight of water, vaporization latent heat, and the universal gas constant [171]. When the humidex is under 30, it can be regarded that there is thermal comfort; when the humidex ranges from 30 to 39, it is defined as some discomfort and moderate outdoor activities are recommended based on age and health; when it reaches 40, it represents great discomfort, and it is recommended that all unnecessary outdoor activities be ceased completely; when humidex is above 45, the thermal environment can be dangerous.

In this study, to simplify the analysis of outdoor thermal comfort, humidity is assumed to be constant, and the dew temperature will not change with the urban morphology and locations. The dew point temperature T_{dew} at each hour in different locations and regions is regarded the same as the boundary inlet.

4.3 Results and Discussion

In this section, CityFFD/CityBEM is applied to investigate the accuracy of urban microclimate estimation during two subsequent days in a heatwave event by comparing it with measurement

data. The onsite measurement data were documented by Environment and Climate Change Canada during a temporary field campaign during the summer of 2013.

Vertical surfaces of the computational domain are inlet or outlet (see Figure 4.6), depending on the wind direction. The floor boundary condition was considered as a wall, and the top boundary condition was symmetry. Buildings' surface temperatures are calculated by CityBEM and used as a boundary condition in CityFFD. The inlet boundary conditions were provided by the weather station located at the Dorval airport, about 13 km away from the LCZ1 of Montreal (Figure 4.6 (b)).

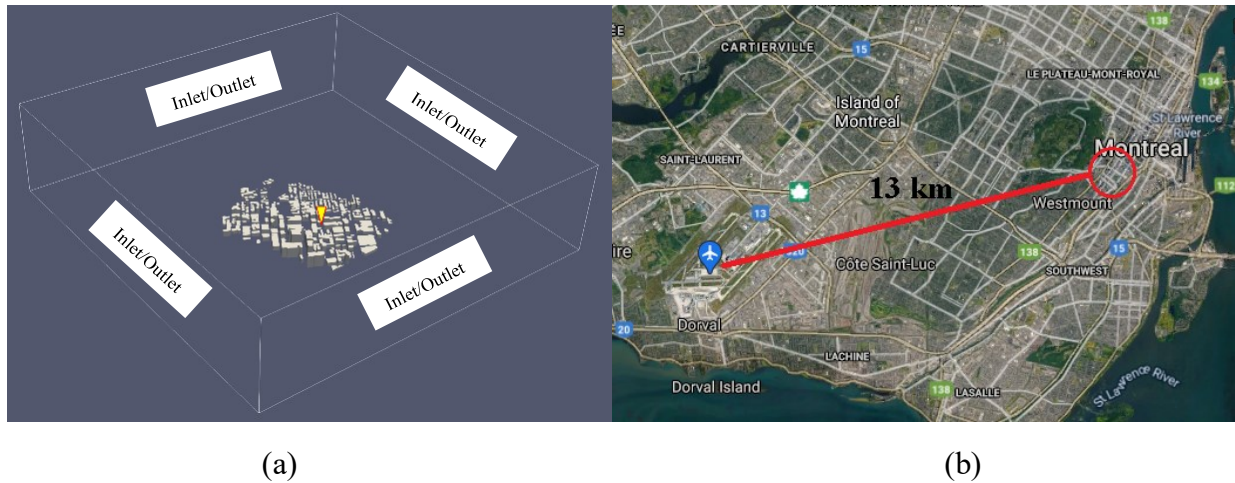


Figure 4.6. (a) Schematic of the computational domain and boundary condition (b) Satellite imagery of Montreal.

Based on the literature, because of urban morphology, building configuration, and terrain impacts, the microclimate properties recorded at the airport are different from the local microclimate near the LCZ1, LCZ3, and LCZ6 regions. We can estimate the variation of wind speed in the three regions empirically by using the airport weather station data. However, it cannot accurately estimate the airflow at the street canyon. Using CityFFD/CityBEM, it is possible to accurately

estimate the wind conditions and air temperature in the urban area by using the weather station data about 13 km away from the case study regions.

The temperature differences were recorded at the Montreal area, and the airport can reach up to 5 degrees. Most temperature differences are observed during the nighttime, possibly due to the UHI effects. Buildings act as solar storage and release the heat into the urban microclimate during the nighttime [172]. Table 4-1 below shows that the proposed integration model could significantly improve the urban temperature accuracy:

Table 4-1 RMSE of validation results for three regions.

	Temperature (C)	Velocity, m/s
Case LCZ1	0.97	0.257
Case LCZ3	0.64	0.103
Case LCZ6	0.458	0.16

The wind speed difference between the airport and the LCZ1 is considerably more significant than the temperature difference, as shown in Table 4-1. Near urban building clusters, the wind speed is reduced significantly. The CityFFD/CityBEM platform could accurately estimate the wind magnitude in the urban area. The RMSE for wind velocity is 0.265 m/s. As mentioned before, CityFFD is equipped with the 4th-order interpolation scheme to reduce numerical dissipation errors and capture wind patterns near the buildings.

In Figure 4.7, the validation results show that the CityFFD/CityBEM is capable of predicting accurate results from large-scale simulations with high resolution at a low computational cost. It

can be beneficial to other urban microclimate investigations like building energy consumption, urban wind energy prediction, and outdoor thermal comfort estimations.

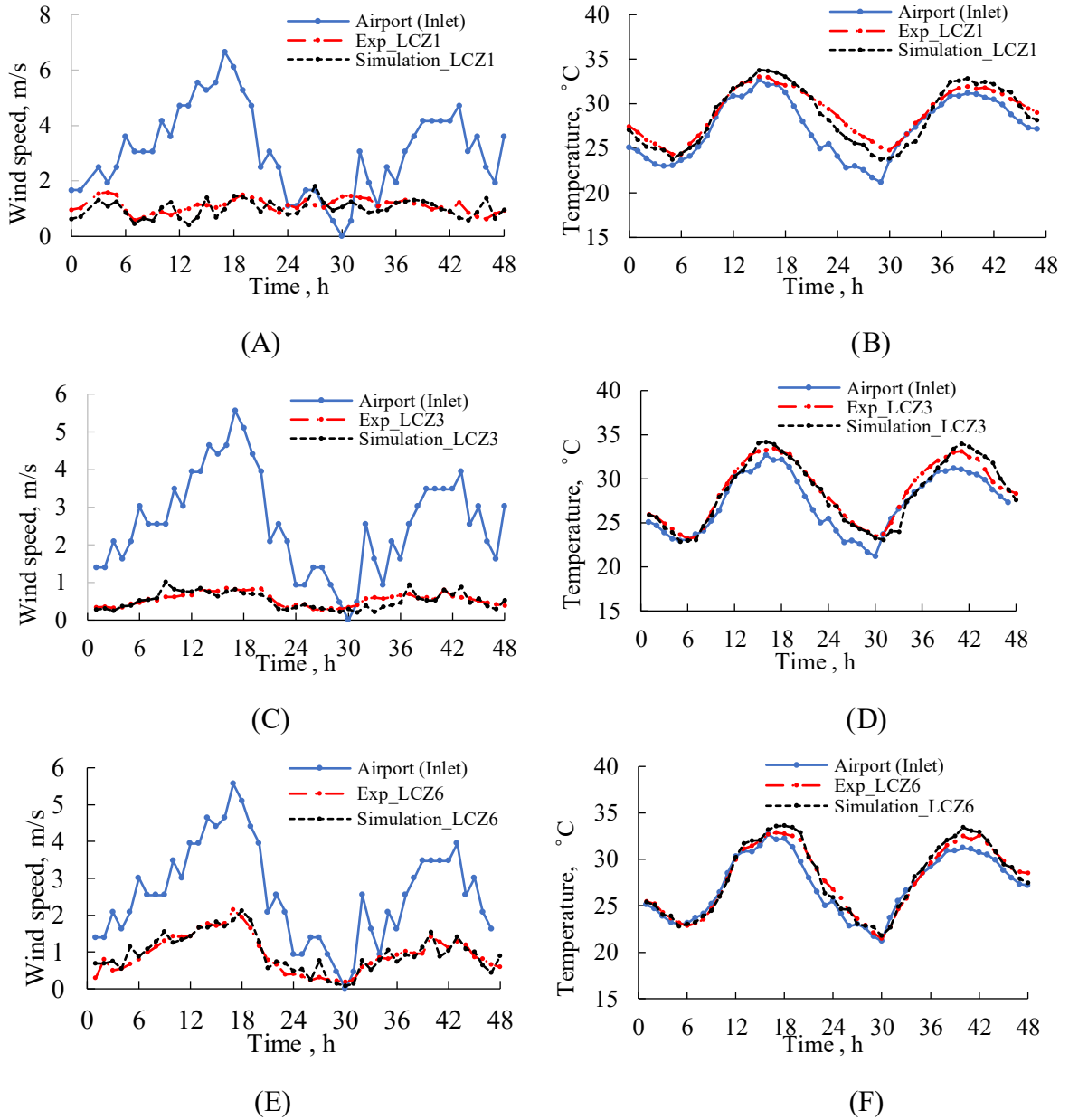


Figure 4.7. Wind velocity (A, C, E) Air temperature (B, D, F) and comparisons between measurements at the airport and at the local, and the simulation at the local station.

Figure 4.8 describes simulation results of the average airflow temperature at pedestrian level (2 m) in the LCZ6 area during the duration 48-hour summer heatwave. The maximum value appears on

July 15th at 18:00, and the average value is 33.2 °C. The lowest value appears on July 16th at 5:00 am, and the average value at the pedestrian level is 21.2 °C. Considering the airflow temperature variation among different detailed locations inside one simulation case, the bar shows the standard deviation for each hour. The maximum standard deviation is 1.89 on July 15th, 20:00. It can also be found that the standard deviation of temperature is smaller at night and larger in the daytime, especially in the afternoon. Because of the solar radiation, buildings' surface temperature is much higher than the adjacent air layer affected by the wind, which will create temperature variation in different locations inside the street canyon. At night, with less effect of solar heat gain, the building surface temperature is close to the air temperature. Thus, there is less temperature variation in different locations compared to daytime conditions.

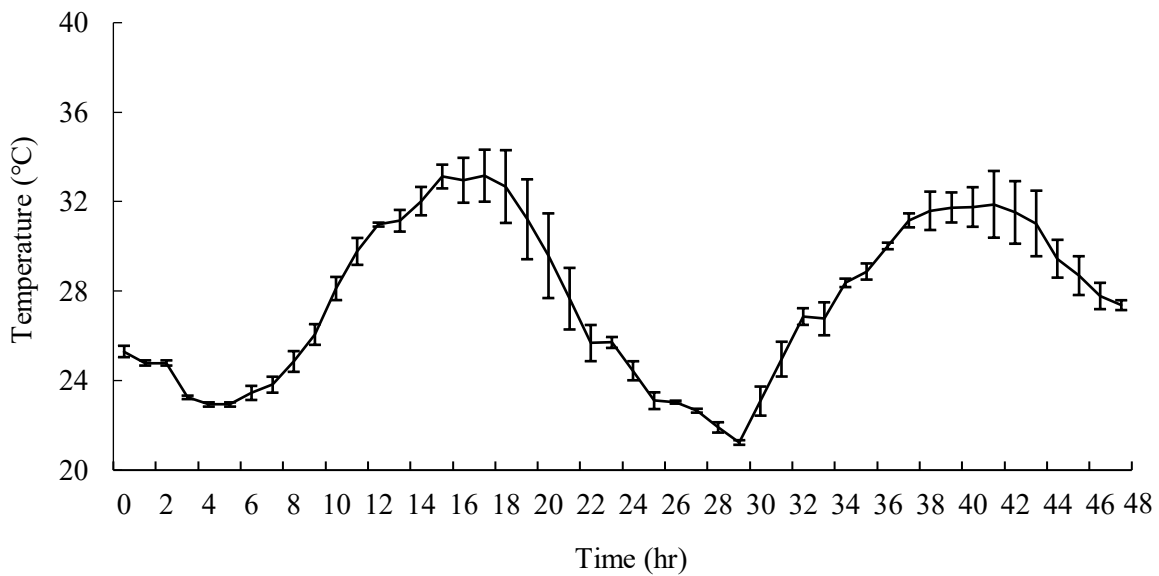


Figure 4.8. Averaged pedestrian level temperature during 48-hour heatwave in LCZ6 area.

Figure 4.9 presents the simulation results similar to the previous paragraph but for the LCZ3 area case study. The maximum value appears on July 15th at 5:00 pm, and the average value is 33.3. The lowest value appears on July 16th at 5:00 am, and the average value at the pedestrian level is

21.32. The maximum standard deviation is 2.85 on July 15th, 18:00. Although the average values are similar to the LCZ6 case study, some locations exhibit larger daytime temperatures in the LCZ3 case study, as seen by the upper range of the standard deviation.

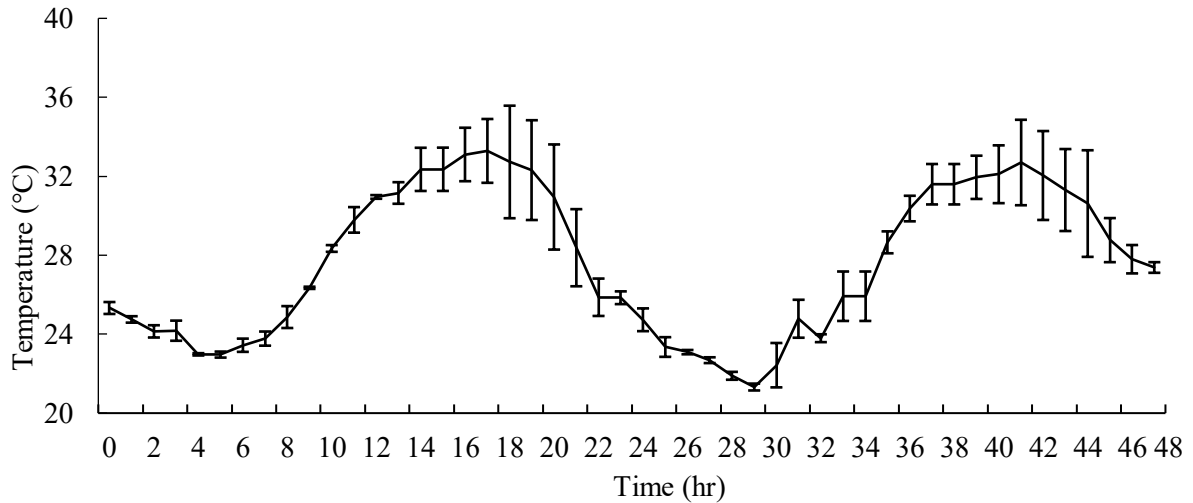


Figure 4.9. Averaged pedestrian level temperature during 48-hour heatwave in LCZ3 area.

Similarly, Figure 4.10 shows simulation results in the LCZ1 area. The maximum value appears on July 15th at 5:00 pm, and the average value is 33.9. The lowest value appears on July 16th at 5:00 am, and the average value at pedestrian level is 21.3. The maximum standard deviation is 3.27 on July 16th, 8 pm. Considering both the standard deviation and the average value of air temperature, the LCZ1 area has the highest airflow-averaged temperature among these three regions. The temperature standard deviation is also higher than the other regions because the LCZ1 area has more heated building surfaces. However, the temperature during the night is close to the other 2 regions.

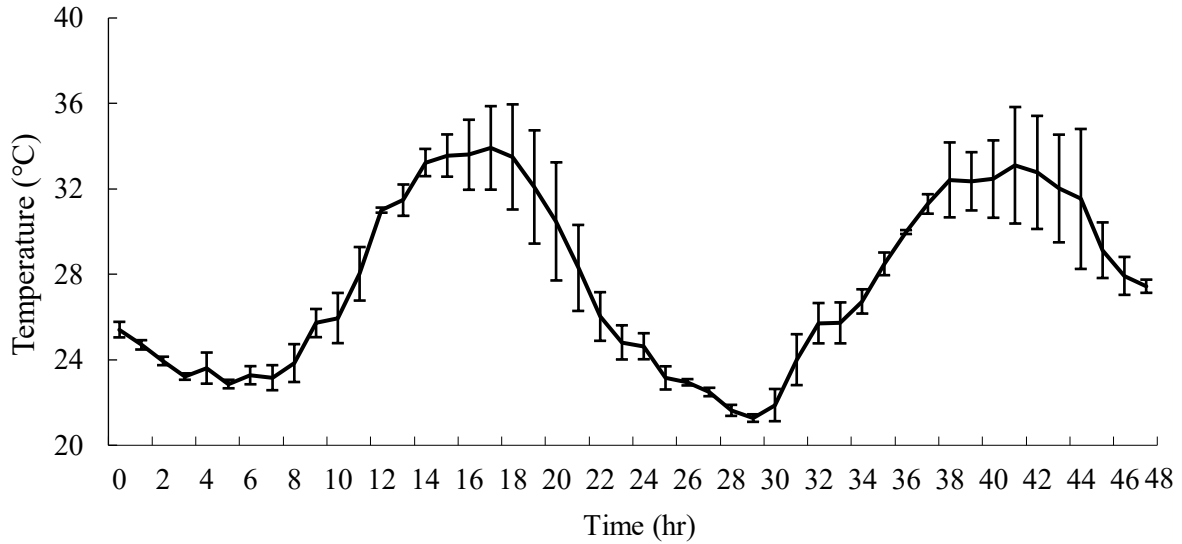


Figure 4.10. Averaged pedestrian level temperature during 48-hour heatwave in LCZ1 area.

It is shown in Figure 4.11 that among the 48-hour simulation results, during the daytime afternoon, the air in the LCZ1 and LCZ6 areas has the highest and the lowest temperature, respectively. In the daytime, higher and denser buildings can absorb solar radiation. Their surface temperature is higher than the surrounding area, and they can act as heat sources to increase the urban airflow temperature. At night, with less effect of solar radiation, the building surface has an impact on the incoming airflow, and the average temperature is quite close.

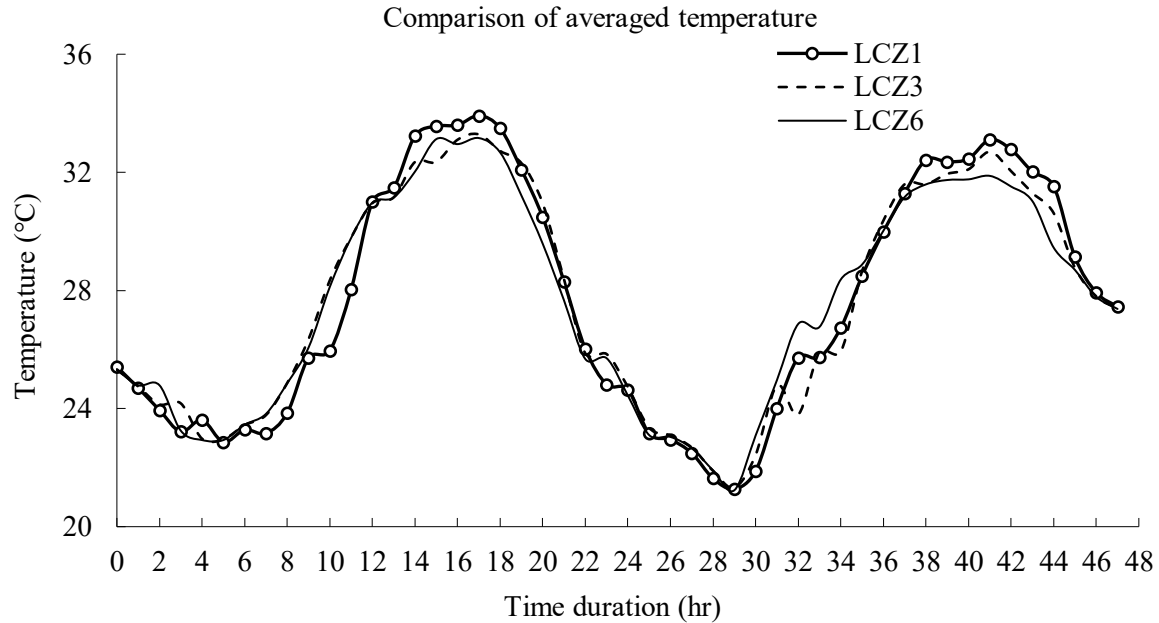


Figure 4.11. Comparison of averaged temperature at pedestrian level in three regions during the heatwave.

4.4 Outdoor Thermal Comfort Analysis

Based on the temperature simulation results and given moisture information from the weather station, the average humidex at a pedestrian level of 2 m is calculated. Figure 4.12 shows the average humidex at pedestrian level (2 m) in the airflow surrounding the buildings in the LCZ6 area. The maximum value appears on July 15th at 6:00 pm, and the average value is 39.5, which means the thermal comfort is close to great discomfort. The lowest value appears on July 16th at 5 am, and the average value at pedestrian level is 26.3, which represents no discomfort. Considering the humidex variation among different detailed locations inside one simulation case, the bar shows the standard deviation of humidex for each hour. The maximum standard deviation is 3.33 on July 15th at 8:00 pm. Considering the average value and standard deviation, most of the time and locations of the LCZ6 area are under some discomfort conditions and there are also few periods under great discomfort.

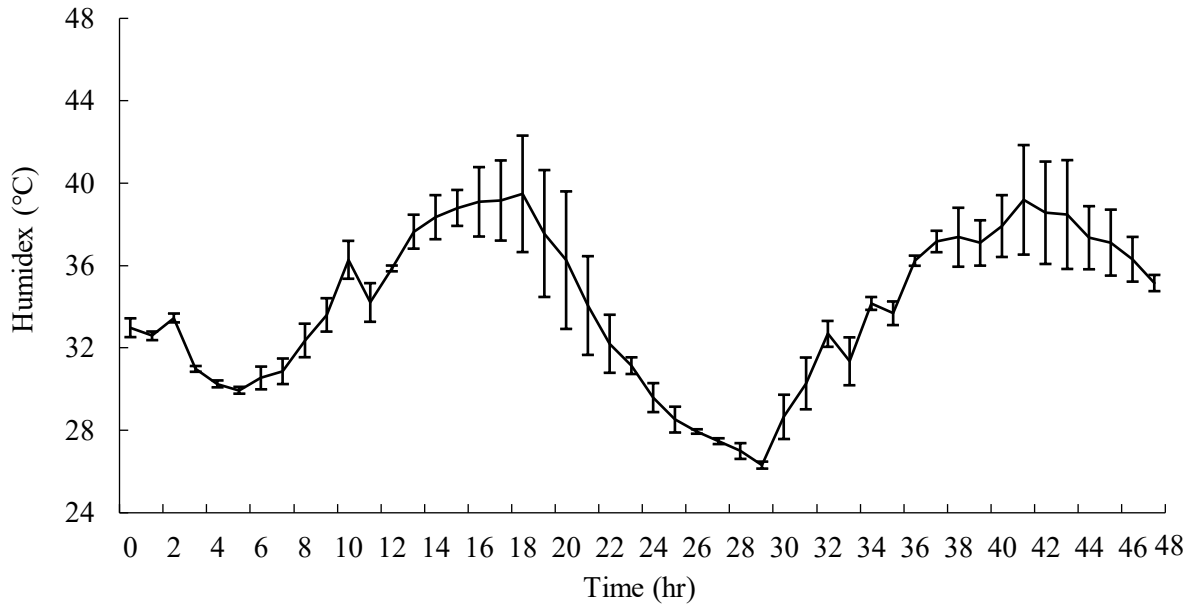


Figure 4.12. Humidex in 48 hours summer heatwave in case LCZ6.

Figure 4.13 shows the average humidex at pedestrian level (2 m) in the airflow surrounding the buildings in the LCZ3 area with dense low-rise buildings. The maximum average humidex appears on July 16th at 5:00 pm and the average humidex is 40.6, which represents great discomfort. The lowest value appears on July 16th at 5:00 am and the average value at the pedestrian level is 26.5, which represents no discomfort. The maximum standard deviation is 5.2 on July 15th 8:00 pm. Considering the average value and standard deviation, great discomfort appeared on July 15th at 4 pm. In part of the locations inside the domain, the exposure period is longer than in the case located in an LCZ6 area.

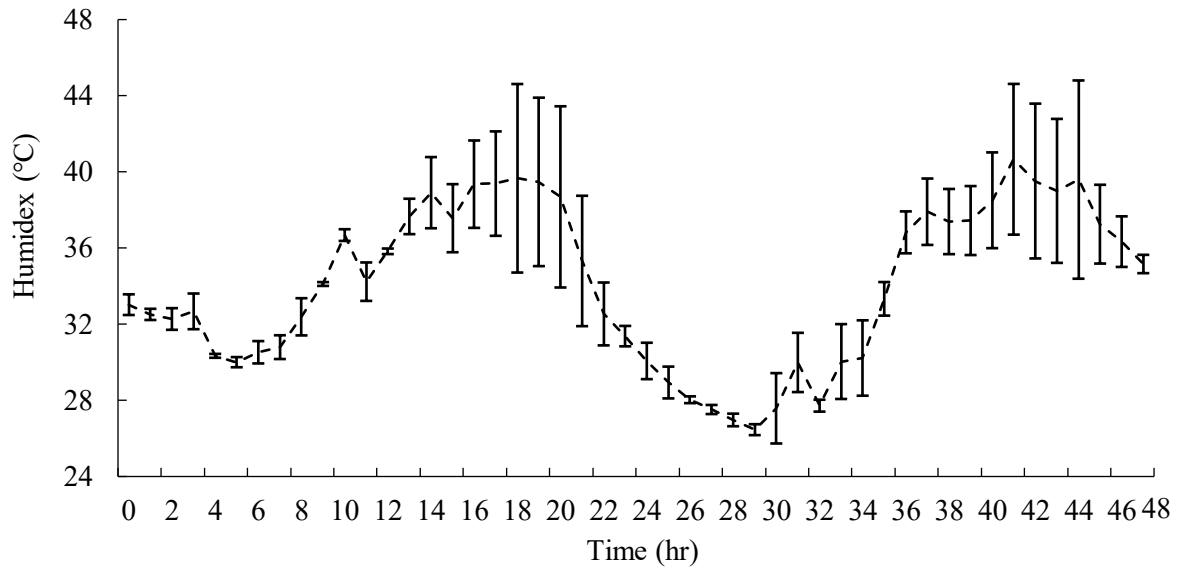


Figure 4.13. The average value and standard deviation of humidex in 48 hours of summer heatwave in case LCZ3.

Figure 4.14 shows the average humidex at pedestrian level (2 m) in the airflow surrounding the buildings in the LCZ3 area with dense low-rise buildings. The maximum average humidex appears on July 16th at 6:00 pm, and the average humidex is 41.4, which represents great discomfort. The lowest humidex value appears on July 16th at 5:00 am, and the average value at the pedestrian level is 26.4, which represents no discomfort. The maximum standard deviation is 5.2 on July 15th 8:00 pm. Considering the average value and standard deviation, great discomfort appeared on July 15th at 2 pm. In some locations inside the domain, because of the increase of heated building surfaces in the LCZ1 area, great discomfort appeared earlier than in the regions of LCZ6 and LCZ3. Besides the higher risk than other regions, the overall exposure period is also longer than that of other cases located in other investigation areas.

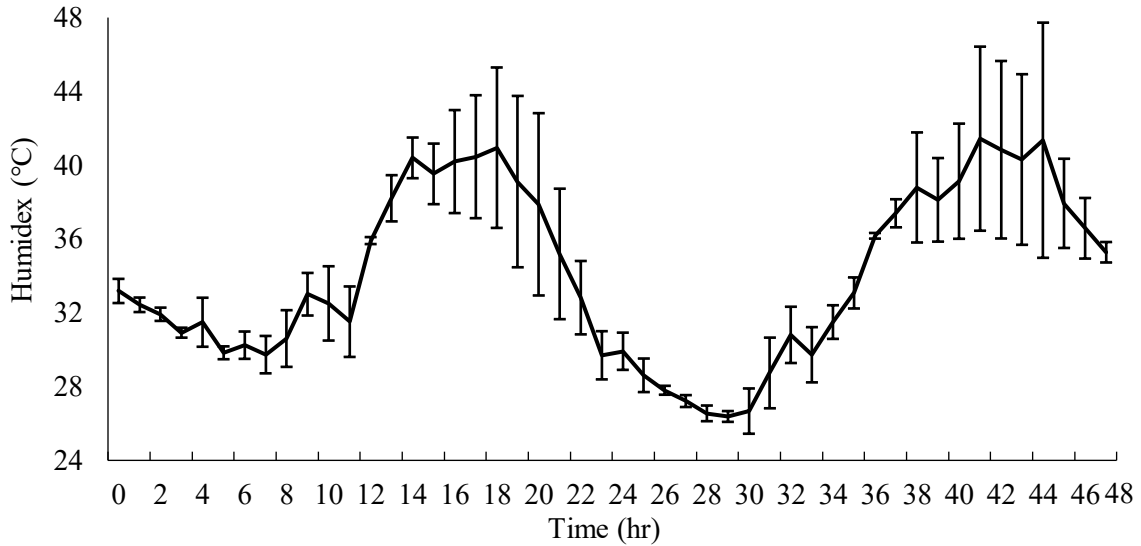


Figure 4.14. Humidex in 48 hours summer heatwave in case LCZ1.

Figure 4.15 shows the humidex variation during 48 hours for all three regions. It can be found that in the daytime, especially in the afternoon, the humidex reaches its peak value. The LCZ1 area has the highest risk and exposure risk compared to other regions. At nighttime, the humidex value for these three zones is quite close. A possible reason could be that, at nighttime, solar radiation plays a less significant role in affecting the building surface temperature so that the surface temperature is close to the surrounding air temperature. Another important point shown in Figure 4.15 is that the humidex on July 16th daytime is higher than that of July 15th owing to the larger synoptic wind speed during the daytime of July 15th. Even though the dry bulb temperature is higher on July 15th, the higher wind speed in the microclimate can still help cool down the city and reduce the humidity compared to wind conditions on July 16th.

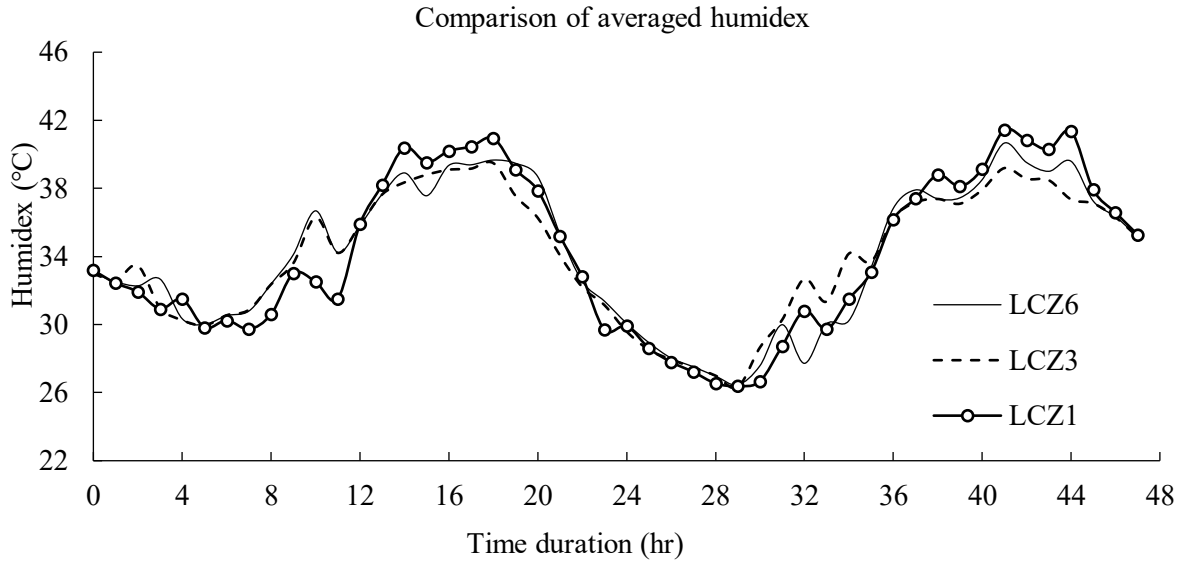
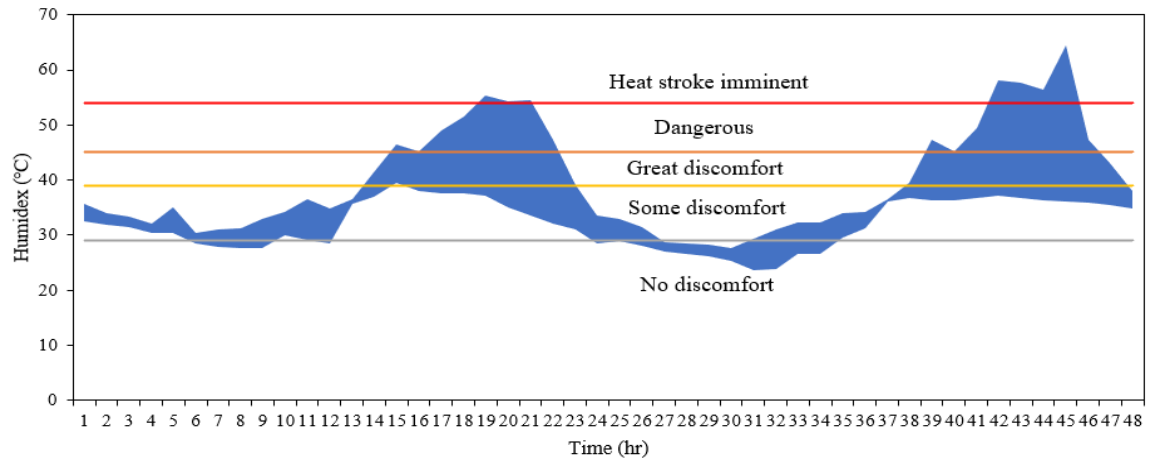


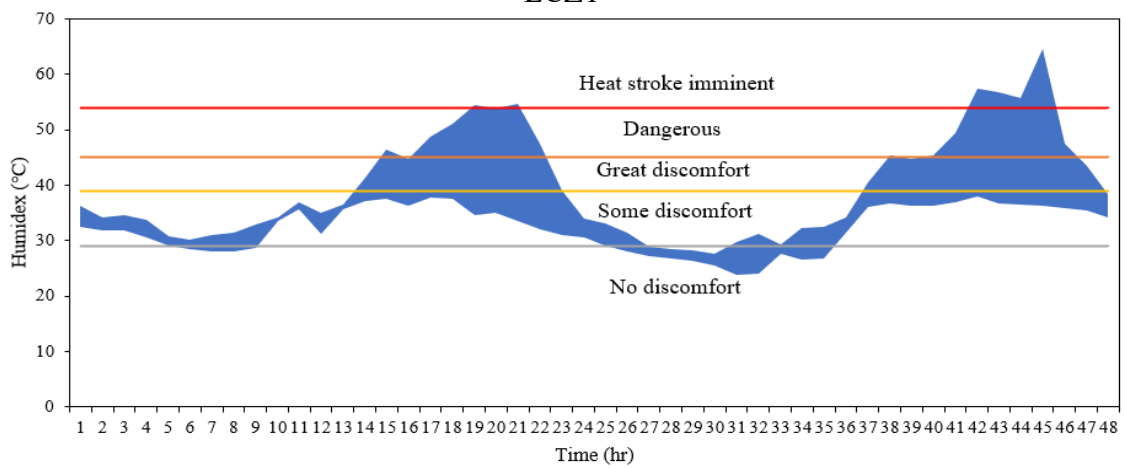
Figure 4.15. Comparison of averaged humidex.

Figure 4.16 shows the distribution of humidex. The blue part represents the humidex inside the selected locations within 48 hours during the heatwave. It could be found from the figures that in the LCZ6 area, no heatstroke will happen during the heatwave, while some parts of the LCZ1 and LCZ3 area under the pedestrian level may suffer from the risk of heatstroke. However, there is no obvious difference in the spatial and temporal distribution of humidex between the LCZ1 and the LCZ3 area (might find some reason from the urban morphology index).

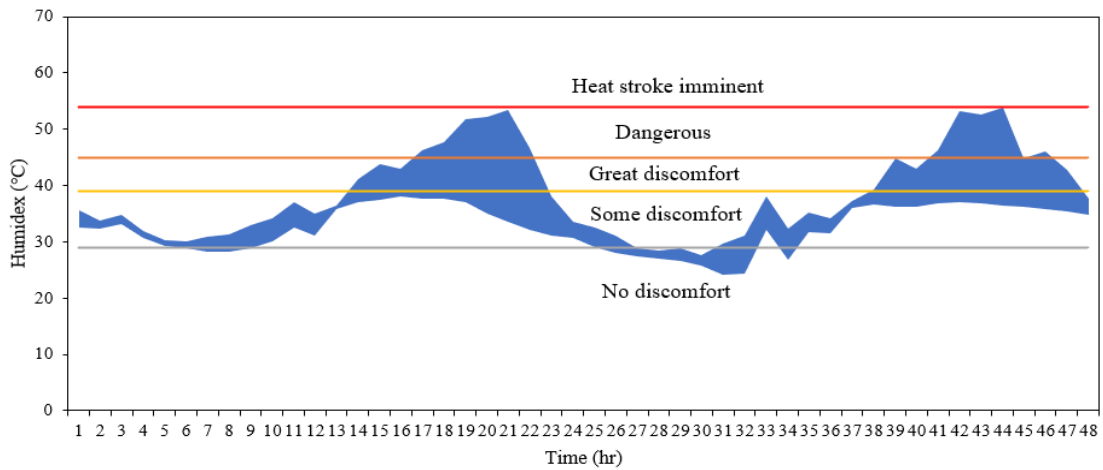
Some parts of the LCZ1 and LCZ3 sites will suffer from heat stroke from 16:00 to 20:00 on July 16th. For all three locations, from 13:00 July 15th to 13:00 July 16th, some parts of the locations will start suffering from great discomfort. For both LCZ1 and LCZ3, dangerous conditions are about 6 hours (from 16:00 to 22:00), but this time for the LCZ6 area can be about 4 to 5 hours. Thus, during the summer heatwave, no matter which urban area, it is suggested that residents go outside before 4 pm or after 10 pm, considering their thermal safety. It might even be fatal if residents go outside between 5 pm and 9 pm.



LCZ1



LCZ3



LCZ6

Figure 4.16. Distribution of humidex among different urban locations.

These results also illustrate the importance of conducting transient simulation for the entire urban area when studying the impact of the summer heatwave on the urban thermal risk or thermal comfort since the environmental parameters and thermal comfort conditions are highly spatially and temporally independent.

Figure 4.17 compares the duration of discomfort exposed during the 48-hour summer heatwave period. Most of the time, these three regions are under the same condition (some discomfort). The LCZ6 area has the longest duration under 'some discomfort' (82%) but the least duration under 'great discomfort' (7%). The LCZ1 area has the longest time duration for 'great discomfort', 21% of 48 hours. There is a dangerous risk for all the zones (above 45). It can be concluded that when an urban site has a large number of high-rise buildings, there will be more risk and longer time duration under the 'great discomfort' condition. For all three areas, the entire duration of 'no discomfort' and 'some discomfort' is almost the same. Although people located in LCZ6 areas experience less extreme heat conditions, they still encounter a long period of thermal discomfort.

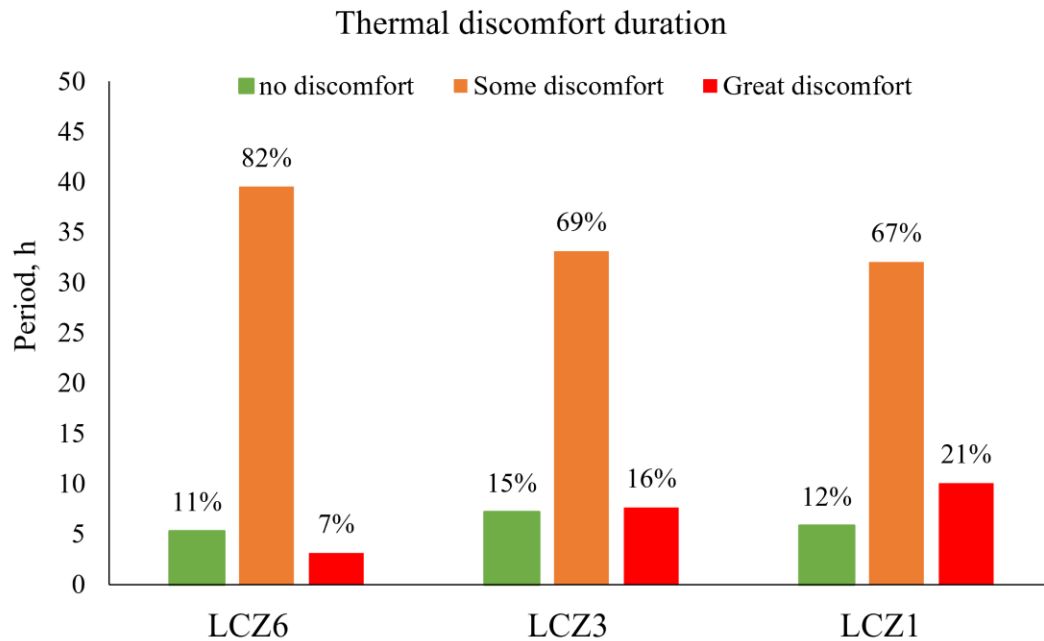


Figure 4.17 Thermal discomfort exposed duration comparison for 3 regions.

In Figure 4.18, maps of the 48-hour averaged velocity, temperature, and humidex are presented. For the three case studies, it is shown that the wind velocity near the building surface is low, while the temperature is large. Among all these three regions, the urban region has the highest wind velocity between buildings while the lowest airflow temperature and humidex are shown in the street canyon. Because of the low and sparse buildings in the LCZ6 location, the airflow is less heated by the buildings. On the other hand, the denser buildings in the LCZ1 and LCZ6 areas led to more heat sources inside the fluid area, which increased the airflow temperature. Meanwhile, the dense building arrangement will also reduce the wind speed inside the street canyon, which prevents the incoming wind from advecting away the heat absorbed by the solar radiation in the urban area. Air temperature spatial patterns are highly influenced by the street canyon geometry and orientation. In particular, the LCZ3 case study exhibits the largest values in obstructed alleys.

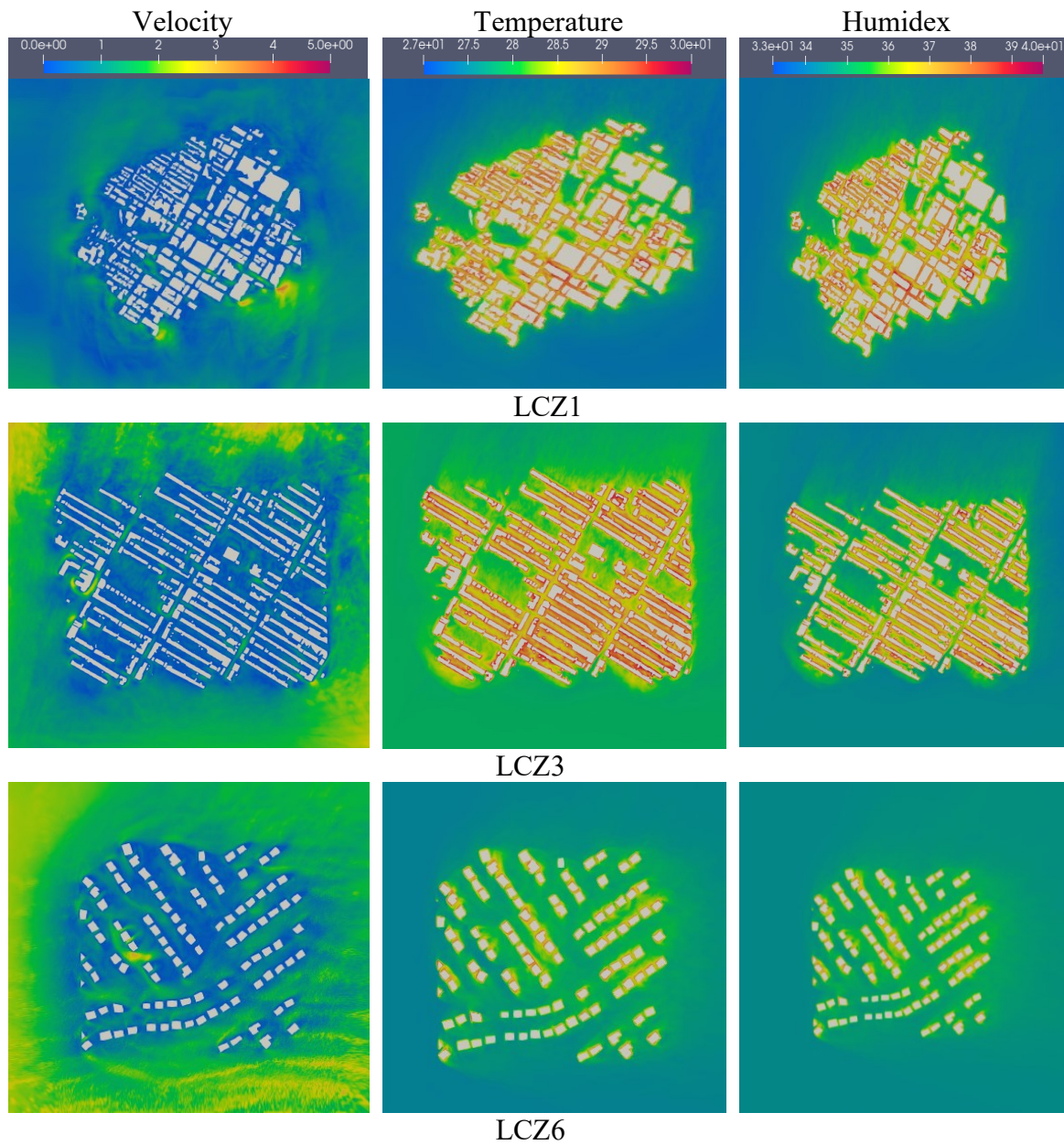


Figure 4.18. Maps of the 48-hour averaged velocity, temperature, and humidex for three case studies.

4.5 Conclusion

In this study, the authors proposed a novel strategy to investigate outdoor thermal discomfort during summertime heat waves using CityFFD/CityBEM. The system was set up over three urban landscapes in Montreal (LCZ 6, LCZ 3, and LCZ 1), and results were obtained during 48 hours on

July 15 and 16, 2013. Comparison of the results with onsite measurements at local weather stations highlights the relatively good accuracy of the method used to simulate the urban thermal environment. RMSE for temperature ranges from 0.5 to 1 degree, and RMSE for wind velocity ranges from 0.1 to 0.26 m s⁻¹.

Based on the validated results, the outdoor thermal, wind, and discomfort conditions of different urban morphologies during the 2013 summer heatwave are analyzed. Here are the main conclusions:

- During the daytime, higher and denser buildings can absorb solar radiation, and their surface temperature is higher than the surrounding airflow. They can also act as heat sources to increase the urban airflow temperature.
- At night, without solar radiation, the building surface temperature is close to the incoming flow air dry-bulb temperature. The airflow temperature inside urban areas is less impacted by the building arrangements.
- With simulated temperature and given moisture information, the thermal discomfort index humidex is calculated and analyzed. The LCZ 1 area has the most duration for great discomfort, 21% of 48 hours, and the LCZ 6 area has the least duration under great discomfort (7%). It can be concluded that the higher the density and elevation of buildings, the more risk and duration there will be for thermal discomfort.
- Meanwhile, the denser building arrangement will also reduce the wind speed inside a street canyon, which prevents the incoming wind from taking away the heat absorbed by solar in the urban area. It can also exacerbate the impact of urban morphology on thermal discomfort.

Chapter 5. Long-term Predictions of Urban Microclimate Impact on Building Energy Consumption

In this section, a machine learning model is developed using on-site monitoring results to establish correlations between public meteorological weather stations and the local urban microclimate. Recognizing the impracticality of conducting long-term simulations for urban regions due to elevated computational costs, the proposed machine learning approach stands as a viable alternative method for examining the impact of urban microclimate on building energy performance.⁴

5.1 Introduction

In the last decades, cities have faced significant challenges from rapid urbanization, mounting energy consumption, and increasing impacts of climate change, such as more heatwaves and other weather extremes [173,174]. By 2050, over 70% of the global population is estimated to live in urban areas [175]. There is an increasing need for energy to support the growing population, demand for better living environments, and rapid construction of residential and industrial buildings. Many of these human activities and their interactions with climate change occur inside the region of urban microclimate [24,176,177]. Urban microclimate refers to the immediate surrounding environment (vertical and horizontal) around building clusters inside the urban boundary layer with a height of 2~5 times the average building, where the close climate-building

⁴ This chapter is partially published in the conference paper: Prediction of the impact of Urban Environment on Building Energy by Artificial Neural Network. Senwen Yang, Dongxue Zhan; Jiwei Zou, Chang Shu, Ted Stathopoulos, Liangzhu (Leon) Wang. International Symposium on Heating, Ventilation and Air Conditioning 2023 Beijing, China (ISHVAC2023).

This chapter is also submitted to peer-reviewed journal: Urban Microclimate Prediction based on Weather Station Data and Artificial Neural Network. Energy and Buildings. Senwen Yang, Dongxue Zhan, Ted Stathopoulos, Jiwei Zou, Chang Shu, Liangzhu (Leon) Wang (2024).

interactions occur, including any climatic phenomenon of urban physics. Extensive research has consistently shown the crucial role of urban microclimate in building energy consumption [178][179]. Heat and mass exchanges between buildings and their surrounding environment significantly contribute to energy loads. In particular, local meteorological conditions near a building are the primary determinants of thermal exchanges through building envelopes in temporal and spatial resolutions [180,181]. Previous reviews summarize that urban microclimate could lead to a median rise of 19% in cooling energy usage and a median reduction of 19% in heating energy usage [182]. The impact varied in different cities, and cooling energy consumption increased from 10% to 120%, and conversely, heating energy consumption decreased from 3% to 45%. It was shown that daily temperature rise increased electrical energy consumption typically by 2.6% during a summer day [73]. The spatial difference of urban microclimate impact, as mostly manifested by urban heat island (UHI) intensity, was found to peak at the urban center and showed a decreasing urban-rural trend. It was indicated that the UHI can contribute to 15% to 200% cooling energy consumption increase [183]. The situation can be elevated during extreme weather. For example, a recent study by Hong et al. [49] showed up to 11 °C outdoor air temperature differences were observed between the coastal and LCZ1 areas in San Francisco during the record 2017 heatwave. Therefore, accurately estimating urban microclimate conditions is imperative for a better prediction of building energy consumption, especially in the context of climate change and increasing weather extremes.

The prediction of urban microclimate conditions for the purpose of building energy modeling has been challenging. The previous review [184] shows that most approaches used to develop building energy models neglect the UHI effect in neighborhoods. Instead, they rely on climate data from meteorological weather stations in more distant rural areas [185]. Recent research highlights that

the estimation of building energy usage varies significantly based on whether the UHI influence on the urban microclimate is considered. However, due to the challenges associated with obtaining accurate temperature data that incorporates the UHI effect and effectively modeling the resultant impact on building energy consumption, only a few studies have explored the interplay between urban microclimate and building energy performance. Most studies nowadays have not taken the impact of UHI into consideration [186].

The quantification of urban microclimate often relies on four approaches: field measurements and meteorological observations, wind tunnel experiments, CFD simulations, and recent developments in artificial intelligence (AI) and machine learning (ML) approaches [177]. A recent review study has documented AI and ML approaches and provided a detailed comparison of all the approaches [177]. Data-driven urban microclimate predictions have progressed well in recent years thanks to advancements in computing power for handling high-dimensional data. One of the first applications may date back to a study in 2016 [92], which categorized the local climate zones with various landscape features, and the number of applications increased in the following years. Artificial intelligence models were applied based on the parameters of interest, including multiple linear regression (MLR) [93][96], nonlinear regression (NLR) [97][96], random forest (RF) [93][96], and artificial neural networks (ANN) [95,98]. For predicting wind speed and wind power, Mortezaadeh et al. [99] adopted the machine learning method with CFD simulation results to assess the wind power potential in the urban region. According to a recent study by Alonso [93], multiple machine-learning models were developed to investigate the relationship between air temperature and different factors (vegetation, sky view factors, the density of water bodies, buildings, moisture, radiation, etc.), and the results showed satisfactory results. The performance of this model still needs further confirmation due to the lack of long-term testing data and multiple

location testing data. Recently, a recurrent neural network was applied to model the variation in time-series temperature under the urban street canyon. Zhang et al. [94] implement the long short-term memory (LSTM) model to forecast the wind speed, wind direction, relative humidity, and solar radiation and then apply the predicted weather parameters for building energy estimation. Their method shows more reliable energy estimation compared with the use of Typical Meteorological Year (TMY) weather data.

ANN was found to perform well in prediction in the urban microclimate [94,95]. Zhang et al. employed long short-term memory (LSTM) to predict urban microclimate and investigated its influence on buildings of different shapes [94,95]. Moghanlo et al. [187] utilized an ANN model to predict the impact of climate changes in the Zanjan region of northwest Iran. The study analyzed daily meteorological data from 2007 to 2018 and 1988 to 2018, considering observed variables such as maximum and minimum temperature and precipitation as predictors in the ANN. Xie et al. utilized an ANN model to predict the mean radiant temperature surrounding buildings [188]. Guijo-Rubio et al. [191] utilized an artificial neural network (ANN) model with three different neural structures to achieve highly accurate predictions of solar radiation using satellite image data. Shboul et al. [189] employed an ANN model to simultaneously predict hourly solar radiation and wind speed. These previous studies applied neural network models to predict the outdoor environment and show acceptable results. However, there are limited studies using ANN investigating the relationship between the rural meteorological weather station and local urban microclimate or heat island.

The process of this study can be divided into three sections: urban microclimate model development and training, local weather prediction and TMY generation, and building energy modeling. As shown in Figure 5.1, this study starts with weather data collected from publicly

available historical airport datasets and onsite collection by local weather stations. Then, an ANN model was trained and tuned to find the connection between airport weather (which is regarded as undisturbed weather) and local weather (weather under the urban microclimate impact). After obtaining the ANN model, the historical long-term weather data were used to generate the long-term local weather data with embedded urban microclimate information. A local TMY weather file was created by following the established statistics method for the building energy analysis by EnergyPlus [190] of the DOE archetype buildings [191].

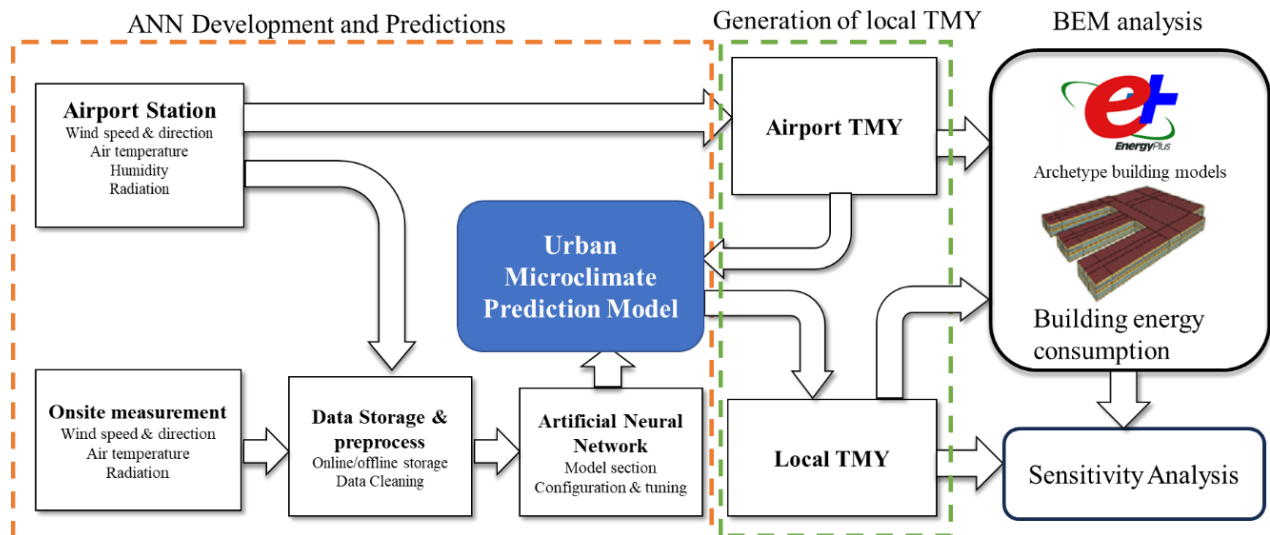


Figure 5.1 Overall schematic for using ANN to estimate building energy.

5.2 Methodology

5.2.1 ANN model for urban microclimate

The ANN model has been used in several studies on urban microclimate [187,188,192,193], which showed that the ANN model can perform well in urban weather prediction. Moghanlo et al. [41] utilized an ANN model to predict the impact of climate change. Xie et al. [42] developed an ANN

model to evaluate the mean radiant temperature surrounding buildings. Zhang et al. [48] evaluated the impact of microclimate on urban microclimate via the ANN model. The ANN model is reported to have good performance compared to other proposed models in solving the problems related to urban microclimate [96, 98, 196]. Thus, this study applied methods similar to those used in previous studies to the current topics, which have not been covered in these previous studies. This study starts with an ANN model with multiple layer perceptron, and its performance was compared to that of other basic machine learning models such as linear regression and random forest.

In this study, airport weather conditions were used as input parameter, while the wind speed, wind direction, and air temperature from local weather station were considered as predicted features of urban microclimate, and multiple layer perceptron (MLP) [189, 195, 197] was used to training the model, as shown in Figure 5.2. By tuning the existing model, the optimized ANN structure consists of one input layer with 24 input neurons, two hidden layers with 40 and 20 neurons, respectively, and one output layer with three neurons for wind speed, direction, and temperature. To consider the thermal storage of the urban underlayer, six hourly data lookback is adopted in the model inputs shown in Figure 5.2. After tuning the model with different dataset settings, including the training dataset random sampling or continuous data of several months as the training dataset, it was found that the proposed approach would not increase the prediction accuracy anymore when adopting more training data than three months. During the tuning, 70% percent of the data was used for training, the rest was for testing and validation. From the testing with model performance with different dataset settings, the accuracy no longer improves when training data involves more than 3 months. This approach focuses on how weather parameters affect the temperature and wind difference between the local environment and the airport. During the training and testing, all the parameters are scaled based on the minimum and maximum values. The model performance in

extreme weather (heatwave) is highlighted in Figure 5.5 and Figure 5.6. The performance for the whole year including hot weather and cold weather is evaluated.

As for the input parameters, temporal weather data from the airport are applied as input. The output labels are the local air temperature, wind speed, and wind direction. Meanwhile, the performance of MLP will be compared with basic machine learning models like multiple linear regression [93,96] and random forest [96,99] used in the previous urban microclimate studies. Comparing an ANN to a basic model provides a benchmark for evaluating the performance of the ANN. Suppose the ANN does not significantly outperform simpler models such as Linear Regression or Random Forest. In that case, it might indicate that the problem is not complex enough to warrant using ANN. Besides, ANNs are prone to overfitting, especially when the dataset is small or the architecture is too complex. Comparing against simpler models helps gauge whether an ANN truly captures meaningful patterns. This study will also compare the proposed method to the LSTM model used in the previous study [94] to see if a more complicated model is required.

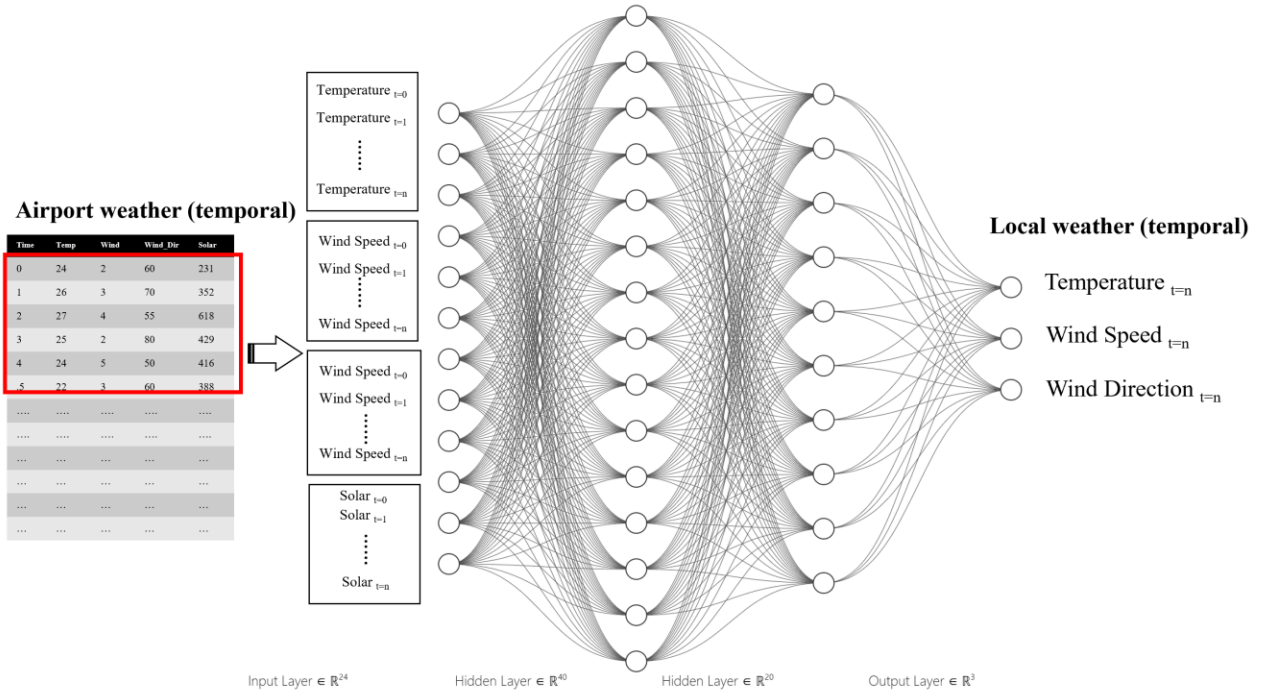


Figure 5.2 Structure of proposed ANN model.

Meanwhile, the accuracy of the model has been tested by calculating the mean absolute error (MAE) in Eq. 5-1 and the correlation coefficient (R^2) of Eq. 5-2. Root mean square error (RMSE) in Eq. 5-3 and Mean absolute percentage error (MAPE) of Eq. 5-4 are also adopted for evaluate wind speed and wind directions.

$$MAE = \frac{\sum_{i=0}^n |y_i - \hat{y}_i|}{n} \quad \text{Equation 5-1}$$

$$R^2 = 1 - \frac{\sum_{i=1}^n (y_i - \hat{y}_i)}{\sum_{i=1}^n (y_i - \bar{y}_i)} \quad \text{Equation 5-2}$$

$$RMSE = \sqrt{\frac{1}{n} \sum_{i=1}^n (y_i - \hat{y}_i)^2} \quad \text{Equation 5-3}$$

$$MAPE = \frac{1}{n} \sum_{i=1}^n \frac{|y_i - \hat{y}_i|}{y_i} \times 100\% \quad \text{Equation 5-4}$$

5.2.2 Onsite data measurement

According to Figure 5.3(a), the study investigated five weather station locations labeled LOC1, LOC2, LOC3, LOC4, and LOC5. These 5 local weather stations are located in 5 schools in the Montreal area. Weather stations use a logger with an LCD screen (HOBO Onset RX3004) and GSM/HSPA cellular communication capability. The chosen weather station (refer to Figure 5.3(b)) consists of various sensors, such as a temperature and humidity sensor (S-THB-M002), pyrometer (S-LIB-M003), wind speed sensor (RM Young Wind Monitor Sensor), wind direction sensor (RM Young Wind Monitor Sensor), and rainfall sensor (S-RGB-M002). These sensors generally measure temperature, wind speed, and wind direction in specific ranges and conditions. It provides a resolution of 0.02°C at 25°C and a temperature accuracy of 0.21°C between 0°C and 50°C. A wind speed range of 0 m/s to 76 m/s can be measured with an accuracy of 1%. The wind direction sensor covers a range of 0° to 355° with a 5° dead band and has an accuracy of ±5°. The installation area was chosen clear of obstructions, HVAC equipment, and exhaust fans to avoid interference with the sensors. Positioning the tripod away from the roof's edge during installation is important to ensure safety. This minimizes the impact of turbulence caused by the roof's edge on wind speed and direction sensors. Using concrete anchor bolts, the feet of the weather station tripod are attached to 12 kg concrete blocks. To protect the roof, the tripod's feet and blocks should be placed on rubber mats, while its legs should remain as level as possible. A total of three guy wires, each 4 meters long, are used to secure the tripods. More than 50 kg of weight is connected to these wires.

For the wind monitor to be placed 3 meters above the roof, the tripod mast is vertically leveled using a bidirectional post level. In a previous study, detailed information can be found [195].

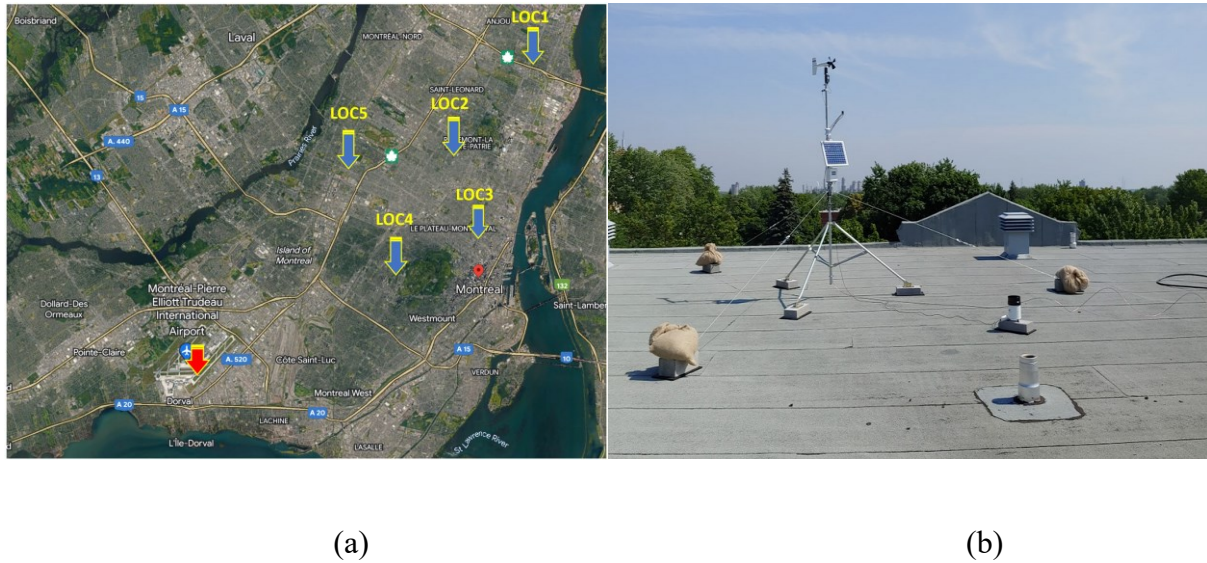


Figure 5.3 (a) Location and installation of roof-mounted weather stations (b) weather station sensors and configuration and installation in LOC1.

5.2.3 Local TMY generation

A Typical Meteorological Year (TMY) is a dataset that represents the long-term average meteorological conditions for a specific location over a one-year period. TMY datasets are commonly used in the field of building energy simulation, solar energy assessment, and other applications where accurate and representative meteorological data are essential.

The TMY dataset is typically derived from actual historical weather data, often spanning 10 to 30 years. However, instead of using the entire historical record, a TMY dataset is created by selecting specific months or days from different years that, when combined, provide a "typical" representation of the climate conditions for that location. The selection process for creating a TMY

dataset involves choosing days or months that are statistically representative of different weather conditions, including typical solar radiation levels, temperatures, wind speeds, and other relevant parameters. The goal is to create a dataset that captures the variability and characteristics of the local climate but in a more condensed and manageable form. Environmental Impact Assessment TMY datasets are used in environmental impact assessments for various projects to understand the potential effects of climate conditions on the environment. TMY data are used to simulate the energy performance of buildings over a year, helping architects and engineers design energy-efficient structures. Heating, ventilation, and air conditioning (HVAC) system designers use TMY data to assess the energy requirements for climate control in buildings.

To evaluate the urban microclimate over a long period of multiple years, the typical meteorological year (TMY) method, a commonly used reference year selection method, is adopted to assess climate impacts. The TMY method was developed by selecting 12 months of weather data from a long-term dataset of at least ten years to represent the typical weather conditions for a specified location instead of considering each year inside the selected period. This method can avoid the need to consider the impact of the specific yearly climatic variation and significantly reduce the computational cost and repetitive labor work [196,197]. In this study, both the airport and local typical meteorological year (TMY) were created based on the EN ISO 15927-4 standard [198,199], which is a combination of multiple typical meteorological months (TMM). TMMs are selected by comparing each month's distribution with that month's long-term distribution for the available climate dataset through the Finkelstein–Schafer statistics based on air temperature, global horizontal irradiance, relative humidity, and wind speed. The detailed procedure for TMY generation in this study is shown below.

First, for a single climate variable and target calendar month, the cumulative distribution function for the selected-year y ($SY(y, i)$) and whole-years dataset ($WY(y, i)$) are calculated by Equation 5-5 and Equation 5-6:

$$SY(y, i) = \frac{S(A_i)}{n + 1} \quad \text{Equation 5-5}$$

$$WY(y, i) = \frac{W(A_i)}{N + 1} \quad \text{Equation 5-6}$$

Where, i is the calendar day of the calendar month, A_i is the daily mean of the selected climate variable at day i , $S(A_i)$ is the rank order of A_i within the calendar month of the selected-year dataset, n is the number of days in the calendar month, $W(A_i)$ is the rank order of A_i within the calendar month of the whole-year dataset, N is the number of days in the calendar month in the whole-year dataset.

With $SY(i)$ and $WY(i)$ in the above equations, the Finkelstein –Schafer statistic for each calendar month could be calculated:

$$Fs(y) = \sum_{i=1}^n |SY(y, i) - WY(y, i)| \quad \text{Equation 5-7}$$

For each climate variable and each calendar month, we obtain the rank score for each year inside the whole-year dataset based on the $Fs(y)$ value. Repeat the above procedures for parameters including air temperature, relative humidity, global horizontal irradiance, etc., and then calculate the sum of $Fs(y)$.

5.2.4 Building Energy Model

Building Energy Modeling (BEM) technologies, developed over decades, play a crucial role in building design, optimization, construction, operation, and research. Commercial BEM tools like TRNSYS, EnergyPlus, and ESP-r primarily utilize physical models (white box modeling) for accurate predictions during a wide range of operating conditions without additional measurement data. These physical models are ideal for the building design stage. In this study, EnergyPlus will be adopted for building energy modeling.

The reference building energy model (BEM) for a primary school building was chosen as the case study for Climate Zone 6A, the Cold-Humid Climate. The reference model was developed by the U.S. Department of Energy (DOE) [200], and in this study, the location of the building is Montreal, Quebec, Canada. To be consistent with the building type of the measurement locations, the primary school archetype from DOE reference models was selected. The primary school building comprises classrooms, a multipurpose room, a cafeteria, and a kitchen with a main corridor and three classroom zones, as shown in Figure 5.4. Specifically, it is a single-story structure with a Gross Floor Area of 6,871 m² (approximately 73,959 ft²) equipped with a Variable Air Volume (VAV) system for 25 zones. The floor-to-ceiling height is 4 meters, and the window-to-wall ratio is 35%. The building properties are defined with the U-factors for the roof of 0.18 W/(m²K), external walls of 0.31 W/(m²K), and windows of 2.65 W/(m²K) with a Solar Heat Gain Coefficient (SHGC) of 0.43. The infiltration rate is 0.46 m³ per m² floor area (1.5 ft³/ft²). The heating setpoint is maintained at 21°C from 6:00 AM to 9:00 PM and 16°C at other times, while the cooling setpoint is 24°C during operational hours and 27°C during non-operational hours. The building occupancy density varies across different spaces, with classrooms allowing 4 m²/person, corridors 10 m²/person, and offices 20 m²/person. In the building energy simulation, there are several

assumptions for analysis of the impact of urban microclimate. The main parameters considered in this study are air temperature, wind speed, and wind direction. The solar radiation is assumed to be the same as the airport data since the local weather station is installed at the top of the roof. Additionally, the shading effect of the surrounding buildings is not covered in this study.

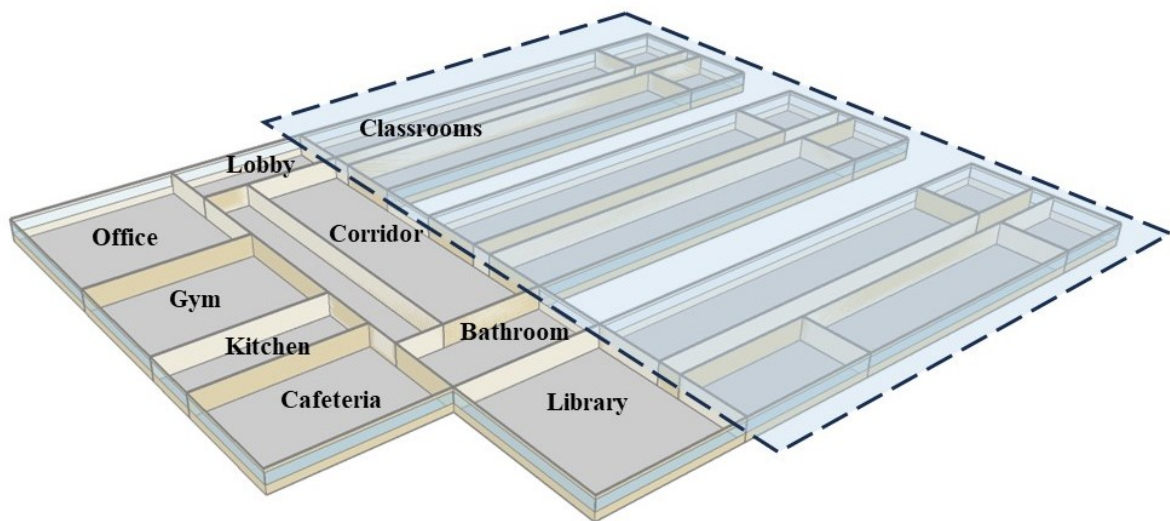


Figure 5.4 DOE Building archetype of primary school.

5.2.5 Sensitivity analysis

To determine the significance of meteorological parameters, we applied a sensitivity analysis (SA) to evaluate the impact of meteorological parameters on the energy performance of buildings by using the Sensitivity Value Index (SVI) method. This method combined three sensitivity techniques: the Standardized Regression Coefficient (SRC), Random Forest Variable Importance, and t-value analysis [201]. The SRC method relies on regression and is commonly used in building energy assessment. A higher SRC value indicates greater importance of the variable. The Random

Forest Variable Importance measures how a model's accuracy is affected by including or excluding a variable, indicating its contribution to output values. The t-value assesses whether the coefficient of a corresponding variable is statistically different from zero. A higher absolute t-value suggests a greater importance of the variable [202]. SRC and t-value are suitable for linear models. The SVI method, as represented by Eq. 5-8 [203], comprehensively evaluates the contribution levels of input parameters, and the sensitivity analyses' results were normalized and combined. This approach ensured a more consistent and aggregated assessment of parameter significance. The candidate meteorological parameters in this study were air temperature, wind velocity, wind direction, relative humidity (RH), diffuse solar radiation, normal solar radiation, and global solar radiation.

$$(SVI) (\%) = \sum_{l=1}^m \frac{\sum_{j=1}^k \left(\frac{V_{i,j}}{\sum_{i=1}^n |V_{i,j}|} \right)}{\frac{k}{m \cdot k}} \times 100 \quad \text{Equation 5-8}$$

where V is the value of a sensitivity analysis method, i is a parameter, n is the total number of the parameters ($n=7$), j is a sensitivity method, k is the total number of sensitivity methods ($k=3$: SRC, random forest variable importance, and T-value), l is the target output, and m is the total number of target outputs ($m=1$: building energy consumption load, repeated for three times for winter, summer and total).

5.3 Results and Discussion

5.3.1 Temperature prediction

Table 5-1 compares the performance based on the coefficient of determination (R²), Mean Absolute Error (MAE), and Root Mean Square Error (RMSE). Compared to the MLR and RF

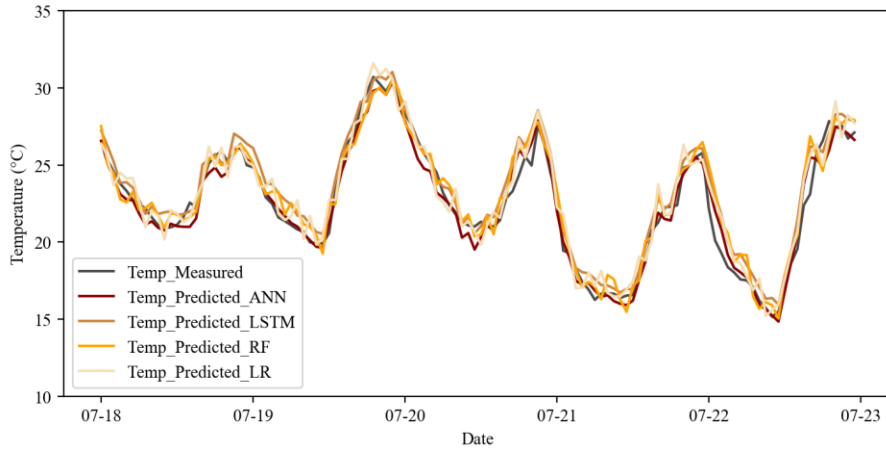
models, the proposed MLP model performs better. Air temperature prediction using the MLP model has an MAE of 0.52 and RMSE of 0.68 degrees, with an R^2 of 0.996. Compared to the literature [93,94], it shows acceptable results. Existing MLP methods still perform better when predicting air temperatures than LSTM methods. Complex neural network models such as LSTM may have worse performance than basic MLP models when solving simple physical problems.

Table 5-1 Machine learning model performance of temperature predictions

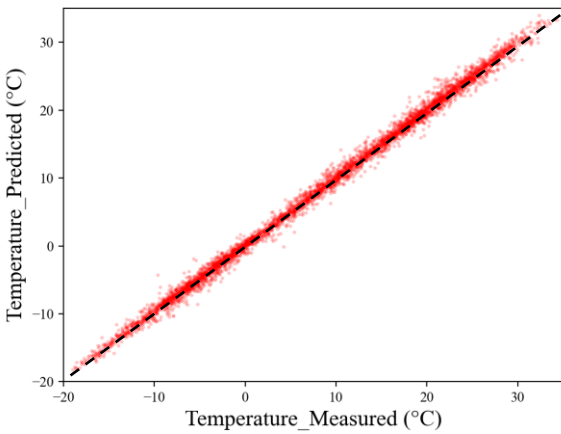
	MLR	RF	LSTM	ANN(MPL)
R^2	0.97	0.96	0.99	0.996
MAE	0.92	0.88	0.68	0.52
RMSE	1.22	1.01	0.85	0.68

Figure 5.5 shows the air temperature comparison between the measurement data and model prediction results for LOC1 in the testing dataset. Figure 5.5 (a) presents four training models for predicting the air temperature. The four models can capture the trend of temperature temporal variation during the five continuous summer days. Among them, the ANN model has the most accurate prediction. Figure 5.5 (b) compares the predicted and measured temperature testing datasets. The prediction shows good agreement with the measurement data. The most error between the measurement and prediction is located ranging from $-0.5\text{ }^{\circ}\text{C}$ to $0.5\text{ }^{\circ}\text{C}$, meanwhile, the sensor measurement accuracy is around $0.2\text{ }^{\circ}\text{C}$. In this study, 5 locations are investigated and trained with different models. The temperature prediction performance is presented in Table 5-2. All the locations and models can achieve R^2 for more than 0.99 and MAE around $0.5\text{ }^{\circ}\text{C}$. It illustrates that the proposed method for predicting air temperature can be applied to different

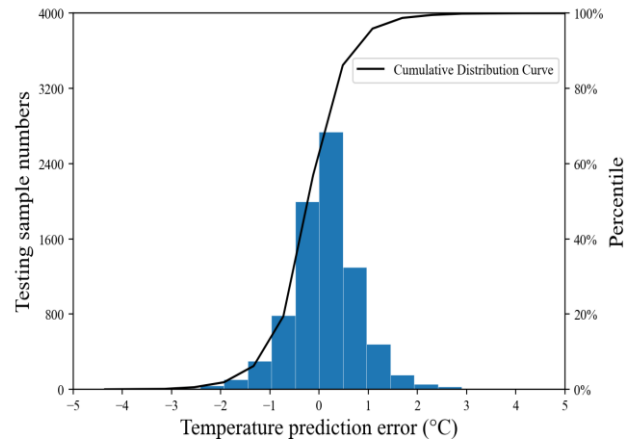
locations. It should be noted that the trained model may be limited to predicting at its own sites, and the model may need to be retrained for another location.



(a)



(b)



(c)

Figure 5.5 (a) Air temperature comparison between prediction and measurement from June 18th to 23rd (b) air temperature prediction accuracy in the testing dataset. (c) air temperature error distribution at LOC1.

Table 5-2 ANN model performance at multiple locations.

	R²	MAE	RMSE	MAPE
LOC1	0.996	0.52	0.68	3.15%
LOC2	0.994	0.54	0.71	3.21%
LOC3	0.995	0.53	0.69	3.08%
LOC4	0.992	0.59	0.8	4.01%
LOC5	0.994	0.55	0.72	3.65%

5.3.2 Wind Speed Prediction

Figure 5.6 (a) shows the effect of urban microclimate on wind speed in LOC1. Between July 18th and July 23rd, the predicted wind speed was consistent with the measured wind speed. Wind prediction is also found to be close to the estimation based on wind power law profile with urban exposure calculated from airport wind speed [204].

$$\frac{V_Z}{V_{Z_g}} = \left(\frac{Z}{Z_g} \right)^\alpha \quad \text{Equation 5-9}$$

Where Z_g is the gradient height, V_{Z_g} is the velocity at gradient height, and α is the roughness exponent. Z_g , and α are functions of ground roughness.

According to Figure 5.6 (b), the prediction errors range from -0.4 m/s to 0.6 m/s, which is acceptable for urban microclimate prediction [96, 97]. Wind speed prediction and power law calculation are compared with measured true data and it shows that the wind speed can have an accuracy of around 0.5 m/s. Considering the difficulties in predicting the temporal wind speed due to the turbulence, as well as the wind sensor accuracy (around 1.1 m/s), close to the previous study

[205], the performance of wind speed prediction might be improved if higher accuracy wind data can be achieved.

Table 5-3 shows the wind speed prediction performance for all 5 locations. The overall R^2 for all locations ranges from 0.5 to 0.6, and the MAE is around 0.5 m/s. It is more challenging to predict wind speed accurately than air temperature because of turbulence and magnitude fluctuation. Another potential reason could be the wind speed measurement accuracy [25]. Data quality and model performance may be improved by using more precise sensors. ANNs are also more accurate at most locations than power law estimations based on roughness calculations. However, based on the R^2 of wind speed prediction, there is still room to improve the ANN model.

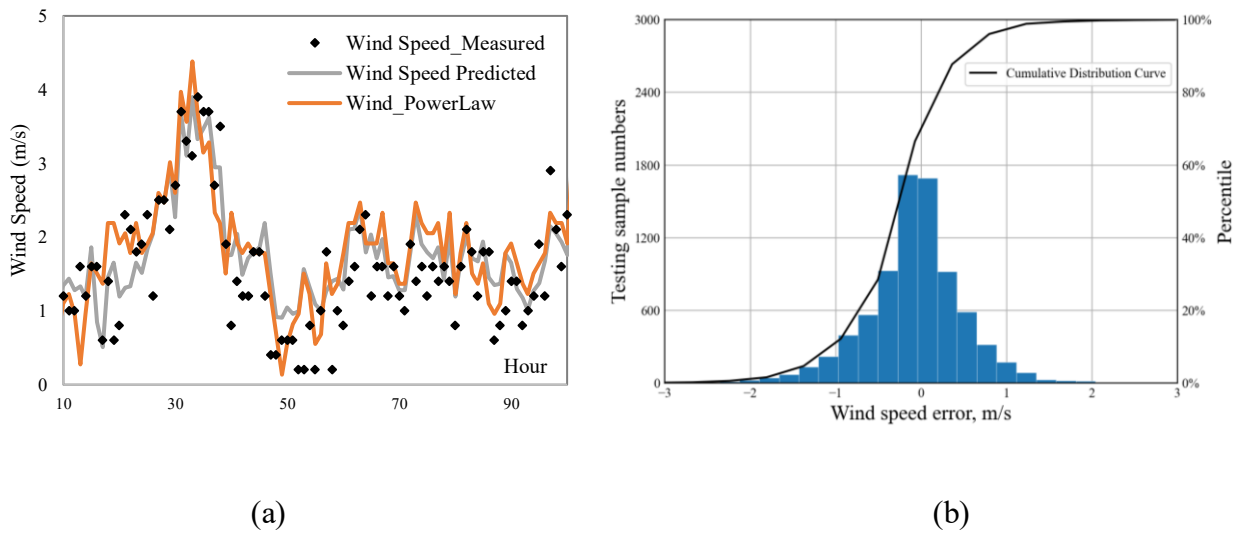


Figure 5.6 (a) Wind speed comparison between measured, predicted and calculated from power law distribution, (b) wind prediction error distribution for LOC1.

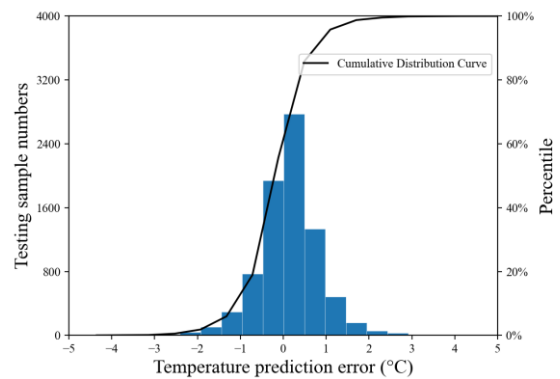
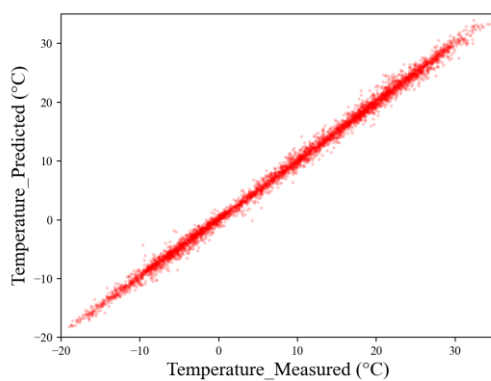
Table 5-3 Wind speed performance and error in all 5 locations

	ANN	Power Law
--	-----	-----------

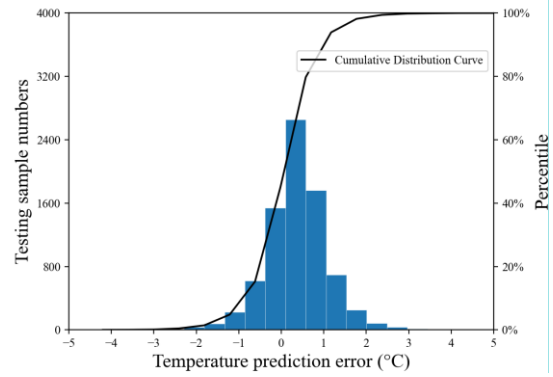
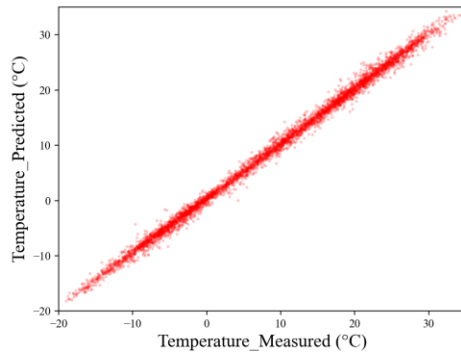
	R ²	MAE (m/s)	α	R ²	MAE (m/s)
LOC1	0.67	0.55	0.25	0.61	0.62
LOC2	0.62	0.62	0.35	0.65	0.58
LOC3	0.66	0.52	0.35	0.68	0.55
LOC4	0.56	0.81	0.35	0.53	1.04
LOC5	0.52	0.87	0.3	0.49	0.92

Figure 5.7 shows the model performance for other locations (LOC2-LOC5), the temperature predictions show good performance, and most of the errors are located within the range from -1 to 1 degree. This figure shows that this method can be applied in different locations.

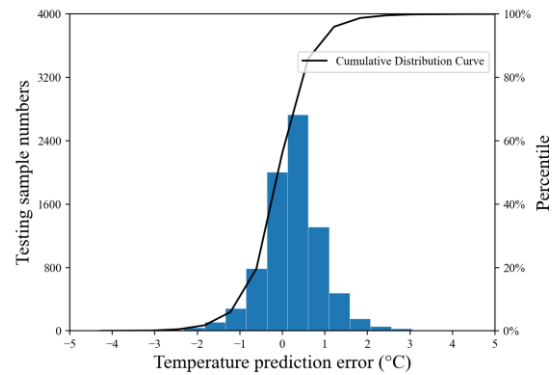
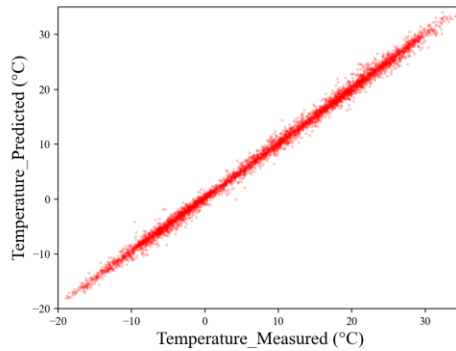
LOC2



LOC3



LOC4



LOC5

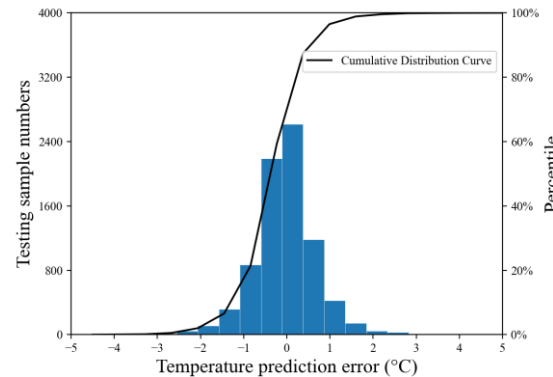
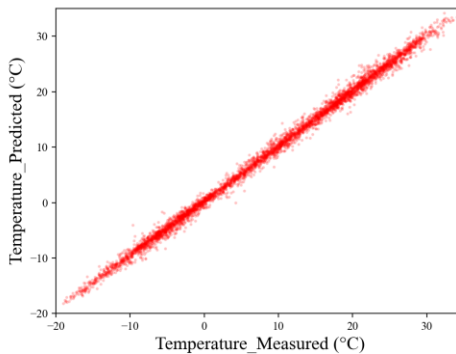
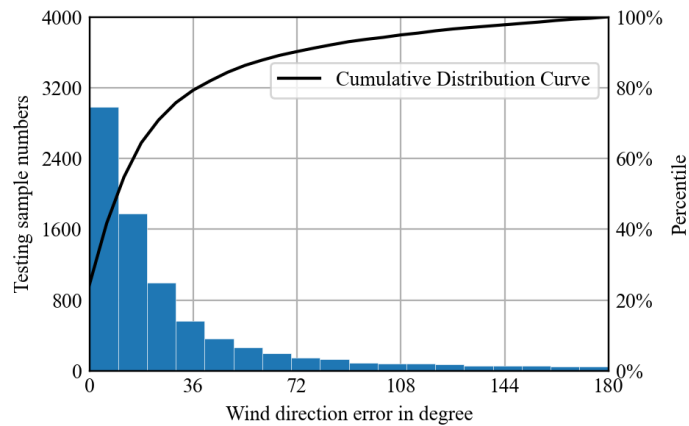
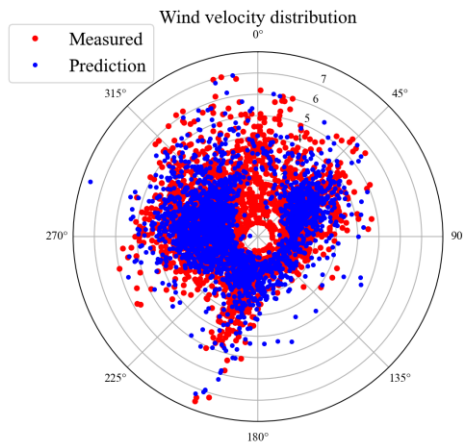
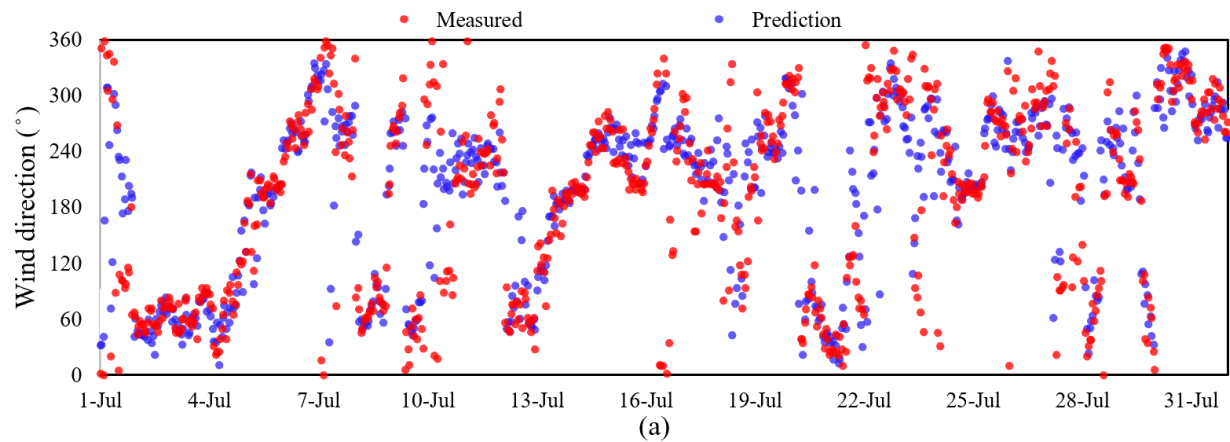


Figure 5.7 Wind speed comparison and wind prediction error distribution for all other locations.

5.3.3 Wind Direction Prediction

Figure 5.8 shows the performance of the wind direction prediction in LOC1. For the North, wind direction is "0", and wind direction in degree increases counterclockwise. Based on Figure 5.8 (a), there is good agreement between measured results and predicted results for the hourly wind

direction. According to Figure 5.8 (b), the overall wind frequency in both magnitude and direction in LOC1 shows a good match for the wind's direction and magnitude. Most of the wind comes from the west direction, 225 to 325. According to Figure 5.8 (c), the majority of wind direction errors fall between 0 and 36 degrees. Similarly, prediction results for other locations are presented in Figure 5.9.



(b)

(c)

Figure 5.8 (a) Temporal wind direction performance in July (b) wind rose for testing dataset comparing the measured and predicted wind direction (c) wind direction prediction error distribution for LOC1.

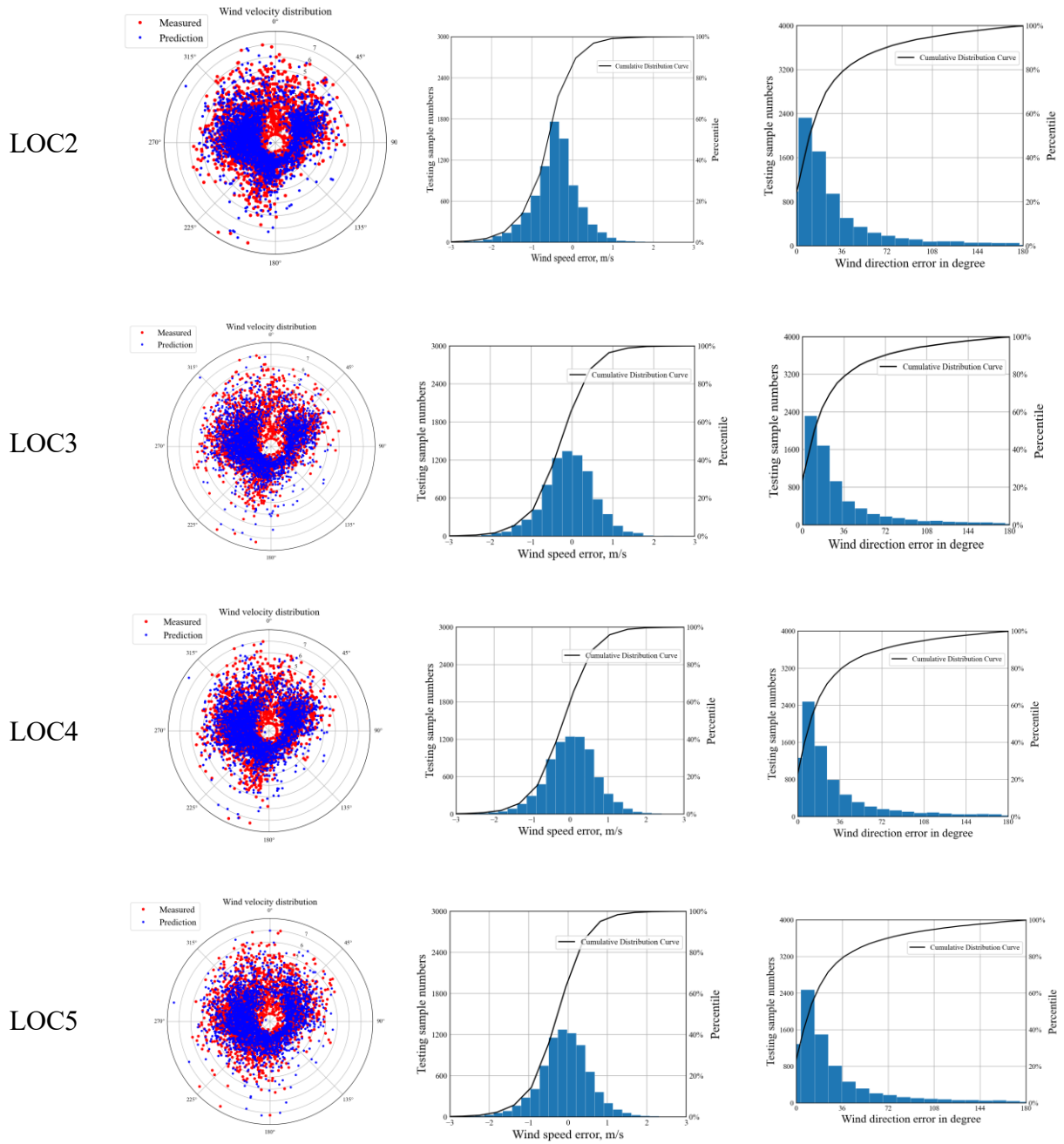


Figure 5.9 Wind direction comparison and wind direction prediction error distribution for all other locations

Table 5-4 shows the wind direction prediction performance for all five locations. Predicted urban MAE, RMSE, and MAPE calculations are presented for wind direction. Overall, LOC3 appears to have the most accurate predictions with the lowest errors, while LOC5 has the least accurate predictions with higher errors. The MAE, RMSE, and MAPE values provide insights into the accuracy and performance of the model at each location. All 5 locations have an MAE close to 30 and an RMSE close to 40 for wind direction, which can be regarded as satisfying results compared to previous machine learning results [94].

Table 5-4 Wind component and directions for 5 locations.

	MAE (degree)	RMSE (degree)	MAPE
LOC1	35	41	9.7%
LOC2	30	35	8.3%
LOC3	27	31	7.5%
LOC4	31	38	8.6%
LOC5	36	43	10.0%

5.3.4 Local TMYs

In urban microclimates, long-term weather can be predicted with acceptable accuracy using projections from long-term historical weather data from airports. The study collects historical weather records from 1997 to 2018 from the same location as the model training (Montréal-Trudeau International Airport). The TMY was calculated based on the weather at Trudeau International Airport for the past 20 years. The first step in obtaining the localized monthly data was to use historical weather station data for projections of local weather with our ANN-trained

model in this study over the past 20 years. After projecting 20 years of microclimate data, the TMY algorithm will produce one-year weather conditions, i.e., local TMY with microclimate information embedded, based on the past 20 years.

A comparison is shown in Figure 5.10 (a) between the traditional TMY results from the airport and the generated local TMY of LOC1. The local temperature from the airport can be up to 8 °C after the TMY algorithm at the airport from July 18th to July 23rd. It was found that urban microclimates under the TMY are different from the airport, which causes traditional methods to underestimate urban outdoor thermal comfort and building energy consumption. The average temperature difference is 3.3 °C between the local and airport during this period. The temperature peak delay in urban microclimate can be observed, which could be caused by the building and road thermal mass. A comparison of wind velocity between airport TMY and local TMY is shown in Figure 5.10 (b). Based on the TMY scale, there is a significant discrepancy between the wind speed at the airport and the local region (scaled on the same elevation by power law). As a result, when evaluating the overall building energy consumption, the wind pressure and CHTC around the building facade can be affected. Hourly comparison of wind direction is not conducted since the TMY method selects wind based on different years, and the variation of wind direction may not make the wind direction consistent in the two TMY methods.

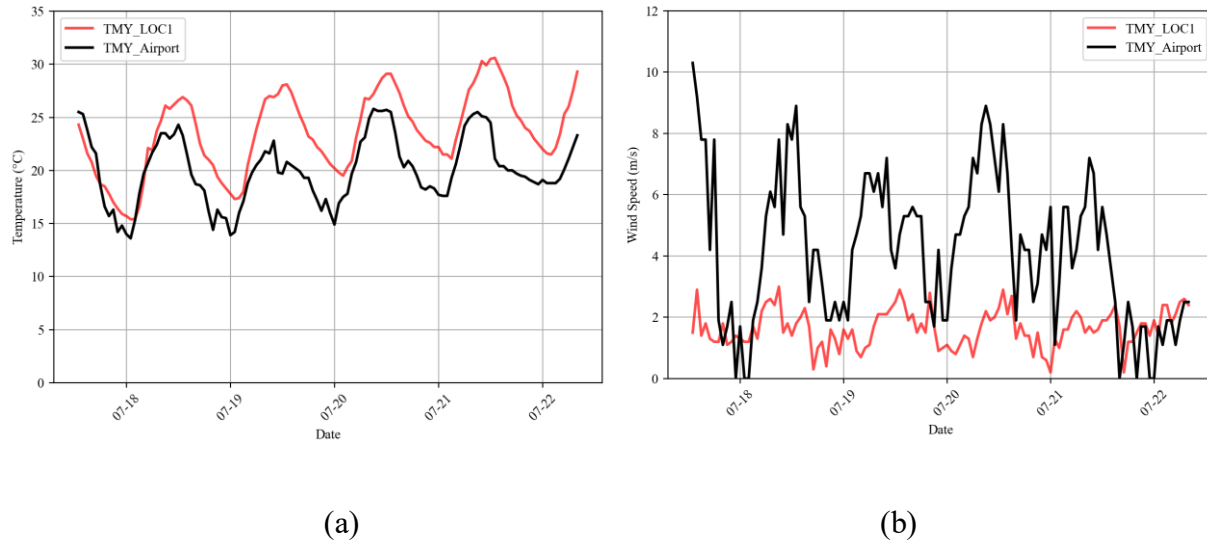


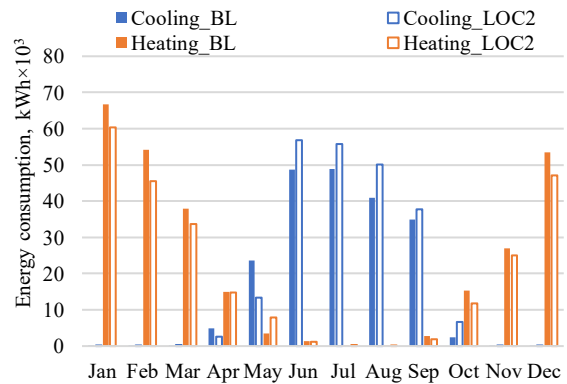
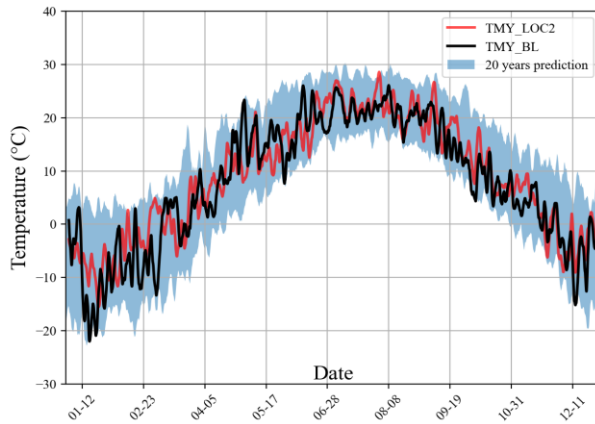
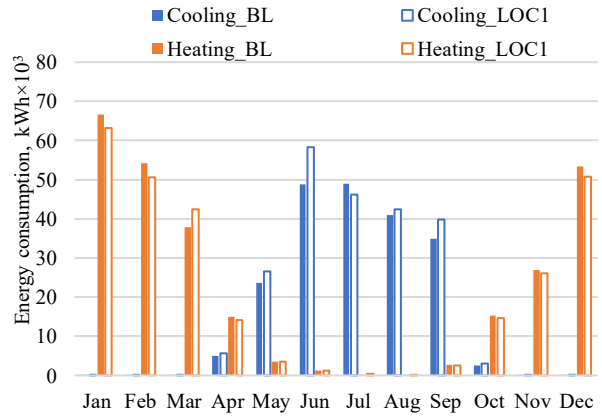
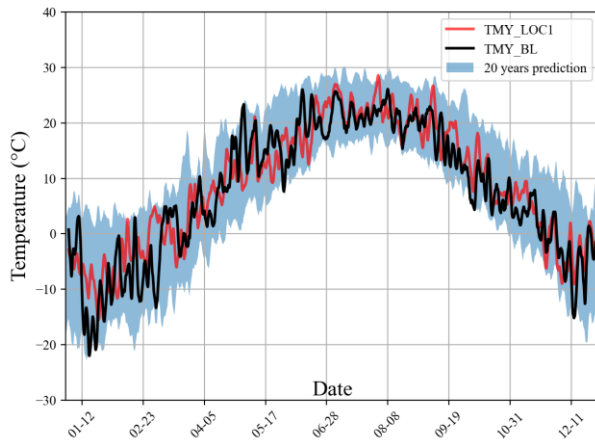
Figure 5.10 TMY air temperature (a) and wind speed (b) at LOC1 from July 18th to 23rd

5.3.5 BEM analysis

In this study, EnergyPlus evaluates building energy consumption based on the local TMY from 20 years of weather predictions for five individual locations. In Figure 5.11, 20 years of weather predictions (e.g., TMY_LOC1) and baseline TMYs (TMY_BL) were calculated from 20 years of airport weather. In addition, the figure presents an evaluation of the cooling and heating loads on an annual basis. There appears to be a trend in the color band between the 20-year airport temperature and the 20-year local prediction temperature for four locations: LOC1, LOC2, LOC3, and LOC5. However, LOC4, which is located near a mountain park at high elevation, is less affected by urban microclimate than other locations. For LOC4, there is a full overlap between the 20 years of airport air temperature distribution and predicted local temperature. This indicates that the urban microclimate has the least impact at LOC4 than other locations.

In each month's analysis of heating and cooling energy, it is determined that 4 of 5 locations affected by urban microclimate will consume more cooling energy in the summer and less heat

energy in the winter due to the higher ambient temperature caused by urban heat islands. Different seasons are affected differently by the urban heat island or urban microclimate. The energy consumption for LOC1-5 has less impact on building energy in spring and fall, when there is less need for cooling or heating. The urban microclimate can have a significant effect on cooling energy, especially in June and July. However, for LOC4, where the ambient temperature differs less from the airport baseline, energy consumption is also close to the airport baseline, and urban microclimate impact becomes minimal compared to other locations.



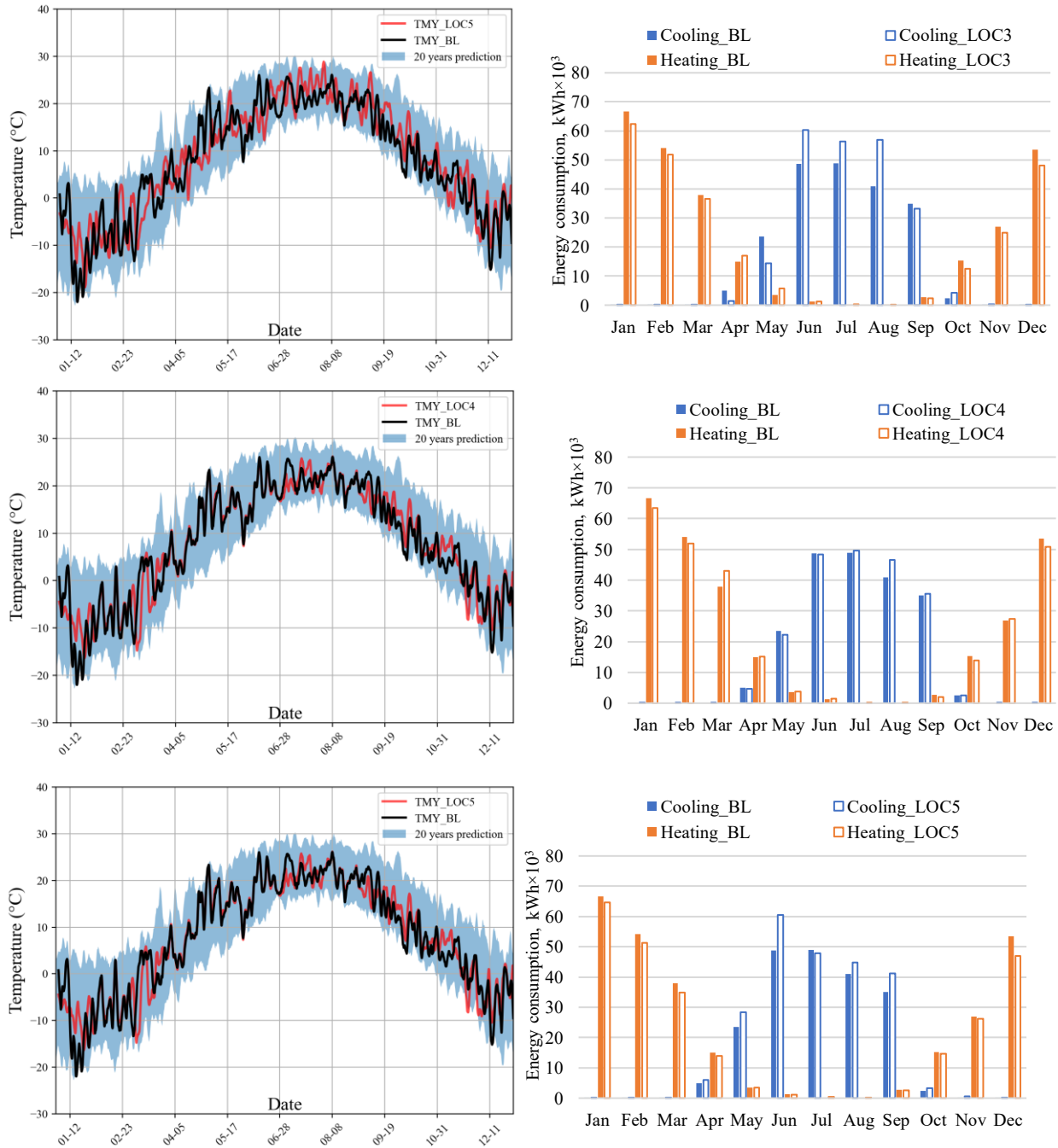


Figure 5.11 Local 20 years weather prediction air temperature variation and related TMY and related annual cooling load and heating load evaluation for 5 Locations (LOC 1-5).

Based on TMY weather from the airport, Figure 5.12 illustrates an increase in cooling and a decrease in heating energy consumption. In this case study, the urban microclimate reduced winter

heating energy consumption by 1% to 10%. Furthermore, it also increases cooling energy consumption by 2% to 14%. This not only shows that urban microclimate significantly impacts energy consumption [182] but also indicates that inside the same city, the spatial difference can also be great.

As a result of the spatial distribution of microclimate effects in Montreal, there is a noticeable spatial variation in energy consumption across locations. Urban heat islands have a lesser impact in places like LOC4, which are situated near mountains and parks. On the other hand, LOC3, located in densely populated areas, is more profoundly affected by the urban microclimate within a proximity of less than 5 km. Consequently, cooling energy consumption at LOC3 has increased by 11%.

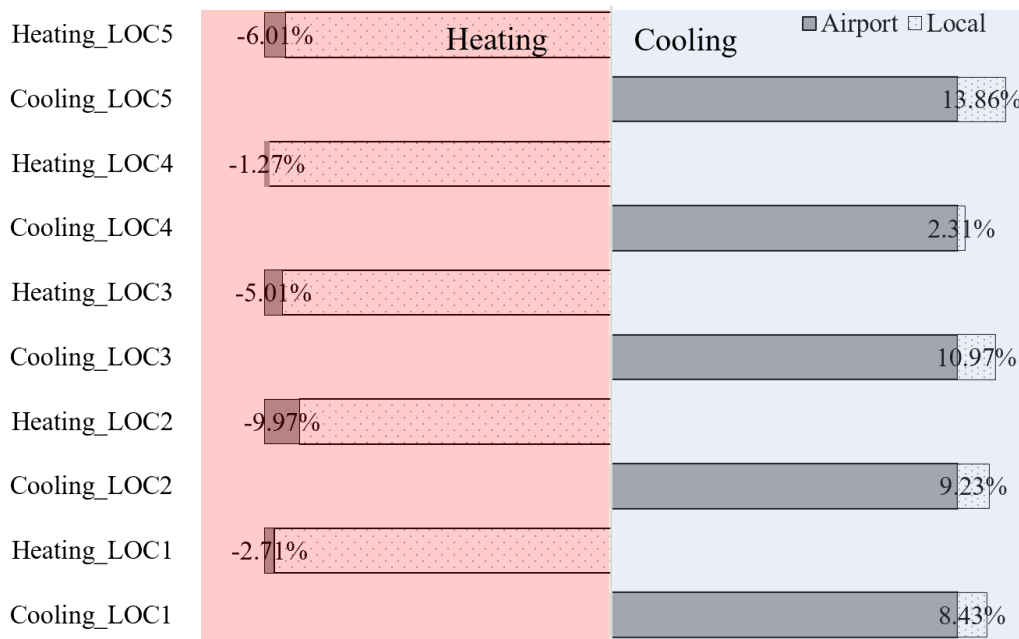


Figure 5.12 Overall cooling energy and heating energy changes in comparison to the traditional method using airport weather for TMY.

In light of this observation, it is important to consider the impact of urban microclimate on energy consumption. It suggests that energy consumption patterns in cities can vary significantly based on their specific location. Using such insights, urban planners and policymakers can optimize energy efficiency and mitigate energy consumption in different parts of cities.

5.3.6 Meteorological sensitivity analysis

In this study, the impact of urban microclimate is determined by air temperature and wind. To evaluate how air temperature, wind, and other meteorological parameters influence the building energy consumption values, a sensitivity analysis is conducted using the generated TMY weather data for LOC1 to investigate the relationship between meteorological parameters and building energy consumption in Table 5-5. A Sensitivity Variance Index (SVI) was calculated to evaluate the influence of seven distinct meteorological parameters. The parameter with the highest impact received a rank of 1. The cooling load, heating load, and total load are exhaustively examined. Every section focuses on a specific parameter and its associated metrics. The parameters under consideration are air temperature, wind speed, wind direction, relative humidity (RH), global solar radiation, diffuse solar radiation, and normal solar radiation. Table 5-5 presents key metrics for each parameter, including the Statistical Relevance Coefficient (SRC), Random Forest importance, T-value, and SVI. The metrics are accompanied by their respective rankings.

Table 5-5 presents a comprehensive assessment of the impact of various environmental parameters on cooling load, heating load, and total load, as well as their respective rankings based on multiple modeling techniques. In the context of cooling load, air temperature emerges as the most critical factor with a high Sensitivity Ratio Coefficient (SRC) of 0.72, a substantial Random Forest value of 308.94, and a significant T-value of 64.05. Following closely, relative humidity (RH) ranks second, emphasizing its substantial influence, while global solar radiation secures the third

position. Wind speed, wind direction, and solar radiation parameters contribute to the overall understanding of cooling load variations.

Shifting the focus to the heating load, the dominance of air temperature is reiterated, holding a prominent SRC of 0.7, a noteworthy Random Forest value of 406.46, and a substantial T-value of 56.93. Global solar radiation plays a crucial role in heating load as well, securing the second position in importance. Wind speed, diffuse solar radiation, and normal solar radiation contribute to the overall understanding of factors affecting heating load.

Considering the total load, air temperature remains pivotal, leading with an SRC of 0.38, a significant Random Forest value of 271.7, and a noteworthy T-value of 25.53. Relative humidity (RH) follows closely in importance, emphasizing its impact on total load variations.

Table 5-5 Building energy sensitivity analysis.

For cooling load					
Parameter	SRC	Random forest	T-value	SVI	Rank
Air temperature	0.72	308.94	64.05	54.05	1
Wind speed	0.05	18.09	4.93	3.64	7
Wind direction	0.05	22.6	4.71	3.82	6
RH	0.13	119.4	12.58	14.33	2
Global solar	0.31	11.37	11.04	10.3	3
Diffuse solar	0.19	10.26	10.89	7.75	4
Normal solar	0.16	11.21	7.22	6.11	5
For heating load					
Parameter	SRC	Random forest	T-value	SVI	Rank
Air temperature	0.7	406.46	56.93	60.98	1
Wind speed	0.05	29.34	4.17	4.28	5
Wind direction	0	42.73	0.27	2.5	7
RH	0.01	53.57	1.11	3.66	6

Global solar	0.19	52.9	6.4	10.07	2
Diffuse solar	0.19	13.94	9.96	9.16	4
Normal solar	0.21	12.9	8.96	9.34	3
For total load					
Parameter	SRC	Random forest	T-value	SVI	Rank
Air temperature	0.38	271.7	25.53	42.55	1
Wind speed	0.08	37.82	5.94	8.14	4
Wind direction	0.05	47.95	3.7	6.39	6
RH	0.13	140.47	9.69	17.91	2
Global solar	0.22	48.21	5.98	13.43	3
Diffuse solar	0.1	20.51	4.21	6.79	5
Normal solar	0.05	39.32	1.7	4.79	7

Figure 5.13 illustrates the impact ranking based on the sensitivity analysis value. For both cooling and heating, the ambient air temperature is the most important parameter. Air temperature is the most significant parameter in the cooling load section, with an SRC value of 0.72 and a top ranking of 1. There is a strong and statistically significant correlation between air temperature and cooling load, thus making it an essential factor to consider when analyzing cooling loads. In addition to its significance in predicting cooling load variations, Random Forest has an importance value of 308.94 for air temperature.

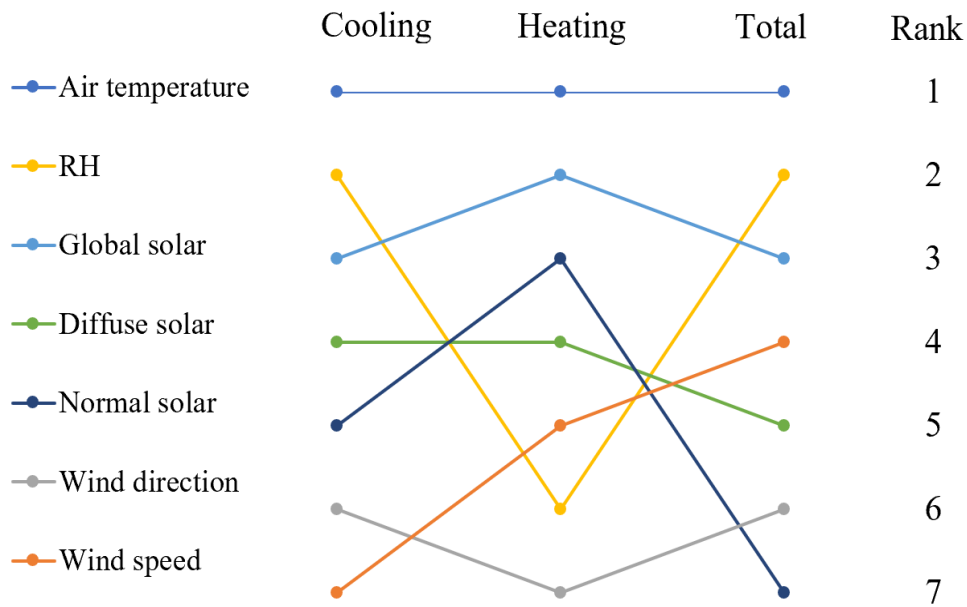


Figure 5.13 Meteorological parameters impact ranking on building energy modeling for LOC1.

SRC values for wind speed and wind direction, however, are lower than those for other parameters, suggesting that they have a weaker correlation with cooling load. The results indicate that they have a relatively low impact, receiving ranks 4 and 6, respectively. Wind speed can impact the building's ventilation energy cost. Wind direction also has a limited impact on building energy modeling. The relative humidity can have a high impact on building cooling in the summer, which can be further investigated if the study focuses on energy consumption during the summer. Solar radiation can also have an impact on energy consumption. However, in the study, the local urban microclimate monitoring is on the roof and there is no shading impact information collected. Solar radiation is considered not to vary with regions. If the specific building is located in a dense urban area, the solar radiation and shading should be considered carefully.

Since the SVIs of other parameters are much lower than the SVIs of air temperature, their impact can be neglected compared to that of air temperature in all three load scenarios [206]. Except for temperature and wind, the other parameters are not discussed further in this study. However, further investigation of relative humidity and solar radiation remains to be done in the future.

5.4 Conclusion

Urban microclimate plays a significant role in the energy consumption of buildings. Accurate prediction of local weather conditions near a target building is crucial for estimating energy consumption under urban microclimate conditions. This study introduces a novel approach using an artificial neural network model to predict microclimate parameters based on long-term onsite measurements, highlighting its importance in building energy analysis.

The primary objective of this study is to establish a connection between urban microclimate parameters and public meteorological weather stations. The trained model utilizes local weather conditions to generate long-term historical local weather data spanning 20 years, in contrast to relying solely on historical weather data from the airport. Subsequently, a localized Typical Meteorological Year (TMY) weather dataset is created using the 20-year predicted weather data. This TMY weather dataset is then input into EnergyPlus, a building energy simulation software, to evaluate building energy consumption.

The study presents the performance of the proposed model and methodology. Statistical investigations are conducted to compare the energy consumption for building heating and cooling against reference models using TMY weather data from the airport and localized weather conditions. Additionally, the study explores the spatial differences among different local weather stations in the urban microclimate's impact on building energy consumption. The findings of this

study reveal that the urban microclimate can contribute to an additional 2% to 14% of building energy consumption across different locations.

Furthermore, the study reveals that air temperature is of the utmost importance in building energy modeling under urban microclimate. The level of relative humidity can significantly influence the cooling of buildings in the summer. Another factor affecting energy consumption is solar radiation. Consequently, solar radiation is assumed to be consistent across regions. Nevertheless, when dealing with buildings situated in densely populated urban areas, it is essential to give thorough consideration to solar radiation and shading effects. Wind speed and wind direction, which may affect building ventilation, play a lesser role compared to ambient air temperature. Parameters, including relative humidity and radiation, are worth further investigation in future studies.

Overall, this study highlights the importance of accurate local weather prediction and its influence on building energy consumption under urban microclimate conditions. The investigation of spatial differences among various local weather stations contributes to a comprehensive understanding of the urban microclimate's impact on building energy consumption.

Chapter 6. Conclusions

From the short-term to long-term evaluation of urban microclimate, Urban microclimate plays a significant role in the energy consumption of buildings. Accurate prediction of local weather conditions near a target building is crucial for estimating energy consumption under urban microclimate conditions. This study introduces a novel approach using an artificial neural network model to predict microclimate parameters based on long-term onsite measurements, highlighting its importance in building energy analysis.

6.1 Contributions

The contributions of this thesis can be generalized as follows:

- Given the limited research on urban wind environments in expansive and realistic urban settings, this study employs CityFFD to assess wind patterns and offers guidance on effectively configuring CityFFD for precise and efficient results.
- The research extends the application of CityFFD and CityBEM to large, realistic urban regions, incorporating detailed building surface information into outdoor simulations.
- This research also explores the spatial differences in outdoor thermal comfort for Montreal during the summer heatwave.
- Furthermore, the study introduces an innovative urban microclimate prediction model based on Artificial Neural Networks (ANN). This model establishes a correlation between data from public meteorological weather stations and urban microclimate conditions, contributing to a deeper understanding of these dynamics.
- Additionally, the research pioneers a method for utilizing long-term meteorological weather records to map extended local weather patterns and generate a local Typical

Meteorological Year (TMY) weather file. The created TMY file is then employed to analyze the impact of urban microclimates on building energy consumption.

This multifaceted approach not only addresses gaps in current research but also provides practical insights and methodologies for efficiently studying and modeling urban microclimates.

6.2 Limitations

While short-term evaluations of urban microclimates through numerical simulations have demonstrated acceptable results compared to actual measurements, limitations exist with the CityFFD simulations. In the present simulation approach, the influence of solar radiation is treated as a component of building surface temperature, overlooking the effects of shading and spatial temperature differences within street canyons. The impact of road and terrain is neglected due to the lack of a method to determine the detailed spatial-temporal road and terrain temperature.

Notably, this study highlights the significance of humidity in influencing outdoor thermal comfort during the summer months, yet the current numerical simulation model lacks the incorporation of relative humidity. Furthermore, the impact of vegetation on urban airflow is acknowledged, but the existing method does not consider vegetation in its calculations.

For long-term evaluation of urban microclimate model by artificial neural network model, the study currently overlooks crucial factors such as solar radiation and shading effects, both of which play a significant role in shaping urban microclimates and influencing building energy consumption. Incorporating these variables into the model would provide a more comprehensive understanding of energy dynamics within urban settings. Furthermore, the existing model lacks consideration for urban geometry as a feature. The layout and form of urban spaces substantially

impact microclimate conditions, affecting wind patterns and heat distribution. Future models would benefit from including urban geometry as a feature, enhancing prediction accuracy and allowing for a more holistic analysis of building energy consumption across diverse urban configurations.

Additionally, the study assumes that the microclimate model for urban areas remains constant over time, disregarding potential changes in the city's urban development. This assumption neglects the dynamic nature of urban environments. To address this, there is a need for additional data to validate the model's time-invariance. Moreover, since the current model requires separate training for each location, it lacks generalization across different urban areas. Introducing urban morphology indicators as input features could offer a potential solution, facilitating the development of a more generalized model applicable to a variety of urban contexts.

6.3 Future Work

In the context of future work for the thesis, several avenues can be explored to enhance the current research:

- Future investigations should include an in-depth analysis of the impact of relative humidity on urban microclimates, particularly during the summer months. This entails integrating relative humidity as a crucial parameter in numerical simulation models.
- To achieve a more comprehensive understanding of the urban microclimate, it is essential to consider water vapor sources such as rivers, lakes, and parks. Future work should explore the influence of these sources on local humidity levels and thermal comfort.
- The role of vegetation, including trees and mountain parks, in shaping urban airflow and microclimatic conditions should be thoroughly investigated. Incorporating vegetation data

into simulation models will contribute to a more accurate representation of the urban environment. The thermal mass or thermal storage impact by the road and terrain can also play an important role, which is worth further investigation. Future research efforts should delve into the effects of shading on urban microclimates, especially within street canyons.

- The inclusion of urban morphology features into artificial neural network models is a promising avenue for future research. In the future, more sophisticated models adding urban morphology indicators, including parameters such as sky view factor, average building height, openness, front area index, etc., as input features could be a potential solution, which can help create a more generalized model applicable to various urban contexts. This entails exploring how the geometric characteristics of urban spaces influence microclimatic conditions, thereby enhancing the predictive capabilities of neural network models.
- Besides, there are also many valuable topics related to urban microclimate that are worth further investigation, including the thermal storage impact of urban roads, and the thermal buoyancy impact on urban pollutant dispersions. Meanwhile, the numerical model can be further improved by adding more detailed urban characteristics, as well as improving the coupling of the CFD models with BES models.

By addressing these areas in future research, the thesis can contribute significantly to advancing our understanding of urban microclimates and refining simulation models for more accurate and comprehensive predictions.

REFERENCES

- [1] P. Bocquier, World urbanization prospects: An alternative to the UN model of projection compatible with the mobility transition theory, *Demogr. Res.* 12 (2005) 197–236. <https://doi.org/10.4054/DemRes.2005.12.9>.
- [2] T.B. Williams, Microclimatic temperature relationships over different surfaces, *J. Geog.* (1991). <https://doi.org/10.1080/00221349108979321>.
- [3] I. Orlanski, A rational subdivision of scales for atmospheric processes, *Bull. Amer. Meteor. Soc.* (1975).
- [4] N. Antoniou, H. Montazeri, M. Neophytou, B. Blocken, CFD simulation of urban microclimate: Validation using high-resolution field measurements, *Sci. Total Environ.* 695 (2019) 133743. <https://doi.org/10.1016/j.scitotenv.2019.133743>.
- [5] G. Chen, D. Wang, Q. Wang, Y. Li, X. Wang, J. Hang, P. Gao, C. Ou, K. Wang, Scaled outdoor experimental studies of urban thermal environment in street canyon models with various aspect ratios and thermal storage, *Sci. Total Environ.* (2020). <https://doi.org/10.1016/j.scitotenv.2020.138147>.
- [6] Y. Toparlar, B. Blocken, B. Maiheu, G.J.F. van Heijst, A review on the CFD analysis of urban microclimate, *Renew. Sustain. Energy Rev.* 80 (2017) 1613–1640. <https://doi.org/10.1016/j.rser.2017.05.248>.
- [7] B. Blocken, J. Carmeliet, Pedestrian wind environment around buildings: Literature review and practical examples, *J. Therm. Envel. Build. Sci.* 28 (2004) 107–159. <https://doi.org/10.1177/1097196304044396>.
- [8] P. Moonen, T. Defraeye, V. Dorer, B. Blocken, J. Carmeliet, Urban Physics: Effect of the micro-climate on comfort, health and energy demand, *Front. Archit. Res.* 1 (2012) 197–228. <https://doi.org/10.1016/j.foar.2012.05.002>.
- [9] L. Howard, *The Climate of London*, vol I, Harvey Dart. (1833).
- [10] M. Santamouris, N. Papanikolaou, I. Livada, I. Koronakis, C. Georgakis, A. Argiriou, D.N. Assimakopoulos, On the impact of urban climate on the energy consumption of building, *Sol.*

- Energy. 70 (2001) 201–216. [https://doi.org/10.1016/S0038-092X\(00\)00095-5](https://doi.org/10.1016/S0038-092X(00)00095-5).
- [11] B.T. Yang, R.N. Meroney, ON DIFFUSION FROM AN INSTANTANEOUS POINT SOURCE IN A NEUTRALLY STRATIFIED TURBULENT BOUNDARY LAYER WITH A LASER LIGHT SCATTERING PROBE., Colo State Univ (Fort Collins), Proj THEMI. (1972).
- [12] P.Y. Cui, Z. Li, W.Q. Tao, Wind-tunnel measurements for thermal effects on the air flow and pollutant dispersion through different scale urban areas, *Build. Environ.* 97 (2016) 137–151. <https://doi.org/10.1016/j.buildenv.2015.12.010>.
- [13] M. Hadavi, H. Pasharshahi, Impacts of urban buildings on microclimate and cooling systems efficiency: Coupled CFD and BES simulations, *Sustain. Cities Soc.* (2021). <https://doi.org/10.1016/j.scs.2021.102740>.
- [14] M. Zeeshan, Z. Ali, Using a blue landscape to mitigate heat stress during a heatwave event: a simulation study in a hot-humid urban environment, *J. Water Clim. Chang.* (2023). <https://doi.org/10.2166/wcc.2023.363>.
- [15] M. Mortezaadeh, L.L. Wang, M. Albettar, S. Yang, CityFFD – City fast fluid dynamics for urban microclimate simulations on graphics processing units, *Urban Clim.* (2022). <https://doi.org/10.1016/j.uclim.2021.101063>.
- [16] C. Shu, A. Gaur, L. (Leon) Wang, M. Bartko, A. Laouadi, L. Ji, M. Lacasse, Added value of convection permitting climate modelling in urban overheating assessments, *Build. Environ.* (2022). <https://doi.org/10.1016/j.buildenv.2021.108415>.
- [17] Z. Gao, Y. Hou, W. Chen, Enhanced sensitivity of the urban heat island effect to summer temperatures induced by urban expansion, *Environ. Res. Lett.* (2019). <https://doi.org/10.1088/1748-9326/ab2740>.
- [18] F. Binarti, M.D. Koerniawan, S. Triyadi, S.S. Utami, A. Matzarakis, A review of outdoor thermal comfort indices and neutral ranges for hot-humid regions, *Urban Clim.* (2020). <https://doi.org/10.1016/j.uclim.2019.100531>.
- [19] A. Abd Razak, A. Hagishima, N. Ikegaya, J. Tanimoto, Analysis of airflow over building arrays for assessment of urban wind environment, *Build. Environ.* (2013).

- <https://doi.org/10.1016/j.buildenv.2012.08.007>.
- [20] F. Salata, I. Golasi, A.D.L. Vollaro, R.D.L. Vollaro, How high albedo and traditional buildings' materials and vegetation affect the quality of urban microclimate. A case study, *Energy Build.* (2015). <https://doi.org/10.1016/j.enbuild.2015.04.010>.
- [21] A. Mochida, I.Y.F. Lun, Prediction of wind environment and thermal comfort at pedestrian level in urban area, *J. Wind Eng. Ind. Aerodyn.* 96 (2008) 1498–1527. <https://doi.org/10.1016/j.jweia.2008.02.033>.
- [22] J. Allegrini, V. Dorer, J. Carmeliet, Buoyant flows in street canyons: Validation of CFD simulations with wind tunnel measurements, *Build. Environ.* 72 (2014) 63–74. <https://doi.org/10.1016/j.buildenv.2013.10.021>.
- [23] L.W. Chew, L.R. Glicksman, L.K. Norford, Buoyant flows in street canyons: Comparison of RANS and LES at reduced and full scales, *Build. Environ.* 146 (2018) 77–87. <https://doi.org/10.1016/j.buildenv.2018.09.026>.
- [24] H. Bherwani, A. Singh, R. Kumar, Assessment methods of urban microclimate and its parameters: A critical review to take the research from lab to land, *Urban Clim.* (2020). <https://doi.org/10.1016/j.uclim.2020.100690>.
- [25] U.K. Priya, R. Senthil, A review of the impact of the green landscape interventions on the urban microclimate of tropical areas, *Build. Environ.* (2021). <https://doi.org/10.1016/j.buildenv.2021.108190>.
- [26] P. Ampatzidis, T. Kershaw, A review of the impact of blue space on the urban microclimate, *Sci. Total Environ.* (2020). <https://doi.org/10.1016/j.scitotenv.2020.139068>.
- [27] Z.T. Ai, C.M. Mak, From street canyon microclimate to indoor environmental quality in naturally ventilated urban buildings: Issues and possibilities for improvement, *Build. Environ.* (2015). <https://doi.org/10.1016/j.buildenv.2015.10.008>.
- [28] A. Shafaghat, G. Manteghi, A. Keyvanfar, H. Bin Lamit, K. Saito, D.R. Ossen, Street geometry factors influence urban microclimate in tropical coastal cities: A review, *Environ. Clim. Technol.* (2016). <https://doi.org/10.1515/rtuct-2016-0006>.

- [29] D. Lai, W. Liu, T. Gan, K. Liu, Q. Chen, A review of mitigating strategies to improve the thermal environment and thermal comfort in urban outdoor spaces, *Sci. Total Environ.* (2019). <https://doi.org/10.1016/j.scitotenv.2019.01.062>.
- [30] Z. Liu, K.Y. Cheng, Y. He, C.Y. Jim, R.D. Brown, Y. Shi, K. Lau, E. Ng, Microclimatic measurements in tropical cities: Systematic review and proposed guidelines, *Build. Environ.* 222 (2022) 109411. <https://doi.org/10.1016/j.buildenv.2022.109411>.
- [31] T. Hu, Y. Hu, K. Qi, Dynamic Evolution of Surface Urban Heat Island in Beijing, in: *Int. Geosci. Remote Sens. Symp.*, 2019. <https://doi.org/10.1109/IGARSS.2019.8898624>.
- [32] D. Mu, N. Gao, T. Zhu, CFD investigation on the effects of wind and thermal wall-flow on pollutant transmission in a high-rise building, *Build. Environ.* (2018). <https://doi.org/10.1016/j.buildenv.2018.03.051>.
- [33] S. Huttner, M. Bruse, Numerical modeling of the urban climate - a preview on ENVI-MET 4.0, *Seventh Int. Conf. Urban Clim.* (2009).
- [34] M. Neophytou, A. Gowardhan, M. Brown, An inter-comparison of three urban wind models using Oklahoma City Joint Urban 2003 wind field measurements, *J. Wind Eng. Ind. Aerodyn.* (2011). <https://doi.org/10.1016/j.jweia.2011.01.010>.
- [35] A.C.S. Lai, A.C.T. So, S.K.C. Ng, D. Jonas, The territory-wide airborne light detection and ranging survey for the Hong Kong special administrative region, in: *33rd Asian Conf. Remote Sens. 2012, ACRS 2012, 2012*.
- [36] R. Byrne, N.J. Hewitt, P. Griffiths, P. MacArtain, A comparison of four microscale wind flow models in predicting the real-world performance of a large-scale peri-urban wind turbine, using onsite LiDAR wind measurements, *Sustain. Energy Technol. Assessments.* (2021). <https://doi.org/10.1016/j.seta.2021.101323>.
- [37] G. Battista, E. Carnielo, R. De Lieto Vollaro, Thermal impact of a redeveloped area on localized urban microclimate: A case study in Rome, *Energy Build.* (2016). <https://doi.org/10.1016/j.enbuild.2016.10.004>.
- [38] W. Liu, Y. Zhang, Q. Deng, The effects of urban microclimate on outdoor thermal sensation and neutral temperature in hot-summer and cold-winter climate, *Energy Build.* (2016).

<https://doi.org/10.1016/j.enbuild.2016.06.086>.

- [39] M. Nikolopoulou, S. Lykoudis, Use of outdoor spaces and microclimate in a Mediterranean urban area, *Build. Environ.* (2007). <https://doi.org/10.1016/j.buildenv.2006.09.008>.
- [40] N. Antoniou, H. Montazeri, M. Neophytou, B. Blocken, CFD simulation of urban microclimate: Validation using high-resolution field measurements, *Sci. Total Environ.* 695 (2019) 133743. <https://doi.org/10.1016/j.scitotenv.2019.133743>.
- [41] L. Klok, S. Zwart, H. Verhagen, E. Mauri, The surface heat island of Rotterdam and its relationship with urban surface characteristics, *Resour. Conserv. Recycl.* (2012). <https://doi.org/10.1016/j.resconrec.2012.01.009>.
- [42] A. M'Saouri El Bat, Z. Romani, E. Bozonnet, A. Draoui, Integration of a practical model to assess the local urban interactions in building energy simulation with a street canyon, *J. Build. Perform. Simul.* (2020). <https://doi.org/10.1080/19401493.2020.1818829>.
- [43] M. Neophytou, P. Fokaidis, I. Panagiotou, I. Ioannou, M. Petrou, M. Sandberg, H. Wigo, E. Linden, E. Batchvarova, P. Videnov, B. Dimitroff, A. Ivanov, Towards Optimization of Urban Planning and Architectural Parameters for Energy use Minimization in Mediterranean Cities, in: *Proc. World Renew. Energy Congr. – Sweden, 8–13 May, 2011, Linköping, Sweden, 2011*. <https://doi.org/10.3384/ecp110573372>.
- [44] M. Doya, E. Bozonnet, F. Allard, Experimental measurement of cool facades' performance in a dense urban environment, in: *Energy Build.*, 2012. <https://doi.org/10.1016/j.enbuild.2011.11.001>.
- [45] M. Shahrestani, R. Yao, Z. Luo, E. Turkbeyler, H. Davies, A field study of urban microclimates in London, *Renew. Energy.* (2015). <https://doi.org/10.1016/j.renene.2014.05.061>.
- [46] G.K.L. Wong, C.Y. Jim, Urban-microclimate effect on vector mosquito abundance of tropical green roofs, *Build. Environ.* (2017). <https://doi.org/10.1016/j.buildenv.2016.11.028>.
- [47] S. Tong, N.H. Wong, C.L. Tan, S.K. Jusuf, M. Ignatius, E. Tan, Impact of urban morphology on microclimate and thermal comfort in northern China, *Sol. Energy.* (2017). <https://doi.org/10.1016/j.solener.2017.06.027>.

- [48] S.A. Zaki, N.E. Othman, S.W. Syahidah, F. Yakub, F. Muhammad-Sukki, J.A. Ardila-Rey, M.F. Shahidan, A.S.M. Saudi, Effects of urban morphology on microclimate parameters in an urban university campus, *Sustain.* (2020). <https://doi.org/10.3390/su12072962>.
- [49] T. Hong, Y. Xu, K. Sun, W. Zhang, X. Luo, B. Hooper, Urban microclimate and its impact on building performance: A case study of San Francisco, *Urban Clim.* (2021). <https://doi.org/10.1016/j.uclim.2021.100871>.
- [50] S.W. Kiyoshi Uehara, Shuzo Murakami, Susumu Oikawa, Wind tunnel experiments on how thermal stratification affects flow in and above urban street canyons, *J. Wind Eng. Ind. Aerodyn.* 94 (2006) 621–636. <https://doi.org/http://dx.doi.org/10.1016/j.jweia.2006.02.003>.
- [51] Y. Ogawa, P.G. Diosey, K. Uehara, H. Ueda, A wind tunnel for studying the effects of thermal stratification in the atmosphere, *Atmos. Environ.* (1981). [https://doi.org/10.1016/0004-6981\(81\)90286-9](https://doi.org/10.1016/0004-6981(81)90286-9).
- [52] J. Allegrini, V. Dorer, J. Carmeliet, Wind tunnel measurements of buoyant flows in street canyons, *Build. Environ.* (2013). <https://doi.org/10.1016/j.buildenv.2012.08.029>.
- [53] J. Allegrini, A wind tunnel study on three-dimensional buoyant flows in street canyons with different roof shapes and building lengths, *Build. Environ.* (2018). <https://doi.org/10.1016/j.buildenv.2018.06.056>.
- [54] Z. Mo, C.H. Liu, Wind tunnel measurements of pollutant plume dispersion over hypothetical urban areas, *Build. Environ.* (2018). <https://doi.org/10.1016/j.buildenv.2018.01.046>.
- [55] T.S. Larsen, P. Heiselberg, Single-sided natural ventilation driven by wind pressure and temperature difference, *Energy Build.* (2008). <https://doi.org/10.1016/j.enbuild.2006.07.012>.
- [56] W. Zhang, C.D. Markfort, F. Porté-Agel, Wind-Turbine Wakes in a Convective Boundary Layer: A Wind-Tunnel Study, *Boundary-Layer Meteorol.* (2013). <https://doi.org/10.1007/s10546-012-9751-4>.
- [57] M.F. Yassin, A wind tunnel study on the effect of thermal stability on flow and dispersion of rooftop stack emissions in the near wake of a building, *Atmos. Environ.* (2013).

<https://doi.org/10.1016/j.atmosenv.2012.10.013>.

- [58] L. Zhang, Y. Feng, Q. Meng, Y. Zhang, Experimental study on the building evaporative cooling by using the Climatic Wind Tunnel, *Energy Build.* (2015). <https://doi.org/10.1016/j.enbuild.2015.07.038>.
- [59] J. Huang, P. Jones, A. Zhang, R. Peng, X. Li, P. wai Chan, Urban Building Energy and Climate (UrBEC) simulation: Example application and field evaluation in Sai Ying Pun, Hong Kong, *Energy Build.* (2020). <https://doi.org/10.1016/j.enbuild.2019.109580>.
- [60] Y. Lin, T. Ichinose, Y. Yamao, H. Mouri, Wind velocity and temperature fields under different surface heating conditions in a street canyon in wind tunnel experiments, *Build. Environ.* (2020). <https://doi.org/10.1016/j.buildenv.2019.106500>.
- [61] Y. Jiang, D. Alexander, H. Jenkins, R. Arthur, Q. Chen, Natural ventilation in buildings: Measurement in a wind tunnel and numerical simulation with large-eddy simulation, *J. Wind Eng. Ind. Aerodyn.* (2003). [https://doi.org/10.1016/S0167-6105\(02\)00380-X](https://doi.org/10.1016/S0167-6105(02)00380-X).
- [62] J. Allegrini, J.H. Kämpf, V. Dorer, J. Carmeliet, Modelling the Urban Microclimate and its Influence on Building Energy Demands of an Urban Neighbourhood, in: *Proc. CISBAT 2013 Cleantech Smart Cities Build.*, EPFL Solar Energy and Building Physics Laboratory (LESO-PB), Lausanne, Switzerland, 2013: pp. 867–872. <http://infoscience.epfl.ch/record/195701>.
- [63] S.M. Salim, R. Buccolieri, A. Chan, S. Di Sabatino, Numerical simulation of atmospheric pollutant dispersion in an urban street canyon: Comparison between RANS and LES, *J. Wind Eng. Ind. Aerodyn.* (2011). <https://doi.org/10.1016/j.jweia.2010.12.002>.
- [64] X. Zheng, H. Montazeri, B. Blocken, CFD simulations of wind flow and mean surface pressure for buildings with balconies: Comparison of RANS and LES, *Build. Environ.* (2020). <https://doi.org/10.1016/j.buildenv.2020.106747>.
- [65] M. Shirzadi, P.A. Mirzaei, Y. Tominaga, CFD analysis of cross-ventilation flow in a group of generic buildings: Comparison between steady RANS, LES and wind tunnel experiments, *Build. Simul.* (2020). <https://doi.org/10.1007/s12273-020-0657-7>.
- [66] ANSYS Fluent Theory Guide, ANSYS Fluent Theory Guide, ANSYS Inc., USA. (2020).

- [67] M. Bruse, ENVI-met 3.0: Updated Model Overview, (2004) 1–12.
- [68] N.G. Jacobsen, D.R. Fuhrman, J. Fredsøe, A wave generation toolbox for the open-source CFD library: OpenFoam®, *Int. J. Numer. Methods Fluids*. (2012). <https://doi.org/10.1002/flid.2726>.
- [69] A. Kamal, S.M.H. Abidi, A. Mahfouz, S. Kadam, A. Rahman, I.G. Hassan, L.L. Wang, Impact of urban morphology on urban microclimate and building energy loads, *Energy Build.* (2021). <https://doi.org/10.1016/j.enbuild.2021.111499>.
- [70] J. Pfafferott, S. Reißmann, M. Sühling, F. Kanani-Sühling, B. Maronga, Building indoor model in PALM-4U: Indoor climate, energy demand, and the interaction between buildings and the urban microclimate, *Geosci. Model Dev.* (2021). <https://doi.org/10.5194/gmd-14-3511-2021>.
- [71] J. Vogel, A. Afshari, G. Chockalingam, S. Stadler, Evaluation of a novel WRF/PALM-4U coupling scheme incorporating a roughness-corrected surface layer representation, *Urban Clim.* (2022). <https://doi.org/10.1016/j.uclim.2022.101311>.
- [72] J. Geletič, M. Lehnert, P. Krč, J. Resler, E.S. Krayenhoff, High-resolution modelling of thermal exposure during a hot spell: A case study using palm-4u in prague, czech republic, *Atmosphere (Basel)*. (2021). <https://doi.org/10.3390/atmos12020175>.
- [73] J. Liu, M. Heidarinejad, S.K. Nikkho, N.W. Mattise, J. Srebric, Quantifying impacts of urban microclimate on a building energy consumption-a case study, *Sustain.* (2019). <https://doi.org/10.3390/su11184921>.
- [74] Z. Zhai, Q. Chen, P. Haves, J.H. Klems, On approaches to couple energy simulation and computational fluid dynamics programs, *Build. Environ.* (2002). [https://doi.org/10.1016/S0360-1323\(02\)00054-9](https://doi.org/10.1016/S0360-1323(02)00054-9).
- [75] J. Allegrini, V. Dorer, J. Carmeliet, Influence of the urban microclimate in street canyons on the energy demand for space cooling and heating of buildings, *Energy Build.* (2012). <https://doi.org/10.1016/j.enbuild.2012.10.013>.
- [76] A. Katal, M. Mortezaadeh, L. (Leon) Wang, Modeling building resilience against extreme weather by integrated CityFFD and CityBEM simulations, *Appl. Energy*. 250 (2019) 1402–

1417. <https://doi.org/10.1016/j.apenergy.2019.04.192>.
- [77] Y. Miao, S. Liu, B. Chen, B. Zhang, S. Wang, S. Li, Simulating urban flow and dispersion in Beijing by coupling a CFD model with the WRF model, *Adv. Atmos. Sci.* (2013). <https://doi.org/10.1007/s00376-013-2234-9>.
- [78] F. Miguet, D. Groleau, Urban bioclimatic indicators for urban planners with the software tool SOLENE, in: *Port. SB 2007 - Sustain. Constr. Mater. Pract. Chall. Ind. New Millenn.*, 2007.
- [79] R. Zhang, K.P. Lam, S. chune Yao, Y. Zhang, Coupled EnergyPlus and computational fluid dynamics simulation for natural ventilation, *Build. Environ.* (2013). <https://doi.org/10.1016/j.buildenv.2013.04.002>.
- [80] K. Perini, A. Chokhachian, S. Dong, T. Auer, Modeling and simulating urban outdoor comfort: Coupling ENVI-Met and TRNSYS by grasshopper, *Energy Build.* (2017). <https://doi.org/10.1016/j.enbuild.2017.07.061>.
- [81] J. Brozovsky, A. Simonsen, N. Gaitani, Validation of a CFD model for the evaluation of urban microclimate at high latitudes: A case study in Trondheim, Norway, *Build. Environ.* (2021). <https://doi.org/10.1016/j.buildenv.2021.108175>.
- [82] N. Fintikakis, N. Gaitani, M. Santamouris, M. Assimakopoulos, D.N. Assimakopoulos, M. Fintikaki, G. Albanis, K. Papadimitriou, E. Chryssochoides, K. Katopodi, P. Doulas, Bioclimatic design of open public spaces in the historic centre of Tirana, Albania, *Sustain. Cities Soc.* (2011). <https://doi.org/10.1016/j.scs.2010.12.001>.
- [83] M.F. Shahidan, P.J. Jones, J. Gwilliam, E. Salleh, An evaluation of outdoor and building environment cooling achieved through combination modification of trees with ground materials, *Build. Environ.* (2012). <https://doi.org/10.1016/j.buildenv.2012.07.012>.
- [84] Y. Toparlar, B. Blocken, P. Vos, G.J.F. Van Heijst, W.D. Janssen, T. van Hooff, H. Montazeri, H.J.P. Timmermans, CFD simulation and validation of urban microclimate: A case study for Bergpolder Zuid, Rotterdam, *Build. Environ.* (2015). <https://doi.org/10.1016/j.buildenv.2014.08.004>.
- [85] X. Yang, L. Zhao, M. Bruse, Q. Meng, Evaluation of a microclimate model for predicting the thermal behavior of different ground surfaces, *Build. Environ.* (2013).

<https://doi.org/10.1016/j.buildenv.2012.11.008>.

- [86] J. Ma, X. Li, Y. Zhu, A simplified method to predict the outdoor thermal environment in residential district, *Build. Simul.* (2012). <https://doi.org/10.1007/s12273-012-0079-2>.
- [87] J. Brozovsky, S. Corio, N. Gaitani, A. Gustavsen, Evaluation of sustainable strategies and design solutions at high-latitude urban settlements to enhance outdoor thermal comfort, *Energy Build.* (2021). <https://doi.org/10.1016/j.enbuild.2021.111037>.
- [88] U. Berardi, Y. Wang, The effect of a denser city over the urban microclimate: The case of Toronto, *Sustain.* (2016). <https://doi.org/10.3390/su8080822>.
- [89] Y. Tominaga, Y. Sato, S. Sadohara, CFD simulations of the effect of evaporative cooling from water bodies in a micro-scale urban environment: Validation and application studies, *Sustain. Cities Soc.* 19 (2015) 259–270. <https://doi.org/10.1016/j.scs.2015.03.011>.
- [90] M. Mortezaadeh, Z. Jandaghian, L.L. Wang, Integrating CityFFD and WRF for modeling urban microclimate under heatwaves, *Sustain. Cities Soc.* (2021). <https://doi.org/10.1016/j.scs.2020.102670>.
- [91] D. Clarke, R. Kinghorn, A. Cam, M. Chui, B. Hall, N. Robert, R. STEFAN, G. CARUTASU, S. Caner, F. Bhatti, H. Michael, K. Andreas, N.R. Mosteanu, S. Weber, A Brief History of Artificial Intelligence: On the Past, Present, and Futur...: Search KCenter resources, McKinsey. (2019).
- [92] K. Hüb, A. Middel, B.L. Ruddell, H. Hagen, A Data-Driven Approach to Categorize Climatic Microenvironments, in: *EnvirVis 2016 - Work. Vis. Environ. Sci.*, 2016. <https://doi.org/10.2312/envirvis.20161105>.
- [93] L. Alonso, F. Renard, A new approach for understanding urban microclimate by integrating complementary predictors at different scales in regression and machine learning models, *Remote Sens.* (2020). <https://doi.org/10.3390/RS12152434>.
- [94] M. Zhang, X. Zhang, S. Guo, X. Xu, J. Chen, W. Wang, Urban micro-climate prediction through long short-term memory network with long-term monitoring for on-site building energy estimation, *Sustain. Cities Soc.* (2021). <https://doi.org/10.1016/j.scs.2021.103227>.

- [95] S. Higgins, T. Stathopoulos, Application of artificial intelligence to urban wind energy, *Build. Environ.* (2021). <https://doi.org/10.1016/j.buildenv.2021.107848>.
- [96] G.Y. Oukawa, P. Krecl, A.C. Targino, Fine-scale modeling of the urban heat island: A comparison of multiple linear regression and random forest approaches, *Sci. Total Environ.* 815 (2022) 152836. <https://doi.org/10.1016/j.scitotenv.2021.152836>.
- [97] C. Ding, K.P. Lam, Data-driven model for cross ventilation potential in high-density cities based on coupled CFD simulation and machine learning, *Build. Environ.* (2019). <https://doi.org/10.1016/j.buildenv.2019.106394>.
- [98] N. Nazarian, J. Fan, T. Sin, L. Norford, J. Kleissl, Predicting outdoor thermal comfort in urban environments: A 3D numerical model for standard effective temperature, *Urban Clim.* (2017). <https://doi.org/10.1016/j.uclim.2017.04.011>.
- [99] M. Mortezaadeh, J. Zou, M. Hosseini, S. Yang, L. Wang, Estimating Urban Wind Speeds and Wind Power Potentials Based on Machine Learning with City Fast Fluid Dynamics Training Data, *Atmosphere (Basel)*. (2022). <https://doi.org/10.3390/atmos13020214>.
- [100] Y. Yao, C. Chang, F. Ndayisaba, S. Wang, A new approach for surface urban heat island monitoring based on machine learning algorithm and spatiotemporal fusion model, *IEEE Access.* (2020). <https://doi.org/10.1109/ACCESS.2020.3022047>.
- [101] I. Abohela, N. Hamza, S. Dudek, Effect of roof shape, wind direction, building height and urban configuration on the energy yield and positioning of roof mounted wind turbines, *Renew. Energy.* (2013). <https://doi.org/10.1016/j.renene.2012.08.068>.
- [102] J. Liu, J. Niu, Y. Du, C.M. Mak, Y. Zhang, LES for pedestrian level wind around an idealized building array—Assessment of sensitivity to influencing parameters, *Sustain. Cities Soc.* (2019). <https://doi.org/10.1016/j.scs.2018.10.034>.
- [103] Q.M. Zahid Iqbal, A.L.S. Chan, Pedestrian level wind environment assessment around group of high-rise cross-shaped buildings: Effect of building shape, separation and orientation, *Build. Environ.* (2016). <https://doi.org/10.1016/j.buildenv.2016.02.015>.
- [104] W.D. Janssen, B. Blocken, T. van Hooff, Pedestrian wind comfort around buildings: Comparison of wind comfort criteria based on whole-flow field data for a complex case

- study, *Build. Environ.* 59 (2013) 547–562. <https://doi.org/10.1016/j.buildenv.2012.10.012>.
- [105] A. Khalilzadeh, H. Ge, H.D. Ng, Effect of turbulence modeling schemes on wind-driven rain deposition on a mid-rise building: CFD modeling and validation, *J. Wind Eng. Ind. Aerodyn.* (2019). <https://doi.org/10.1016/j.jweia.2018.11.012>.
- [106] K. Pettersson, S. Krajnovic, A.S. Kalagasidis, P. Johansson, Simulating wind-driven rain on building facades using Eulerian multiphase with rain phase turbulence model, *Build. Environ.* (2016). <https://doi.org/10.1016/j.buildenv.2016.06.012>.
- [107] C. Yuan, L. Norford, E. Ng, A semi-empirical model for the effect of trees on the urban wind environment, *Landsc. Urban Plan.* (2017). <https://doi.org/10.1016/j.landurbplan.2017.09.029>.
- [108] M.G. Giometto, A. Christen, P.E. Egli, M.F. Schmid, R.T. Tooke, N.C. Coops, M.B. Parlange, Effects of trees on mean wind, turbulence and momentum exchange within and above a real urban environment, *Adv. Water Resour.* (2017). <https://doi.org/10.1016/j.advwatres.2017.06.018>.
- [109] G. Kang, J.J. Kim, W. Choi, Computational fluid dynamics simulation of tree effects on pedestrian wind comfort in an urban area, *Sustain. Cities Soc.* (2020). <https://doi.org/10.1016/j.scs.2020.102086>.
- [110] P. Höppe, The physiological equivalent temperature - A universal index for the biometeorological assessment of the thermal environment, *Int. J. Biometeorol.* (1999). <https://doi.org/10.1007/s004840050118>.
- [111] D. Fiala, G. Havenith, P. Bröde, B. Kampmann, G. Jendritzky, UTCI-Fiala multi-node model of human heat transfer and temperature regulation, *Int. J. Biometeorol.* (2012). <https://doi.org/10.1007/s00484-011-0424-7>.
- [112] P. Kumar, A. Sharma, Study on importance, procedure, and scope of outdoor thermal comfort –A review, *Sustain. Cities Soc.* (2020). <https://doi.org/10.1016/j.scs.2020.102297>.
- [113] H.M. Imran, J. Kala, A.W.M. Ng, S. Muthukumaran, Effectiveness of vegetated patches as Green Infrastructure in mitigating Urban Heat Island effects during a heatwave event in the city of Melbourne, *Weather Clim. Extrem.* (2019).

<https://doi.org/10.1016/j.wace.2019.100217>.

- [114] Y. Jamei, P. Rajagopalan, Q. (Chayn) Sun, Spatial structure of surface urban heat island and its relationship with vegetation and built-up areas in Melbourne, Australia, *Sci. Total Environ.* (2019). <https://doi.org/10.1016/j.scitotenv.2018.12.308>.
- [115] H. Li, Y. Zhou, X. Wang, X. Zhou, H. Zhang, S. Sodoudi, Quantifying urban heat island intensity and its physical mechanism using WRF/UCM, *Sci. Total Environ.* (2019). <https://doi.org/10.1016/j.scitotenv.2018.10.025>.
- [116] Y. Li, S. Schubert, J.P. Kropp, D. Rybski, On the influence of density and morphology on the Urban Heat Island intensity, *Nat. Commun.* (2020). <https://doi.org/10.1038/s41467-020-16461-9>.
- [117] C. Ren, K. Wang, Y. Shi, Y.T. Kwok, T.E. Morakinyo, T. cheung Lee, Y. Li, Investigating the urban heat and cool island effects during extreme heat events in high-density cities: A case study of Hong Kong from 2000 to 2018, *Int. J. Climatol.* (2021). <https://doi.org/10.1002/joc.7222>.
- [118] F. Salamanca, M. Georgescu, A. Mahalov, M. Moustaoui, M. Wang, Anthropogenic heating of the urban environment due to air conditioning, *J. Geophys. Res.* (2014). <https://doi.org/10.1002/2013JD021225>.
- [119] S.W. Kim, R.D. Brown, Urban heat island (UHI) intensity and magnitude estimations: A systematic literature review, *Sci. Total Environ.* (2021). <https://doi.org/10.1016/j.scitotenv.2021.146389>.
- [120] J. Kong, Y. Zhao, J. Carmeliet, C. Lei, Urban heat island and its interaction with heatwaves: A review of studies on mesoscale, *Sustain.* (2021). <https://doi.org/10.3390/su131910923>.
- [121] G. Xian, H. Shi, R. Auch, K. Gallo, Q. Zhou, Z. Wu, M. Kolian, The effects of urban land cover dynamics on urban heat Island intensity and temporal trends, *GIScience Remote Sens.* (2021). <https://doi.org/10.1080/15481603.2021.1903282>.
- [122] K.B. Moffett, Y. Makido, V. Shandas, Urban-rural surface temperature deviation and intra-urban variations contained by an urban growth boundary, *Remote Sens.* (2019). <https://doi.org/10.3390/rs11222683>.

- [123] R. Yao, L. Wang, X. Huang, W. Gong, X. Xia, Greening in Rural Areas Increases the Surface Urban Heat Island Intensity, *Geophys. Res. Lett.* (2019). <https://doi.org/10.1029/2018GL081816>.
- [124] D. Zhou, S. Zhao, S. Liu, L. Zhang, C. Zhu, Surface urban heat island in China's 32 major cities: Spatial patterns and drivers, *Remote Sens. Environ.* (2014). <https://doi.org/10.1016/j.rse.2014.05.017>.
- [125] S.I. Bohnenstengel, S. Evans, P.A. Clark, S.E. Belcher, Simulations of the London urban heat island, *Q. J. R. Meteorol. Soc.* (2011). <https://doi.org/10.1002/qj.855>.
- [126] S. Peng, S. Piao, P. Ciais, P. Friedlingstein, C. Oettle, F.M. Bréon, H. Nan, L. Zhou, R.B. Myneni, Surface urban heat island across 419 global big cities, *Environ. Sci. Technol.* (2012). <https://doi.org/10.1021/es2030438>.
- [127] M. Santamouris, Analyzing the heat island magnitude and characteristics in one hundred Asian and Australian cities and regions, *Sci. Total Environ.* (2015). <https://doi.org/10.1016/j.scitotenv.2015.01.060>.
- [128] A. Dimoudi, A. Kantzioura, S. Zoras, C. Pallas, P. Kosmopoulos, Investigation of urban microclimate parameters in an urban center, *Energy Build.* (2013). <https://doi.org/10.1016/j.enbuild.2013.04.014>.
- [129] F. Peron, M.M. De Maria, F. Spinazzè, U. Mazzali, An analysis of the urban heat island of Venice mainland, *Sustain. Cities Soc.* (2015). <https://doi.org/10.1016/j.scs.2015.05.008>.
- [130] P. Rajagopalan, K.C. Lim, E. Jamei, Urban heat island and wind flow characteristics of a tropical city, *Sol. Energy.* (2014). <https://doi.org/10.1016/j.solener.2014.05.042>.
- [131] E.L. Ndetto, A. Matzarakis, Effects of urban configuration on human thermal conditions in a typical tropical African coastal city, *Adv. Meteorol.* (2013). <https://doi.org/10.1155/2013/549096>.
- [132] C.A.Souch, C.Souch, The effect of trees on summertime below canopy urban climates: a case study Bloomington, Indiana, *J. Arboric.* (1993).
- [133] A. Aboelata, S. Sodoudi, Evaluating the effect of trees on UHI mitigation and reduction of

- energy usage in different built up areas in Cairo, *Build. Environ.* (2020). <https://doi.org/10.1016/j.buildenv.2019.106490>.
- [134] X.X. Li, L.K. Norford, Evaluation of cool roof and vegetations in mitigating urban heat island in a tropical city, Singapore, *Urban Clim.* (2016). <https://doi.org/10.1016/j.uclim.2015.12.002>.
- [135] M.O. Mughal, A. Kubilay, S. Fatichi, N. Meili, J. Carmeliet, P. Edwards, P. Burlando, Detailed investigation of vegetation effects on microclimate by means of computational fluid dynamics (CFD) in a tropical urban environment, *Urban Clim.* (2021). <https://doi.org/10.1016/j.uclim.2021.100939>.
- [136] P. Ramamurthy, E. Bou-Zeid, Heatwaves and urban heat islands: A comparative analysis of multiple cities, *J. Geophys. Res.* (2017). <https://doi.org/10.1002/2016JD025357>.
- [137] D. Li, E. Bou-Zeid, Synergistic interactions between urban heat islands and heat waves: The impact in cities is larger than the sum of its parts, *J. Appl. Meteorol. Climatol.* (2013). <https://doi.org/10.1175/JAMC-D-13-02.1>.
- [138] D. Founda, M. Santamouris, Synergies between Urban Heat Island and Heat Waves in Athens (Greece), during an extremely hot summer (2012), *Sci. Rep.* (2017). <https://doi.org/10.1038/s41598-017-11407-6>.
- [139] D. Founda, F. Pierros, M. Petrakis, C. Zerefos, Interdecadal variations and trends of the Urban Heat Island in Athens (Greece) and its response to heat waves, *Atmos. Res.* (2015). <https://doi.org/10.1016/j.atmosres.2015.03.016>.
- [140] S. Jiang, X. Lee, J. Wang, K. Wang, Amplified Urban Heat Islands during Heat Wave Periods, *J. Geophys. Res. Atmos.* (2019). <https://doi.org/10.1029/2018JD030230>.
- [141] L.W. Chew, X. Liu, X.X. Li, L.K. Norford, Interaction between heat wave and urban heat island: A case study in a tropical coastal city, Singapore, *Atmos. Res.* (2021). <https://doi.org/10.1016/j.atmosres.2020.105134>.
- [142] A. Dimoudi, S. Zoras, A. Kantzioura, X. Stogiannou, P. Kosmopoulos, C. Pallas, Use of cool materials and other bioclimatic interventions in outdoor places in order to mitigate the urban heat island in a medium size city in Greece, *Sustain. Cities Soc.* (2014).

<https://doi.org/10.1016/j.scs.2014.04.003>.

- [143] J.P. Gastellu-Etchegorry, F. Zagolski, J. Romier, A simple anisotropic reflectance model for homogeneous multilayer canopies, *Remote Sens. Environ.* (1996). [https://doi.org/10.1016/0034-4257\(95\)00221-9](https://doi.org/10.1016/0034-4257(95)00221-9).
- [144] F. Lindberg, B. Holmer, S. Thorsson, SOLWEIG 1.0 - Modelling spatial variations of 3D radiant fluxes and mean radiant temperature in complex urban settings, *Int. J. Biometeorol.* (2008). <https://doi.org/10.1007/s00484-008-0162-7>.
- [145] V. Dorer, J. Allegrini, K. Orehounig, P. Moonen, G. Upadhyay, J. Kämpf, J. Carmeliet, Modelling the urban microclimate and its impact on the energy demand of buildings and building clusters, in: *Proc. BS 2013 13th Conf. Int. Build. Perform. Simul. Assoc.*, 2013.
- [146] Y. Toparlar, B. Blocken, B. Maiheu, G.J.F. van Heijst, Impact of urban microclimate on summertime building cooling demand: A parametric analysis for Antwerp, Belgium, *Appl. Energy.* (2018). <https://doi.org/10.1016/j.apenergy.2018.06.110>.
- [147] L. Malys, M. Musy, C. Inard, A hydrothermal model to assess the impact of green walls on urban microclimate and building energy consumption, *Build. Environ.* (2014). <https://doi.org/10.1016/j.buildenv.2013.12.012>.
- [148] M. Shirzadi, M. Naghashzadegan, P. A. Mirzaei, Improving the CFD modelling of cross-ventilation in highly-packed urban areas, *Sustain. Cities Soc.* (2018). <https://doi.org/10.1016/j.scs.2017.11.020>.
- [149] M. Shirzadi, Y. Tominaga, P.A. Mirzaei, Wind tunnel experiments on cross-ventilation flow of a generic sheltered building in urban areas, *Build. Environ.* (2019). <https://doi.org/10.1016/j.buildenv.2019.04.057>.
- [150] M. Shirzadi, Y. Tominaga, P.A. Mirzaei, Experimental and steady-RANS CFD modelling of cross-ventilation in moderately-dense urban areas, *Sustain. Cities Soc.* (2020). <https://doi.org/10.1016/j.scs.2019.101849>.
- [151] Y. Tominaga, T. Stathopoulos, CFD simulation of near-field pollutant dispersion in the urban environment: A review of current modeling techniques, *Atmos. Environ.* (2013). <https://doi.org/10.1016/j.atmosenv.2013.07.028>.

- [152] B. Blocken, Y. Tominaga, T. Stathopoulos, CFD simulation of micro-scale pollutant dispersion in the built environment, *Build. Environ.* (2013). <https://doi.org/10.1016/j.buildenv.2013.01.001>.
- [153] P. Gousseau, B. Blocken, T. Stathopoulos, G.J.F. van Heijst, CFD simulation of near-field pollutant dispersion on a high-resolution grid: A case study by LES and RANS for a building group in downtown Montreal, *Atmos. Environ.* 45 (2011) 428–438. <https://doi.org/10.1016/j.atmosenv.2010.09.065>.
- [154] S. Yang, L. (Leon) Wang, P. Raftery, M. Ivanovich, C. Taber, W.P. Bahnfleth, P. Wargocki, J. Pantelic, J. Zou, M. Mortezaadeh, C. Shu, R. Wang, S. Arnold, Comparing airborne infectious aerosol exposures in sparsely occupied large spaces utilizing large-diameter ceiling fans, *Build. Environ.* (2023). <https://doi.org/10.1016/j.buildenv.2023.110022>.
- [155] M. Chavez, B. Hajra, T. Stathopoulos, A. Bahloul, Near-field pollutant dispersion in the built environment by CFD and wind tunnel simulations, *J. Wind Eng. Ind. Aerodyn.* 99 (2011) 330–339. <https://doi.org/10.1016/j.jweia.2011.01.003>.
- [156] L. Soulhac, P. Salizzoni, P. Mejean, R.J. Perkins, Parametric laws to model urban pollutant dispersion with a street network approach, *Atmos. Environ.* (2013). <https://doi.org/10.1016/j.atmosenv.2012.10.053>.
- [157] M. Carpentieri, P. Hayden, A.G. Robins, Wind tunnel measurements of pollutant turbulent fluxes in urban intersections, *Atmos. Environ.* (2012). <https://doi.org/10.1016/j.atmosenv.2011.09.083>.
- [158] C. Yuan, E. Ng, L.K. Norford, Improving air quality in high-density cities by understanding the relationship between air pollutant dispersion and urban morphologies, *Build. Environ.* (2014). <https://doi.org/10.1016/j.buildenv.2013.10.008>.
- [159] J.F. Sini, S. Anquetin, P.G. Mestayer, Pollutant dispersion and thermal effects in urban street canyons, *Atmos. Environ.* (1996). [https://doi.org/10.1016/1352-2310\(95\)00321-5](https://doi.org/10.1016/1352-2310(95)00321-5).
- [160] B. Blocken, Computational Fluid Dynamics for urban physics: Importance, scales, possibilities, limitations and ten tips and tricks towards accurate and reliable simulations, *Build. Environ.* 91 (2015) 219–245. <https://doi.org/10.1016/j.buildenv.2015.02.015>.

- [161] B. Blocken, 50 years of Computational Wind Engineering: Past, present and future, *J. Wind Eng. Ind. Aerodyn.* (2014). <https://doi.org/10.1016/j.jweia.2014.03.008>.
- [162] A. Zhang, C. Gao, L. Zhang, Numerical simulation of the wind field around different building arrangements, *J. Wind Eng. Ind. Aerodyn.* 93 (2005) 891–904. <https://doi.org/10.1016/j.jweia.2005.09.001>.
- [163] Y. Jiang, Q. Chen, Effect of fluctuating wind direction on cross natural ventilation in buildings from large eddy simulation, *Build. Environ.* (2002). [https://doi.org/10.1016/S0360-1323\(01\)00036-1](https://doi.org/10.1016/S0360-1323(01)00036-1).
- [164] Y. Tominaga, R. Yoshie, A. Mochida, H. Kataoka, K. Harimoto, T. Nozu, Cross Comparisons of CFD Prediction for Wind Environment at Pedestrian Level around Buildings Part 2 : Comparison of Results for Flowfield around Building Complex in Actual Urban Area, *Sixth Asia-Pacific Conf. Wind Eng.* (2005).
- [165] Y. Tominaga, A. Mochida, R. Yoshie, H. Kataoka, T. Nozu, M. Yoshikawa, T. Shirasawa, AIJ guidelines for practical applications of CFD to pedestrian wind environment around buildings, *J. Wind Eng. Ind. Aerodyn.* 96 (2008) 1749–1761. <https://doi.org/10.1016/j.jweia.2008.02.058>.
- [166] M. Mortezaadeh, L. (Leon) Wang, Solving city and building microclimates by fast fluid dynamics with large timesteps and coarse meshes, *Build. Environ.* (2020). <https://doi.org/10.1016/j.buildenv.2020.106955>.
- [167] A. Katal, M. Mortezaadeh, L. (Leon) Wang, Modeling building resilience against extreme weather by integrated CityFFD and CityBEM simulations, *Appl. Energy.* (2019). <https://doi.org/10.1016/j.apenergy.2019.04.192>.
- [168] J. Hensen, *Modelling Coupled Heat and Air Flow: Ping-Pong vs Onions*, IEA Air Infiltration Vent. (1995).
- [169] J.M. Masterton, F.A. Richardson, C.E. Canada, C.A.E. Service, *Humidex: A Method of Quantifying Human Discomfort Due to Excessive Heat and Humidity*, Environment Canada, Atmospheric Environment, 1979. <https://books.google.ca/books?id=IVETzQEACAAJ>.
- [170] L. Monteiro, M. Alucci, *Outdoor thermal comfort: comparison of results of empirical field*

- research and predictive models simulation, in: *Comf. Energy Use Build. Get. It Right*, 2006.
- [171] É. Mekis, L.A. Vincent, M.W. Shephard, X. Zhang, Observed Trends in Severe Weather Conditions Based on Humidex, Wind Chill, and Heavy Rainfall Events in Canada for 1953-2012, *Atmos. - Ocean.* 53 (2015) 383–397. <https://doi.org/10.1080/07055900.2015.1086970>.
- [172] J.M. Sobstyl, T. Emig, M.J.A. Qomi, F.J. Ulm, R.J.M. Pellenq, Role of City Texture in Urban Heat Islands at Nighttime, *Phys. Rev. Lett.* (2018). <https://doi.org/10.1103/PhysRevLett.120.108701>.
- [173] L. Ji, A. Laouadi, C. Shu, A. Gaur, M. Lacasse, L. (Leon) Wang, Evaluating approaches of selecting extreme hot years for assessing building overheating conditions during heatwaves, *Energy Build.* (2022). <https://doi.org/10.1016/j.enbuild.2021.111610>.
- [174] C. Shu, A. Gaur, L. Wang, M.A. Lacasse, Evolution of the local climate in Montreal and Ottawa before, during and after a heatwave and the effects on urban heat islands, *Sci. Total Environ.* (2023). <https://doi.org/10.1016/j.scitotenv.2023.164497>.
- [175] L.H.U.W. Abeydeera, J.W. Mesthrige, T.I. Samarasinghalage, Global research on carbon emissions: A scientometric review, *Sustain.* (2019). <https://doi.org/10.3390/su11143972>.
- [176] Z. Zeng, X. Zhou, L. Li, The Impact of Water on Microclimate in Lingnan Area, in: *Procedia Eng.*, 2017. <https://doi.org/10.1016/j.proeng.2017.10.082>.
- [177] S. Yang, L. (Leon) Wang, T. Stathopoulos, A.M. Marey, Urban microclimate and its impact on built environment – A review, *Build. Environ.* 238 (2023) 110334. <https://doi.org/10.1016/j.buildenv.2023.110334>.
- [178] K. Lundgren, T. Kjellstrom, Sustainability challenges from climate change and air conditioning use in urban areas, *Sustain.* (2013). <https://doi.org/10.3390/su5073116>.
- [179] J. Allegrini, V. Dorer, J. Carmeliet, Coupled CFD, radiation and building energy model for studying heat fluxes in an urban environment with generic building configurations, *Sustain. Cities Soc.* (2015). <https://doi.org/10.1016/j.scs.2015.07.009>.
- [180] A. Aboelata, Vegetation in different street orientations of aspect ratio (H/W 1:1) to mitigate

- UHI and reduce buildings' energy in arid climate, *Build. Environ.* (2020). <https://doi.org/10.1016/j.buildenv.2020.106712>.
- [181] A. Katal, S. Leroyer, J. Zou, O. Nikiema, M. Albettar, S. Belair, L. (Leon) Wang, Outdoor heat stress assessment using an integrated multi-scale numerical weather prediction system: A case study of a heatwave in Montreal, *Sci. Total Environ.* (2023). <https://doi.org/10.1016/j.scitotenv.2022.161276>.
- [182] X. Li, Y. Zhou, S. Yu, G. Jia, H. Li, W. Li, Urban heat island impacts on building energy consumption: A review of approaches and findings, *Energy.* (2019). <https://doi.org/10.1016/j.energy.2019.02.183>.
- [183] M. Palme, L. Inostroza, G. Villacreses, A. Lobato, C. Carrasco, Urban weather data and building models for the inclusion of the urban heat island effect in building performance simulation, *Data Br.* (2017). <https://doi.org/10.1016/j.dib.2017.08.035>.
- [184] N. Sezer, H. Yoonus, D. Zhan, L. (Leon) Wang, I.G. Hassan, M.A. Rahman, Urban microclimate and building energy models: A review of the latest progress in coupling strategies, *Renew. Sustain. Energy Rev.* (2023). <https://doi.org/10.1016/j.rser.2023.113577>.
- [185] N. Lauzet, A. Rodler, M. Musy, M.H. Azam, S. Guernouti, D. Mauree, T. Colinart, How building energy models take the local climate into account in an urban context – A review, *Renew. Sustain. Energy Rev.* (2019). <https://doi.org/10.1016/j.rser.2019.109390>.
- [186] S. Tsoka, K. Tolika, T. Theodosiou, K. Tsikaloudaki, D. Bikas, A method to account for the urban microclimate on the creation of 'typical weather year' datasets for building energy simulation, using stochastically generated data, *Energy Build.* (2018). <https://doi.org/10.1016/j.enbuild.2018.01.016>.
- [187] S. Moghanlo, M. Alavinejad, V. Oskoei, H. Najafi Saleh, A.A. Mohammadi, H. Mohammadi, Z. DerakhshanNejad, Using artificial neural networks to model the impacts of climate change on dust phenomenon in the Zanzan region, north-west Iran, *Urban Clim.* (2021). <https://doi.org/10.1016/j.uclim.2020.100750>.
- [188] Y. Xie, W. Hu, X. Zhou, S. Yan, C. Li, Artificial Neural Network Modeling for Predicting and Evaluating the Mean Radiant Temperature around Buildings on Hot Summer Days,

- Buildings. (2022). <https://doi.org/10.3390/buildings12050513>.
- [189] B. Shboul, I. AL-Arifi, S. Michailos, D. Ingham, L. Ma, K.J. Hughes, M. Pourkashanian, A new ANN model for hourly solar radiation and wind speed prediction: A case study over the north & south of the Arabian Peninsula, *Sustain. Energy Technol. Assessments*. (2021). <https://doi.org/10.1016/j.seta.2021.101248>.
- [190] D.B. Crawley, L.K. Lawrie, F.C. Winkelmann, W.F. Buhl, Y.J. Huang, C.O. Pedersen, R.K. Strand, R.J. Liesen, D.E. Fisher, M.J. Witte, J. Glazer, EnergyPlus: creating a new-generation building energy simulation program, *Energy Build.* 33 (2001) 319–331. [https://doi.org/10.1016/S0378-7788\(00\)00114-6](https://doi.org/10.1016/S0378-7788(00)00114-6).
- [191] C.Y. Siu, Z. Liao, Is building energy simulation based on TMY representative: A comparative simulation study on doe reference buildings in Toronto with typical year and historical year type weather files, *Energy Build.* (2020). <https://doi.org/10.1016/j.enbuild.2020.109760>.
- [192] J. Zhang, F. Zhang, Z. Gou, J. Liu, Assessment of macroclimate and microclimate effects on outdoor thermal comfort via artificial neural network models, *Urban Clim.* (2022). <https://doi.org/10.1016/j.uclim.2022.101134>.
- [193] X. Wu, J. Hou, J. Hui, Z. Tang, W. Wang, Revealing Microclimate around Buildings with Long-Term Monitoring through the Neural Network Algorithms, *Buildings*. (2022). <https://doi.org/10.3390/buildings12040395>.
- [194] M. Mangiameli, G. Mussumeci, A. Gagliano, Evaluation of the Urban Microclimate in Catania using Multispectral Remote Sensing and GIS Technology, *Climate*. (2022). <https://doi.org/10.3390/cli10020018>.
- [195] C. Shu, Assessment of the Effects of Extreme Heat Events on Buildings, (2021).
- [196] J. Zou, A. Gaur, L. (Leon) Wang, A. Laouadi, M. Lacasse, Assessment of future overheating conditions in Canadian cities using a reference year selection method, *Build. Environ.* (2022). <https://doi.org/10.1016/j.buildenv.2022.109102>.
- [197] J. Zou, H. Lu, C. Shu, L. Ji, A. Gaur, L. (Leon) Wang, Multiscale numerical assessment of urban overheating under climate projections: A review, *Urban Clim.* 49 (2023) 101551.

<https://doi.org/https://doi.org/10.1016/j.uclim.2023.101551>.

- [198] C.; Zhang, O.B. Kazanci, S. Attia, R. Levinson, S.H. Lee, P. Holzer, A. Salvatif, A. Machard, M. Pourabdollahtookaboni, A. Gaur, B.W. Olesen, P. Heiselberg, General rights IEA EBC Annex 80-Dynamic simulation guideline for the performance testing of resilient cooling strategies, Citation. (2021).
- [199] M. P.tootkaboni, I. Ballarini, M. Zinzi, V. Corrado, A comparative analysis of different future weather data for building energy performance simulation, *Climate*. (2021). <https://doi.org/10.3390/cli9020037>.
- [200] M. Deru, K. Field, D. Studer, K. Benne, B. Griffith, P. Torcellini, B. Liu, M. Halverson, D. Winiarski, M. Rosenberg, M. Yazdanian, J. Huang, D. Crawley, U.S. Department of Energy commercial reference building models of the national building stock, *Publ.* (2011) 1–118. http://digitalscholarship.unlv.edu/renew_pubs/44.
- [201] K. Menberg, Y. Heo, R. Choudhary, Sensitivity analysis methods for building energy models: Comparing computational costs and extractable information, *Energy Build.* (2016). <https://doi.org/10.1016/j.enbuild.2016.10.005>.
- [202] T. Wei, A review of sensitivity analysis methods in building energy analysis, *Renew. Sustain. Energy Rev.* (2013). <https://doi.org/10.1016/j.rser.2012.12.014>.
- [203] H. Lim, Z.J. Zhai, Comprehensive evaluation of the influence of meta-models on Bayesian calibration, *Energy Build.* (2017). <https://doi.org/10.1016/j.enbuild.2017.09.009>.
- [204] E.W. Peterson, J.P. Hennessey, ON THE USE OF POWER LAWS FOR ESTIMATES OF WIND POWER POTENTIAL., *J. Appl. Meteorol.* (1978). [https://doi.org/10.1175/1520-0450\(1978\)017<0390:OTUOPL>2.0.CO;2](https://doi.org/10.1175/1520-0450(1978)017<0390:OTUOPL>2.0.CO;2).
- [205] S. Magli, C. Lodi, L. Lombroso, A. Muscio, S. Teggi, Analysis of the urban heat island effects on building energy consumption, *Int. J. Energy Environ. Eng.* (2015). <https://doi.org/10.1007/s40095-014-0154-9>.
- [206] D. Hou, I.G. Hassan, L. Wang, Review on building energy model calibration by Bayesian inference, *Renew. Sustain. Energy Rev.* (2021). <https://doi.org/10.1016/j.rser.2021.110930>.